AN ABSTRACT OF THE DISSERTATION OF

Arpan Biswas for the degree of Doctor of Philosophy in Mechanical Engineering presented on December 4, 2020.

Title: Hybrid Statistical and Engineering Optimization Architectures in Early Multidisciplinary Designs of Resilience and Expensive Black-box Complex Systems

Abstract approved:

_____

Christopher Hoyle

Practical engineering design problems are generally multi-disciplinary with limited budget and high risk in terms of life loss, economic resources, etc. In the early phase of such problems, selection of true efficient designs is desired while minimizing overall design cost by avoiding expensive search processes. However, the task is difficult for a simple optimization framework due to the formulation complexity, high function evaluation cost, uncertain design parameters etc. Thus, the overall research goal is to develop complex, hybrid optimization architectures for solving early design problems considering the trade-off among model complexity, performance and cost. We start by comparing multiple architectures, and investigated a *nested bi-level architecture* for early resilience design with discrete design space and with a trade-off among multiple objectives at different risk level scenarios. The work then focused on increased problem complexity with black-box functions in a mechanical design classification problem with discontinuous design space using a *sequential Bayesian Optimization* (BO) architecture to locate an unknown creep-fatigue failure constraint boundary. The work then extends a *weighted Tchebycheff black-box multi-objective BO* (MO-BO) architecture for mechanical design with a trade-off between design risk and cost, with model calibration through regression analysis of unknown parameters. Finally, we investigate an iterative regression model selection procedure, nested into the proposed MO-BO, to enhance design flexibility, estimation and overall performance. This work can be applicable to any domains of complex or/and expensive black-box system design problems.

# Hybrid Statistical and Engineering Optimization Architectures in Early Multidisciplinary Designs of Resilience and Expensive Black-box Complex Systems

by
Arpan Biswas

A DISSERTATION

submitted to

Oregon State University

in partial fulfillment of
the requirements for the
degree of

Doctor of Philosophy

Presented December 4, 2020
Commencement June 2021

Doctor of Philosophy dissertation of Arpan Biswas presented on December 4, 2020

APPROVED:

Major Professor, representing Mechanical Engineering

Head of the School of Mechanical, Industrial and Manufacturing Engineering

Dean of the Graduate School

I understand that my dissertation will become part of the permanent collection of Oregon State University libraries. My signature below authorizes release of my dissertation to any reader upon request.

Arpan Biswas, Author

# ACKNOWLEDGEMENTS

The author expresses sincere appreciation to everyone who has helped him to achieve the degree successfully.

I would like to thank to almighty GOD for the blessing I needed in every path.

To my advisors Dr. Christopher Hoyle and Dr. Claudio Fuentes for showing such faith in me to work with them and guiding me to complete my dissertation. Their continuous guidance and feedback have helped me to grow immensely both as a person and a researcher. It's been an honor to work with them.

To my committee members, Dr. Matt Cambell and Dr. Nathan Gibson to guide and provide feedbacks of my research whenever requested. Also, the design optimization and the mathematical courses taught by them have broaden my horizon and deepen my concepts, which is one of the major reason to the completeness of this dissertation.

To my lovely wife Ananya for being so supportive throughout my good and bad phases of my life.

To my parents for giving me continuous moral support for my study.

And lastly to everyone who has directly or indirectly provided a significant impact in completing my dissertation successfully.

# CONTRIBUTION OF AUTHORS

For the manuscript: Exploring Architectures for Integrated Resilience Optimization.
Co-authors: Daniel Hulse, Christopher Hoyle, Irem Y. Tumer, Chetan Kulkarni, Kai Goebel

For the manuscript: An Approach to Bayesian Optimization for Design Feasibility Check on Discontinuous Black-Box Functions.
Co-author: Christopher Hoyle

For the manuscript: An Approach to Bayesian Optimization in Optimizing Weighted Tchebycheff Multi-Objective Black-Box Functions.
Co-authors: Claudio Fuentes, Christopher Hoyle

For the manuscript: A MO-Bayesian Optimization Approach Using the Weighted Tchebycheff Method: A Case Study of Cyclic Pressure-Temperature Loaded Thin Tube Design.
Co-authors: Claudio Fuentes, Christopher Hoyle

For the manuscript: A Nested Weighted Tchebycheff MO-Bayesian Optimization Approach for Flexibility in Utopia Point Estimation: A Case Study of Cyclic Pressure-Temperature Loaded Thin Tube Design.
Co-authors: Claudio Fuentes, Christopher Hoyle

# TABLE OF CONTENTS

Page

TABLE OF CONTENTS (Continued)

Page

TABLE OF CONTENTS (Continued)

Page

TABLE OF CONTENTS (Continued)

Page

# TABLE OF CONTENTS

Page

# LIST OF FIGURES

Figure Page

# LIST OF FIGURES (Continued)

Figure Page

# LIST OF FIGURES (Continued)

Figure Page

# LIST OF TABLES

# LIST OF APPENDIX FIGURES

Figure Page

# LIST OF APPENDIX TABLES

Table Page

DEDICATED
TO

My wife, Ananya Sinha Chowdhury

My mother, Kabita Biswas

My father, Nepal Biswas

# CHAPTER 1

# General Introduction

## 1.1.Motivation

Practical engineering design problems are generally complex with limited budget. However, due to the involvement of high risk in terms of public safety, economic resources, etc. in such design problems, we require our design decisions to be as accurate as possible. A risk in engineering design can be defined as the potential for a design to fail to meet critical requirements due to being flawed, infeasible, inefficient etc. In the early design phase, it is very important for the designers to able to identify the interesting regions in the large complex design space when the cost is low; this helps in guidance as the designers can avoid investing on detailed and expensive design analysis on infeasible or inefficient designs. Thus, the goal is to provide efficient design decisions in the early design phase to reduce the overall cost of the design process. It is impossible to conduct expensive evaluations of every possible design, therefore, low-cost optimization models are necessary, specific to the domain of design problem, to help the designers with efficient decisions in early design phase. However, such practical design problems are hard to implement in a simple optimization framework, due to the complexity in the formulation of objective functions and constraints, high simulation or function evaluation cost, inclusion of uncertain design parameters, etc. Also, approximating a complex design problem into much simpler problem can lead to the negligence of original complex constraints and, thus, can result in infeasible designs and not be a useful choice for practical decisions. This motivates us to consider an appropriate optimization framework for a complex design problem to obtain better decisions in the early design phase, which can reduce higher cost in the later design phase. Practically, there is a cost consideration with the complexity in the optimization framework due to complex function evaluations, large constraints validation, complex simulations, etc. which act as a counter-balance for better decisions. Some practical design problems have been investigated where complex optimization frameworks have been modeled [1], [2]. In this work, we are focused on the application of *sequential* and *hierarchical* optimization frameworks to solve complex design problems, representing

the domain of problems practiced in different industries. Different sequential [3], [4] and hierarchical or nested methods [5], [6] have been attempted to solve these problems. This research is focused on the investigation of the *bi-level* (nested) and *Bayesian* (sequential) design techniques. Thus, the overall research goal is to investigate hybrid optimization architectures in solving early phase design problems with a trade-off among model complexity, performance, and cost.

### 1.2. Research Objectives and Contribution

The four research objectives of this dissertation are now presented:

***RO-1: Investigating bi-level design architectures in early resilient system design optimization:***

In the domain of complex dynamic system engineering, we generally have a high failure cost: for example, life loss from aircraft disasters due to any system failures. The goal for this study is to investigate an appropriate design architecture for efficient, high resilience design solutions, reducing risk of failures. A *resilient design* is the design of a system which has the ability to recover from faults, partially or completely, to attain a desired level of performance and mitigate risk. Redundancy in engineering design, is the duplication or installation of critical components or functions of a system with the intention of increasing reliability of the system or to improve actual system performance. Redundancy is one method of achieving system resilience. Figure 1.1 is an example of a resilient commercial aircraft complex engineered system. However, in such complex system design problems (e.g. aircraft systems), the challenges or the complexities involve a challenging design space due to a mixed-integer problem from discrete choices of systems and subsystems (eg. airfoil, flaps, propellers, battery etc.), and continuous operational variables (flight height, speed etc.) with multiple considerations of costs from design, manufacturing, operation and safety measures. An efficient design solution should have the best trade-off among these costs. With such complexities in the early integrated resilient system design problem, this research contributes by investigating a *nested bi-level* design architecture and compares this with other common simpler optimization architectures like *single stage* and *sequential* in

terms of the solution quality, time complexities and general usefulness. The research will benefit the domain of complex engineering systems and the proposed bi-level optimization framework (nested design) can be applicable in such practical design problems where in the early design stage, the designer will be able to consider multiple design options (concepts), compare numerically among those design options (concepts), and find true efficient designs (concept selection in terms of low risk factor) for future consideration in manufacturing or implementation.

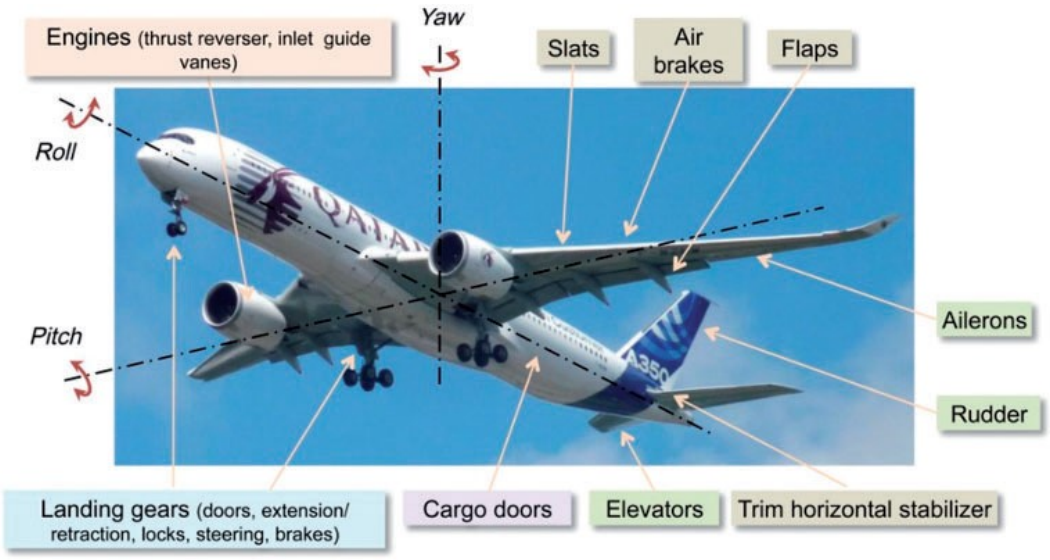


Figure 1.1. Example of a resilience system (commercial aircraft) (from google)

***RO-2: Developing a sequential Bayesian optimization design architecture as a design classifier:***

In addition to the challenges in the first research objective, in other complex design problems, the objective or constraint functions might also be represented by many mathematical equations or need very costly simulation models. These kind of functions are called *black-box functions* and such design problems are called black-box problems. Figure 1.2 shows a conceptual comparison between white-box and black-box models in software testing. In the white-box, we know the complete application codes, whereas in the black-box model, the complex and expensive application codes are too complicated for a human brain to interpret or are unknown to the designer. Thus, unlike

a white-box model, we know only the model inputs and outputs but not any mapping equations from input to output. Generally, these kind of black-box problems can be solved by a Bayesian optimization (BO) [7]. Bayesian optimization is a low-cost black-box global optimization tool in the sequential design method where we learn and update our knowledge from prior evaluated designs (data), and proceed to the selection (sampling) of new designs for future expensive evaluation, with a target to find the optimal region at minimal evaluation cost. In the complex design problems like in the domain of complex engineered system (Aircraft design) or in physical and mechanical systems of material science and manufacturing, there can lie a *discontinuity* from discrete choice of designs, discrete design domain (or regions) or discontinuity in material properties etc. However, one of the challenges is that the standard BO assumes a continuous black-box function [7] and therefore, with a discontinuous space in a black-box design problem, the performance of BO does not guarantee true convergence and thereby raises the concern on the quality of the solution. As in the black box design problem, there can also lie an unknown location of a black-box constraint, which with neglecting can also lead to provide solution inaccuracy, posing high risk designs. Focusing on these challenges on a discontinuous black-box design problem with unknown constraints, this research contributes in tackling these with adopting a design space-partitioning approach. This research investigates integrating a classification technique into the existing efficient sampling method of BO, with no constraint on the amount and quality of pre-existing training data, which any existing machine learning classifiers are dependent to [8], [9].

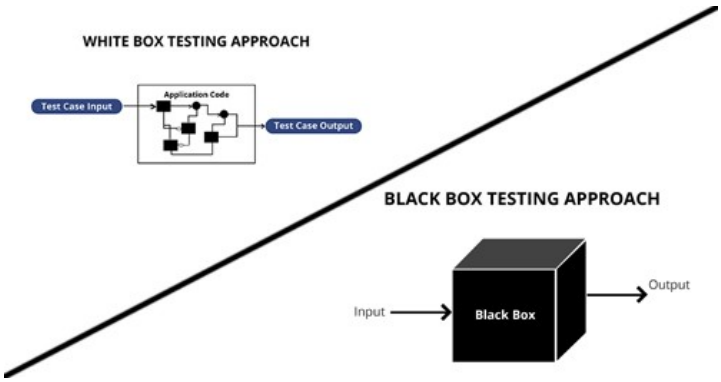


Figure 1.2. Comparison between white-box and black-box models

***RO-3: Stage 2: Developing a weighted Tchebycheff multi-objective Bayesian optimization with regression-based model calibration:***

In the black-box design problems in the domain of complex static or dynamic systems, one can have multiple black-box objectives with respect to design, operational, safety measures etc. In optimizing the problems, a multi-objective Bayesian optimization (MOBO) architectures is generally suited. In recent years, two common approaches that has been taken: 1. formulating a multi-objective (hyper-volume) acquisition function [10], [11] and 2. building a combined (single) multi-objective function and treat it as a single acquisition function [12] . The first approach however possesses significant model complexity with large number of objectives [12]. The second approach does not possess such limitations, however, but requires a special consideration of the choice of the method to formulate the multi-objective. A *global criterion method*, such as the weighted Tchebycheff method, is well suited for this second approach; however, a challenge of this method is the need for prior knowledge of *utopia values*. A utopia value in a multi-objective problem is the optimal solution of the objective when the same is optimized independently (not considering other objectives). As computational cost grows significantly with multiple BO for optimizing each objective independently (to find utopia), this research contributes in developing a weighted Tchebycheff MOBO with a regression based model calibration approach, where the utopia values are iteratively estimated from regression analysis of the available sampled data, guided by the acquisition function of weighted Tchebycheff black-box multi-objective function to minimize computational expense.

***RO-4: Developing a nested weighted Tchebycheff multi-objective Bayesian optimization, embedded with a regression model selection algorithm for utopia estimation:***

In the black-box multi-objective optimization problem in the domain of complex system design, the objectives are unknown (black-box) and due to the sequential sampling in a MOBO, the challenge further lies in the prior choice of *regression models* to be fitted in the weighted Tchebycheff MOBO, to best represent the black-box objectives from the available sampled data. Also, with an efficient choice of a regression model fitting the limited data (early knowledge), the efficiency of a given

regression model in estimating utopia values can degrade with the availability of more data through sequential sampling (increasing knowledge). With an inappropriate regression model estimating unknown model parameters (like utopia), large errors can also lead to the concern in solution accuracy in the MOBO setting, which ultimately leads to potentially inefficient or high-risk design solutions in any complex system design. Thus, to overcome these challenges and in the common focus of this dissertation to identify appropriate design architecture for better decisions, this research contributes in developing a *nested* weighted Tchebycheff MOBO. Here, to add flexibility, a regression model selection procedure is nested into the weighted Tchebycheff MO-BO design architecture, ultimately to find an appropriate regression model from a finite set of pre-defined models. The research contribution also includes investigating this flexible MO-BO design architecture by comparing the performance with earlier developed non-flexible architectures and architectures with other model selection procedures.

### 1.3.Case Studies

This dissertation uses two primary case studies to demonstrate the methods from this research. They are described as follows:

*Case Study 1*: The first case study, as a motivational problem to the first research objective, is the design of a *multirotor drone model*. In this problem, a trade-off between different cost objectives like design, operational and resilience cost are considered with different choices of systems (battery, rotor or line architectures), operations (flight height) and different choices of resilience policy in response to system (battery, rotor or line architectures) failures. This problem represents the early system resilience design under fault-scenario simulation. The problem considers two extreme flight scenarios representing different levels of flight risk: 1. A *Rural* scenario with relatively low cost of failure and 2. A *Congested* scenario with very high cost of failure. While design resiliency in this work is considered the system's ability to recover from faults to avoid from any disaster (high decrease in failure cost relative to low increase in design or operational cost), design redundancy in this work is defined

as the intention of installing more complex systems than required to increase system dependability (low decrease in failure cost relative to high increase in design cost).

*Case Study 2*: The second case study, from the domain of mechanics and manufacturing, is a *cyclic pressure-temperature loaded thin tube design*. This can be considered as a high-risk design problem due to having high failure outcomes of the material structures due to cyclic loading. Focusing on practical challenges of a black-box design problems as discussed earlier, this second case study represents a motivational example to the second, third and fourth research objectives, assuming multiple black-box objectives and an unknown creep-fatigue failure constraint boundary along the discontinuity of the discrete design domain of safe and unsafe region.

The roadmap for this dissertation is as follows. Chapter 2 uses the first case study and compares multiple architectures, and selects a nested bi-level architecture for early design resilience with discrete-continuous design space, and with a trade-off among multiple objectives. Chapters 3-5 focus on the second case study of the cyclic loaded thin tube design. Chapter 3 builds a sequential BO architecture as a design classifier by optimizing the location of the unknown constraint boundary (also representing the discontinuity) within a pseudo-continuous design space, which partitions and classifies safe and unsafe thin tubes in terms of creep-fatigue failure. Chapter 4 solves the multi-objective black-box problem with weighted Tchebycheff MO-BO and regression-based model calibration for utopia value estimation. Chapter 5 investigates the model selection procedure in an attempt to add flexibility and enhance the overall performance of the weighted Tchebycheff MOBO, leading to a nested weighted Tchebycheff MOBO. Chapter 6 concludes the dissertation with overall research accomplishments, current limitations, and future research directions.

### 1.4. Intellectual Merit

The principle purpose of the research is to provide an appropriate optimization framework and its application to complex engineering design problems during the early design process. The development of different architectures to mitigate several design

challenges mentioned earlier, extends the practical application of bi-level and Bayesian optimization for the design of experiment problems with discontinuous response surface, and solving machine learning classification problems. This efficient sequential learning will allow for better resource allocation to experiments, providing efficient investments. Furthermore, the reduction of model complexities with large number of objectives, and the additional knowledge in Bayesian Optimization framework through model calibration from low-cost statistical approach, increases the efficiency and thus align towards practical implementation. Finally, the development of Bi-level framework, representing a nested approach, opens a new direction in solving complex engineering system designs which are subject to high risk to failure consequences.

### 1.5. Broader Impact

The research in this dissertation will make significant steps as a positive impact on society. As practical engineering design problems are generally complex with limited budget, for the betterment of the society, we will need our design decisions to be as accurate as possible. It is very unlikely for a simple standard optimization formulation to be applicable for industrial problems due to the complexity in formulation of objective and constraints. Considering an oversimplified or inappropriate model for a design problem can lead to providing incorrect solutions, which can cause negative impact on society, especially when there is an involvement of high risk. Such high risk can be measured in terms of life loss or loss of resources as in the nuclear sectors, aerospace industries, pharmaceutical industries, consumer industries etc. In another way, any redundant costly design architectures should also be avoided in the early design to avoid the increase in cost of the overall design process. Thereby, by developing an efficient optimization models to solve such complex engineering design problems with a trade-off between solution accuracy and model cost in a decision making process in the early design phase, we can help the designers in reducing such risks while minimizing costs. The research also considers uncertainty in the optimization process, and towards minimizing prediction error of such uncertain parameters, which further reduces the risk in design decisions. Therefore, the outcome

of the research reduces the gap between design optimization theory and its practical application to reduce risk of failure due to any catastrophic incidents, thus maximizing design safety.

# CHAPTER 2

## An Approach to Bi-level Architectures in Early Resilience Designs

**Authors:**

**Arpan Biswas**

Department of Mechanical Engineering

Oregon State University

Corvallis, Oregon 97331

biswasar@oregonstate.edu

**Daniel Hulse**

Department of Mechanical Engineering

Oregon State University

Corvallis, Oregon 97331

hulsed@oregonstate.edu

**Christopher Hoyle**

Department of Mechanical Engineering

Oregon State University

Corvallis, Oregon 97331

chris.hoyle@oregonstate.edu

Chapter 2 manuscript is partly contributed from the below journal paper where I am the second author:

Paper Name: Exploring Architectures for Integrated Resilience Optimization.

**Status: Submitted ( AIAA Journal of Aerospace Information Systems)**

Texts and sections of chapter 2 marked with ** are the contribution of the author only of this dissertation.

Remaining texts and sections of chapter 2 NOT marked with ** are taken from the journal with a contribution of the first author: Daniel Hulse.

**ABSTRACT****

*In large scale complex engineered system design problems, multidisciplinary optimization has been utilized and plays a key role in design research. In such problems, it is often difficult to optimize for the whole system in a single level consisting of large numbers of design variables, objective functions and constraints. Also, it is often necessary to ensure that the design will be resilient to hazardous events to ensure safe, sustainable, and economical operations. To design resilience into the complex engineered system, it is necessary to consider a trade-off among high-level design redundancy of systems, operations, and the resilience policy used to respond and mitigate any hazardous contingencies. Therefore, it can be helpful to break down the overall problem into several sub-problems where optimizing each of the sub-problems guarantees an optimal solution to the main problem. With high risk of failure consequences in this early resilient design, an appropriate optimization architecture is necessary. This chapter compares different architectures for the resilient design of a drone model, finally selecting a bi-level architecture. In a nested bi-level design architecture, a decision at the upper level provides a unique projection to the lower level design space. In this architecture, the lower level problem is solved for each candidate design at the upper level, leading to an optimal solution at both levels. Though the computational cost of the bi-level architecture is the highest, it provides an overall better performance than simpler architectures like single-stage and sequential in terms of the optimal tradeoffs of design redundancy (design and operational cost) and resiliency for a low risk design solution.*

## 2.1.Introduction

Incorporating resilience in the design of a system is beneficial to ensure it operates as safely, sustainably, and economically as possible when there are hazardous events [13]–[15]. Optimizing resilience can involve the physical design of the system (e.g. redundancy and sensors) and the contingency management of the system (how it responds to hazardous events). Prior work [16]–[20] has shown both of these types of resilience optimization in the design of aerospace systems. For example, the resilience

optimization of a health management system in a power balance model of the Space Shuttle Main Engine involved the allocation of sensors needed to detect a hazard [16]--an instance of optimizing a design for resilience. Other work has focused on optimizing the resilience of in-flight aircraft fault accommodation (e.g. trim, throttle, and switch adjustments for various hazards) [17] -one of many instances (see: [18]–[20]) of optimizing the contingency management for resilience. These approaches complement each other, since contingency management must have some inherent flexibility afforded to it from the design features to operate effectively and resilient design features must likewise be leveraged effectively by contingency management to effectively mitigate hazards. Designing resilience into a system thus can and should involve optimizing both its high-level design and operational features and its contingency management.

However, while there have been design studies which optimize the either design or contingency management individually, there has been much less research dedicated to optimizing both in an integrated framework. This joint optimization of design and resilience policy is somewhat analogous to the co-design problem. In co-design, one simultaneously optimizes the plant (or architecture) of the system and its control system [21]. There are two main formulations which can be used in co-design: a bi-level architecture (called a nested strategy) and a single-stage architecture (called a simultaneous strategy). In the bi-level architecture, the lower-level control optimization is performed at each iteration of the upper-level plant or architecture optimization. In the all-in-one architecture, on the other hand, both the plant design and control policy are optimized at the same time in a single problem [21]. Neither approach is universally preferred; the best strategy depends on considerations such as the computational time of inner and outer loops and the computational complexity of the problem [Sec. 3.3.3, [21]]. In the emerging area of reliability-based co-design, one optimizes the design and performance of a system while maintaining a desirable reliability for the system (i.e. keeping the probability of certain limiting states below specified constraint thresholds [22]. While this reliability-based co-design problem is similar to resilience-based design in intention--minimizing the cost of the system and ensuring it mitigates

hazards--the formulation is different because of the consideration of hazards: in reliability based design, risk is dealt with as a constraint on the system failure probability, while in resilience-based design risk is represented as a cost used in the objective.

### *2.1.1. Research motivation*

Previous approaches in resilience optimization, on the other hand, have used three architectures to structure the optimization problem: a sequential approach, a bi-level approach, and an all-in-one approach. In the sequential approach, the upper-level optimization allocates resilience lower-level control sub-problems based on a high-level model of design risk [23], [24]. Thus, there is an underlying assumption that the upper and lower levels are not coupled--that no solution in the second stage will change the optimal decision made in the first stage. If this assumption does not hold, e.g., if the value of a sensor or redundancy depends on how it can be leveraged to reconfigure the system, then it could cause the optimization approach to output a sub-optimal solution. In a nested bi-level design architecture, a decision at the upper level provides a unique projection to the lower level design space. In this architecture, on the other hand, the lower-level optimizes resilience strategies as a single iteration of the top-level optimization [25], [22], leading to increased computational cost. In simultaneous approaches, both the design and control of the system are considered in one problem [26] -often by focusing on either the design or control of the system. Despite the presentation of various methods to solve individual design problems, little has been done to understand the performance and suitability of these methods for the general case of resilience optimization. To understand how optimization architectures can affect solution quality and computational performance, there is first a need to formalize the integrated (design, operational, and contingency management) optimization of resilience. This type of problem is shown in fig. 2.1, which shows the variables, models, cost functions, and interactions between each optimization sub-problem. Considering a problem like this is challenging, because one must jointly structure the problems in such a way that the interactions between design, operational, and resilience models are

modelled and taken into account effectively with the need of an appropriate design architecture.

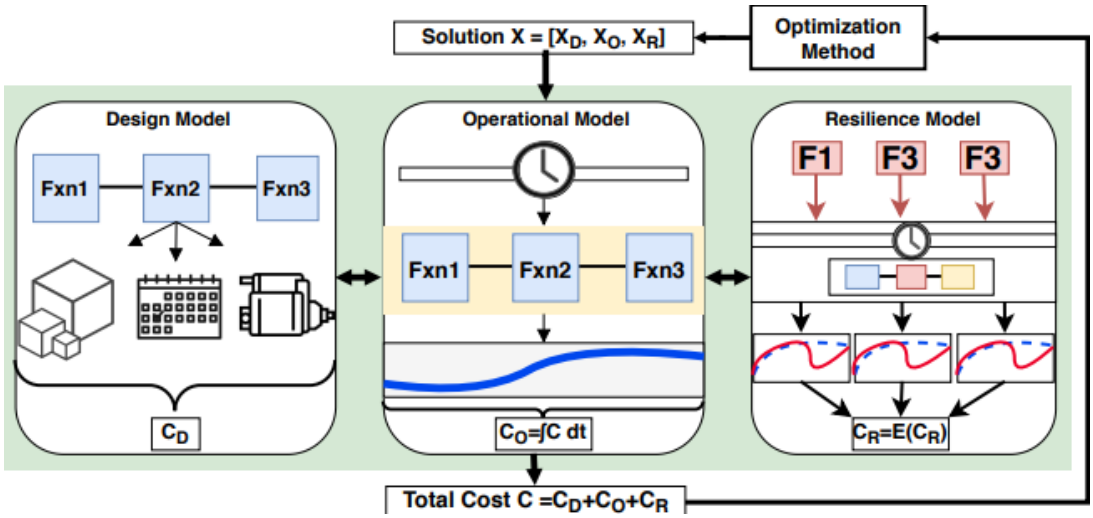


Fig.2.1. Integrated Resilience Optimization framework pursued in this work where design, operational, and resilience variables are jointly optimized.

### *2.1.2. Research contribution*

To meet this need, this chapter presents two main contributions:

- The formalization of the integrated resilience optimization problem shown in fig. 2.1 as a joint optimization of design, operational, and resilience variables in a value-based framework, and
- The elaboration and comparison of optimization architectures which may be applied to the integrated resilience optimization problem in terms of solution quality, computational cost and general usefulness.

To demonstrate this framework and compare architectures, this work considers the high-level optimization a multirotor drone's battery pack and rotor architecture, operational altitude, and battery and rotor fault-based flight reconfiguration. This model is composed of a high-level design cost model, a flight simulation operational model, and a resilience model where the flight simulation is injected with a number of faults. Using the integrated resilience optimization formulation, this model illustrates both the need to consider problem architecture when design and resilience models are

coupled and the computational cost needs in resilience optimization when the resilience model involves a large set of independent operational model simulations.

**The remaining sections elaborate upon these contributions. Section 2.2 presents prior research about structuring optimization problems and previous applications of mathematical optimization in the design of resilience. Section 2.3 then presents a drone resilience problem with formulation of design, operational and resilience costs. Section 2.4 formalizes the integrated resilience optimization problem with several optimization architectures like single-stage, sequential and nested bi-level. Section 2.5 then provides a trade-space analysis of the design space of the drone problem, and then a comparative study among different architectures in terms of effectiveness and computational cost. Finally, Section 2.6 summarizes the findings, identifies limitations with the methods, and offers potential directions for future work.**

## 2.2. Background

Prior work has studied the use different optimization architectures and presented different frameworks for resilience optimization. This section discusses this work and how it relates to the contributions in this paper.

### *2.2.1. Optimization architectures*

The complexity inherent to optimizing large-scale and multi-disciplinary systems has led to the study of distributed optimization architectures in the field of multidisciplinary design optimization (MDO) [27]. Unfortunately, the development of a distributed optimization architecture that consistently converges across a wide range of problems is still an open problem, and distributed approaches often have increased computational cost compared to monolithic formulations [27]. However, while architectures can increase solution difficulty, the heterogeneous design spaces often approached in complex systems design make it necessary to break the problem into components for ease of solution [28]. Because aircraft design is a multidisciplinary design problem like this, with multiple models and coupled objectives, interest in the area has resulted in application tools for real problems [29]–[31] and frameworks for integrating MDO in design [32], [33].

*Bi-level optimization* architectures are often used in multidisciplinary design optimization for large scale complex systems when the optimal decision in one model depends on the optimal decision in another model. Bi-level optimization was first realized in the field of game theory by economist Heinrich Freiherr von Stackelberg in 1934 [34] that described this hierarchical problem, where one problem, the lower level-level problem, is embedded (nested) within another problem, called the upper-level problem, acting as a constraint. To solve the problem, each iteration of the optimization of the upper level corresponds to a full optimization of the lower-level problem at a specific set of values used in the upper level problem [35]. While these approaches are applicable to certain classes of problems such as competitive games where one wants to know the best strategy to defeat the opponent's best strategy [36], computational cost is an issue when they are used on traditional problems instead of a monolithic approach [35]. Nevertheless, Stackelberg games have been used to represent complex robust design problems where one wishes to design the system to be as robust as possible to adverse events, because these events are analogous to the lower-level "adversaries" in traditional Stackelberg games [37].

**A simple formulation of Bi-Level Optimization problem can be written as below:

$$\min_x F(x,y) \quad (\underline{\textit{Upper Level}})$$

s.t (*Upper Level Constraints*)

$$G_i(x,y) \leq 0 \; for \; i = \{1,2 \dots N\}$$

$$x \in X \text{ and } y \in S(x) \tag{2.1}$$

$$\min_y f(x,y) \; (\underline{\textit{Lower Level}})$$

s.t (*Lower Level Constraints*)

$$g_j(x,y) \leq 0 \; for \; j = \{1,2 \dots n\}$$

$$y \in Y \tag{2.2}$$

In this formulation, $x$ and $y$ are upper and lower level decision variables, respectively; $G_i$ and $g_j$ are the $i^{th}$ and $j^{th}$ inequality constraints in upper and lower level, respectively; $F(x,y)$ and $f(x,y)$ are upper and lower level objective functions,

respectively; and S(x) is the solution set of the lower level problem for the upper level candidate decision *x*.

Papers have been published attempting bi-level programming in various complex design problems. This approach has been extensively applied in the field of transportation and defense strategy. Labbe, Marcotte and Savard in 1998 proposed a bilevel model of taxation and its application in toll-setting problem in highways. In this bilevel model the leader wants to maximize revenue from taxation schemes, while the follower rationally reacts to those tax levels [38]. Chen and Subprasom [39] formulated a stochastic bilevel programming model for a Build-Operate-Transfer (BOT) road pricing problem under demand uncertainty. Braken and McGill [40] proposed a bilevel optimization model in defense applications which includes strategic force planning problems and two general purpose force planning problems. In recent years, this approach has been accepted and is being widely used in strategic bomber force structure, and allocation of tactical aircraft to missions. Roghanian et. al. [41] presented a bilevel multi-objective programming model in enterprise-wide supply chain planning problems considering uncertainties on market demand, production capacity and resource availability. Recently, Biswas et. al. [42] developed a bilevel flexible robust design on complex large scale multi-reservoir system under risk of future shortage of energy, which provides better optimal decision (higher revenue) than a standalone framework. Since bilevel optimization is computationally expensive, mathematical and dimension reduction approaches have also been taken in [42] to reduce the computational cost at minimal loss of information.**

*Two-stage Optimization* is an architecture used in mathematical optimization to consider uncertainty in decision-making [43]. Two-stage optimization was introduced by Dantzig [44] and Beale [45] as a way of solving linear programming problems with stochastic variables. In these formulations, the first stage optimizes the decisions available before the uncertain variable is known, while the second stage optimizes the decisions available after the uncertain variable is realized. However, since taking the uncertainty into account in the first stage requires taking into account the second-stage actions, a recourse function for the optimal second-stage response must be provided.

This recourse function is the optimal resilience cost given realized values of the uncertain variables, which can either be derived analytically and/or approximated using a discrete set of scenarios (stochastic programming problems of this type are usually formulated to be linear) [46], [47]. Thus, where a bi-level approach might find the optimal policy over a space of uncertainty (e.g. finding the best design and operational policy over the set), two-stage approaches find the best policy before and after uncertain variables have been realized. However, inherent to this framework is the idea that the second-stage variables can or will be optimized after the fact. For engineered systems, this may not necessarily be the case: while a PHM system might be able to identify a fault, it may not necessarily be able to optimize the response to the fault in real time, instead using a predetermined contingency management scheme for that particular fault. Thus, this work focuses on the optimization of that policy before the uncertainty is realized (where all variables are optimized together), rather than after (where two-stage approaches are applied).

Recent developments in the field of multidisciplinary design optimization have considered the unique situation of combined plant and control design [48]. Co-design is the special application of multidisciplinary design optimization to the simultaneous design of the plant (or design) of a system and its dynamic control policy or architecture which is used when control and design considerations are coupled. Co-design can be performed in a nested (bi-level) or simultaneous (all-at-once) architecture [49], and has been used in a number of applications for combined plant, control system, and architecture optimization [21]. For example, co-design has previously been applied in aircraft design to the aerodynamics and control of tail-fin controlled supersonic missiles, where the choice of optimal tail planform is coupled with the choice of optimal tail control profile [50]. This situation is similar to the resilience optimization problem--except that in the resilience optimization problem the control of the system must be optimal not only over the nominal scenario, but over the set of fault scenarios.

### *2.2.2. Design and optimization of resilience*

There are a number of competing definitions for resilience in the literature, including resistance, absorption, restoration, and recovery [15]. The definition used in this is the

common engineering definition: the ability of the system to prevent and recover from hazards [51] with a focus on system recoverability [52]. While one could improve resilience at all costs, there are often design trade-offs to incorporating resilience, since design features (e.g., safety margin, redundancy) can also affect performance. To enable the trading of resilience with performance and other considerations, many design frameworks have been put forward which quantify the value of resilience in the overall cost function used to assess the merit of designs [53], [54], [26] (though other approaches exist, see [55]–[57]). One major advantage of value-of-resilience design frameworks is that they provide an objective which can be used by an optimization method to find the most resilient set of parameters for a system and can incorporate the designer's valuation of uncertainty [24]. Thus, many optimization frameworks and applications use an overall life-cycle cost function as the overall objective, which incorporates both the cost of resilience and the cost of performance and design considerations [58]–[62].

In resilience-based design, there have been some previous efforts to optimize the contingency management policy of a system together with its physical design and operations. Mehr et. al. [63] proposed the unified optimization of a mission's prognostic and health management, asset design, and asset management as three disciplines in a multi-objective multi-disciplinary optimization of mission price, vehicle weight, and launch availability. Since then, major works in resilience-based design have theorized the general early-stage resilience allocation problem as a sequential problem of first allocating resilience to subsystems and then optimizing the reliability and health management of those systems to achieve the required resilience [23], [54]. Additionally, in a prognostics and health management application, Niu and Jiang used a sequential approach, first optimizing the “local” usage profile of a braking system to reduce maintenance and then optimizing the “global” maintenance policy for the brake to minimize the maintenance cost-per-braking-distance, finding that optimizing both resulted in less overall cost than only optimizing one or the other [64].

Finally, there have also been examples of bilevel and two-stage (a related architecture, see Section 2.2.1 architectures for use in resilience optimization. Two-

stage approaches are often used in the resilient design of infrastructure networks [65]–[67], though have recently been introduced in a general systems design context [24]. Similar to the bi-level approach, the two-stage approach optimizes the system to prepare for adverse events in the first stage (upper level) and optimizes the system to mitigate and recover from adverse events in the second stage (lower level). The difference between the two-stage approach and the integrated resilience optimization formulation pursued in this work is that a two-stage formulation assumes that one can optimize the second-stage variables after the hazard has occurred, rather than relying on a predetermined policy (as is done in this work). More recently, Zhang et al. have used a bi-level optimization approach to determine the optimal construction and capacities of service centers that maximizes resilience in the case of service center disruptions [68]. One goal of this work is to compare the merit of bi-level approaches like this (e.g.[68]) with the sequential approaches previously (i.e. [23], [54]) presented for the general design of resilience.

## 2.3. Early Resilience Design Problem

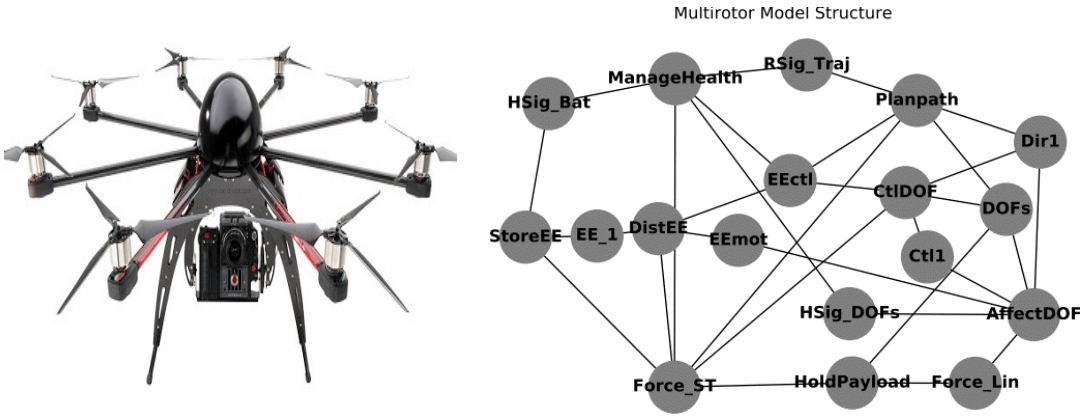


Fig. 2.2. (Left) Multi-rotor (Octa-copter) drone (from google); (Right) Functions and Flows of Multi-rotor Model Represented as an Undirected Graph. The Battery (StoreEE) powers the system while the rotor lines (AffectDOF) use the system control commands (Ctl1 and Dir1) to change the position of the aircraft (DOFs).

To demonstrate the utility of the architectures in the design of resilience, this work considers a multirotor drone case study representative of a typical early resilience-

based design scenario. This model has been implemented in the `fmdtools` software package [69] and is publicly-available in the examples repository [70]. The structure of the multirotor model is shown in fig. 2.2. This case study focuses on the design of the rotor line architecture (AffectDOF), battery pack architecture (StoreEE), flight planning (Planpath), and recovery (ManageHealth) functions. The objective is to design a resilient architecture, operational profile, and resilience policy which will minimize the cost of failures while minimizing total operational and design cost.

The design of the battery and line architectures is motivated by minimizing design cost, minimizing weight (to increase operational performance), and enabling reconfiguration in case of the individual battery and rotor failures in to increase resilience. To achieve this in the battery, four structures are considered--monolithic, parallel, series, or series-parallel. When a battery fault occurs, a parallel architecture enables a reconfiguration which keeps the same voltage at a lower maximum current draw while a series architecture enables a reconfiguration which can keep the same current draw at a lower voltage. Series-parallel enables both types of reconfiguration at the expense of increased weight and cost. Three line architectures are also considered--a quad-copter configuration with four rotors, a hexa-copter configuration with six rotors, and an octo-copter configuration with eight rotors. While these line architectures increase resilience by enabling the system to remain stable in the case of individual line faults, they also increase weight and design cost (which can also harm resilience). The resulting design cost of the system is:

$$C_D = c_b(x_b) + c_l(x_l) \quad 2.3$$

where the cost functions $c_b$ and $c_l$, as well as the total design $C_D$ are for each value of design variables: the battery pack architecture $x_b$ and line architecture $x_l$ respectively. The design costs are provided in Table 2.1.

| Battery | $C_D(\$)$ | Line/Rotor | $C_D(\$)$ |
|---|---|---|---|
| Monolithic | 0 | Quad-copter | 0 |
| Series-split | 300 | Hexa-copter | 1000 |
| Parallel-split | 300 | Octa-copter | 2000 |
| Split-both | 600 | | |

Table 2.1. Design costs for the battery and line architectures of multi-rotor drone**

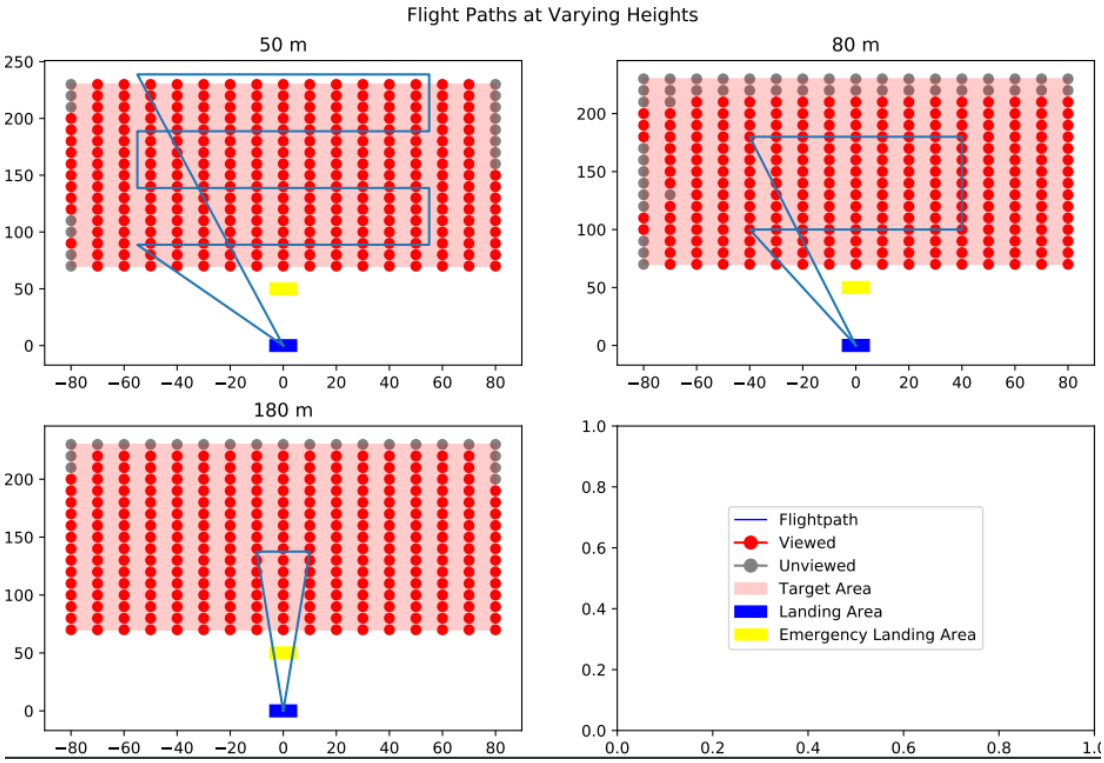


Fig. 2.3. Flight Plans of Multirotor at Different Operational Altitudes. A higher operational altitude leads to a shorter flight but results in lower-quality imagery.

The purpose of this drone is to surveil a given area. To perform this task, it must fly over the area at a specific operational altitude and sense (e.g., photograph) the area below it at that altitude. As shown in fig. 2.3, different operational altitudes lead to different flight-plans which cause the drone to fly for a longer or shorter amount of time. When the drone flies lower, it must fly for longer, but it also senses more information, yielding higher operational revenue. This relationship is quadratic and related to the number of points viewed, according to the operational cost function:

$$C_O = -n \sum_{p \in A} 0.5 + \frac{2}{e_{h,p}^2(x_h, x_b, x_l)} \qquad 2.4$$

where $C_O$ is the operational cost, $n$ is the number of flights, $p$ is an individual viewed grid point in the set of viewed gridpoints shown in fig. 3, the operational variable $x_h$ is the input flight altitude, and the resulting altitude at each point in the simulation is $e_{h,p}$. **It is to be noted that by providing the minus (-) sign in eqn. 2.4, the operational revenue is transformed to cost and thereby we transform our objective from the

maximization of operational revenue to minimization of operational cost**. In addition to costs, the design of the operations is subject to constraints:

- It must return to the starting location with at least 20% charge.
- It must return with no faults present.
- It must stay within a feasible range of operational altitudes over the flight simulation.

Finally, to mitigate failures in the drone, it may be helpful to have different recovery strategies for specific detectable faults. In the multirotor case, two sets of faults are considered: faults in the rotor lines and faults in the battery. When these faults are detected, the drone has a number of options for flight recovery: continuing the mission, returning to base, flying to the closest safe landing point, or landing immediately (options 0,1,2,3 in the model). The resilience costs of the system depend on the performance of resilience policy, flight-plan, and design architectures over the given set of fault scenarios:

$$C_R = \sum_{s \in S} n r_s c_s(x_{bp}, x_{lp}, x_h, x_b, x_l) \quad 2.5$$

where $C_R$ is the overall resilience cost, $s$ is a scenario in the set of fault scenarios $S$, $n$ is the number of flights, $r_s$ is the per-flight scenario rate, $c_s$ is the cost of a scenario, and the resilience variables are $x_{bp}$, the battery reconfiguration policy, and $x_{lp}$, the line reconfiguration policy. The cost of each scenario comes from the flight, landing or crashing, and repair costs of each modelled simulation, as shown below.

$$c_s = c_f + c_l + c_r \quad 2.6$$

The flight costs $c_f$ come from the safety cost of flying with a fault, amount of time flying with a fault, and the viewed operational value of the mission. The landing costs $c_l$ come from the impact to safety from landing in the target area as well as the cost of landing in an area with property restrictions (which is anywhere but the landing areas). Finally, $c_r$ is the repair cost which is the minimum between the replacement and the repaired costs of the system.

## 2.4. Design Architectures for Early Resilience System Optimization**

In this section, we have presented three different optimization frameworks which are commonly applied in a design problem. The optimization frameworks are *Bi-level optimization*, *Sequential optimization* and *single stage optimization*. Considering the example problem of resilient design of a multirotor drone, our objective is to investigate these optimization frameworks in order to provide the optimal resilient design which gives the best trade-off between design, operation and failure cost.

### *2.4.1. Bi-level design architecture for the multi-rotor drone resilience design*

Figure 2.4 shows the bi-level framework for the complex system design, considering an example problem of the multirotor drone problem. The upper level is focused on the system design in a nominal environment whereas the lower level is focused on the resilience policy design in a fault-injected environment. In this framework (fig. 2.4), the lower level problem optimizes for each iteration of the upper level problem. Thus, following the multirotor problem, below is the formulation of the upper and lower level optimization problem.

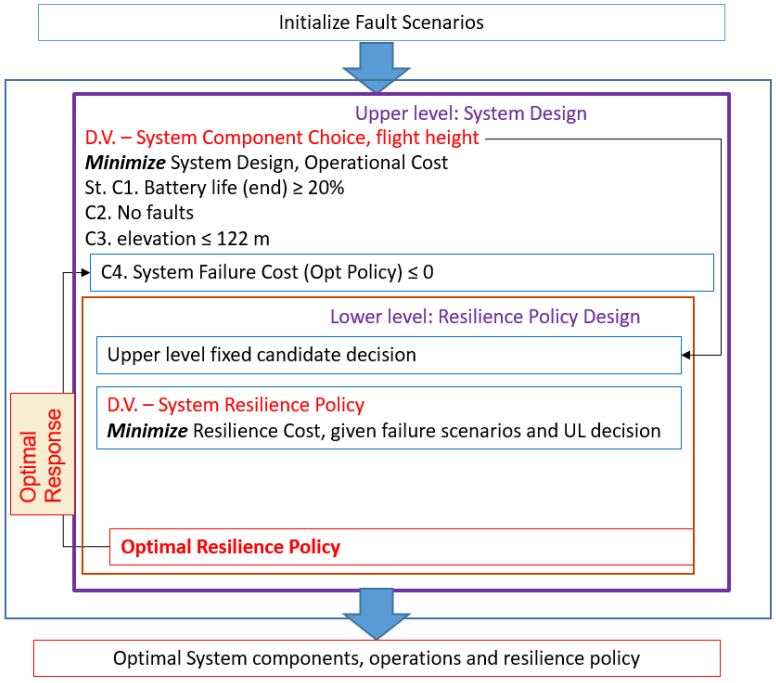


Fig. 2.4. Bi-level design architecture of the early drone resilient design problem**

#### *2.4.1.1. Upper level*

The upper level decision variable, objective function and constraints are stated as follows

*Decision Variable:*

The upper level decision variables are battery $x_b$, line architectures $x_l$ and the operational height $x_h$.

*Objective Function*:

We minimize the total Design and Operational Cost, considering two exterior penalties for both independent upper level and lower level decision dependent constraints violation:

$$\min_{x_b, x_l, x_h} \; C_D + C_O + \mathcal{P}_1 + \mathcal{P}_2 \tag{2.7}$$

$$\mathcal{P}_1 = \max(0, G_1)^2 + \mathcal{M}_2 G_2 + G_3^2 \tag{2.8}$$

$$\mathcal{P}_2 = \mathcal{M}_r \max(0, g_4) \tag{2.9}$$

where $C_D$ and $C_O$ are the normalized design and operational costs; $\mathcal{P}_1$ and $\mathcal{P}_2$ are the upper and lower level penalty functions; $G_1$, $G_2$ and $G_3$ are the upper level constraints dependent to only upper level decision variables; $\mathcal{M}_2$ is a very large penalty value for $G_2$ violation; $\mathcal{M}_r$ is a penalty value for constraint $g_4$, which depends on both upper and lower level decision variables.

*Constraint Functions*:

The constraint functions are as follows:

- Battery Life percent at the end of flight:

$$g_1 = 20 - I_e \tag{2.10}$$

- Fault checking at the end of flight:

$$g_2 = \begin{cases} 1 \; if \; \mathcal{F}_{end} \; exists \\ 0 \qquad\quad else \end{cases} \tag{2.11}$$

- Maximum flight elevation at each timesteps:

$$g_3 = \sum_{p \in A} \max(0, e_{h,p} - 122) \tag{2.12}$$

- Failure Cost (need to run lower level problem):

$$g_4 = C_{R,opt,k} \tag{2.13}$$

where $C_{R,opt,k}$ is the optimal resilience cost at iteration $k$ of the upper level. To find the value of $C_{R,opt,k}$, below lower level problem is optimized iteratively.

*2.4.1.2. Lower level*

The lower level problem in this drone example is an unconstrained problem. However, it is noted that any constraints related to the resilience policy design can be incorporated. The upper level inputs and lower level decision variables and objective function are stated as follows:

*Input Variables*:

For iteration $k$ of the upper level optimization problem, the input candidate decisions are battery $x_b$, line architectures $x_l$ and the operational height $x_h$

*Decision Variable*:

The lower level decision variables are the resilience policy for battery $x_{bp}$ and line architectures $x_{lp}$.

*Objective Function*:

We minimize the total resilience cost, given the fault scenarios.

$$\min_{x_{bp},\, x_{lp}} \; C_R(x_{bp}, x_{lp}, x_h, x_b, x_l) \qquad 2.14$$

where $C_R$ is the resilience costs which is the function of both upper and lower level decisions.

*Final Output*:

The optimal solutions after meeting the user specified convergence criteria of both upper and lower levels are optimal battery $x_{b,opt}$, line architectures $x_{l,opt}$, operational height $x_{h,opt}$, resilience policy for battery $x_{bp,opt}$ and line architectures $x_{lp,opt}$; design cost $C_{D,opt}$, operational cost $C_{O,opt}$ and resilience costs $C_{R,opt}$ at optimal decisions.

In order to lower the computational cost, we have modified the architecture where the lower level problem is only executed if the current upper level decision is feasible, i.e, no violation of constraints 2.10 - 2.12. This eliminates any redundant lower level optimization as any optimal solution of the lower level is optimal to the infeasible projected upper level design space, thus the lower level solution is also infeasible. Thus, instead of lower level execution and thereby to increase the computational efficiency of the bi-level design, a very large value of $\mathcal{P}_2$ is inputted in the penalized objective function 2.7.

### *2.4.2. Sequential design architecture for the multi-rotor drone resilience design*

Figure 2.5 shows the sequential framework for the complex system design, considering an example problem of multirotor drone problem. The stage 1 is focused on the system design in the nominal environment whereas the stage 2 is focused on the resilience policy design in the fault injected environment. In this framework (fig. 2.5), the two stages optimize sequentially where the Stage 1 problem runs first, and then the optimal solution of stage 1 is passed as the input parameters into the stage 2 optimization. Below, we provided the changes in the formulation from the bi-level design.

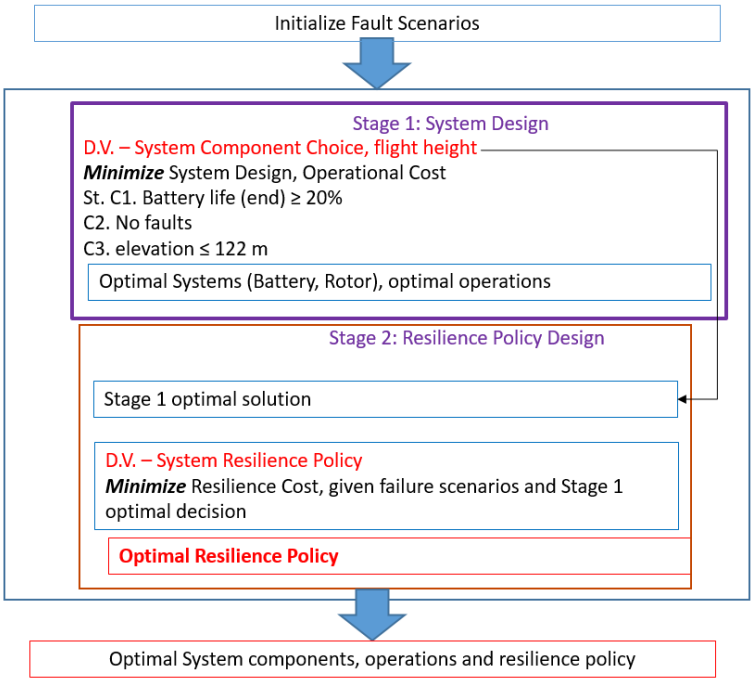


Fig. 2.5. Sequential design architecture of the early drone resilient design problem**

The stage 1 optimization problem is mostly similar to the upper level problem in bi-level design with decision variables as battery $x_b$, line architectures $x_l$ and the operational height $x_h$; and the objective function to minimize the total Design and Operational cost, considering exterior penalty (refer eqn. 2.8) for violation of constraints equations (2.10 – 2.12). Thus, in the sequential framework as the stage 1 runs independently to stage 2, we omit the last term $\mathcal{P}_2$ of equation (2.7). Likewise, we do not have the constraint equation (2.13). After the convergence criteria is met, we get

the stage 1 optimal solution as optimal battery $x_{b,opt}$, line architectures $x_{l,opt}$, operational height $x_{h,opt}$; design cost $C_{D,opt}$, operational cost $C_{O,opt}$ at optimal decisions.

The stage 2 problem mostly resembles the lower level problem in the bi-level design, however, runs for single time after considering the stage 1 optimal solutions as the input parameters. Thus, the decision variables in stage 2 are the resilience policy for battery $x_{bp}$ and line architectures $x_{lp}$ with minimizing total resilience cost, given the fault scenarios. Thus, the equation 2.14 is modified to 2.15:

$$\min_{x_{bp},\, x_{lp}} C_R(x_{bp}, x_{lp}, x_{h,opt}, x_{b,opt}, x_{l,opt}) \quad 2.15$$

Finally, the stage 2 problem converges to provide optimal resilience policy for battery $x_{bp,opt}$ and line architectures $x_{lp,opt}$; resilience cost $C_{R,opt}$ at optimal decisions.

### *2.4.3. Single-Stage design architecture for the multi-rotor drone resilience design*

Figure 2.6 shows the all-in-one framework for the complex system design, considering an example problem of multirotor drone problem. Here, both the upper and lower levels of the bi-level design have been compacted into a single framework. Thus, all the decision variables such as battery $x_b$, line architectures $x_l$, the operational height $x_h$, resilience policy for battery $x_{bp}$ and line architectures $x_{lp}$ have been considered together. Likewise, we consider a multi-objective framework where we together minimize the objective 1: *total design and operational cost* and objective 2: *resilience cost*. We formulated the weighted Tchebycheff multi-objective function [71]–[73] as below:

$$\min_{x_b, x_l, x_h, x_{bp}, x_{lp}} \max_{i \in N} \{w_i |Y_i - u_i|\} + \mathcal{P}_1 \quad 2.14$$

$$Y_1 = C_D + C_O \quad 2.15$$

$$Y_2 = C_R \quad 2.16$$

where $\mathcal{P}_1$ is the penalty factor (refer eqn. 2.8) for violation of constraints equations (2.10 – 2.12); $Y_i$ is the $i^{th}$ objective with $w_i$and $u_i$ are the weight preferences and the utopia values of the $i^{th}$ objective respectively; $N = 2$ is the number of objectives in this problem. The utopia values are the optimal solution when the respective objective is

optimized individually. The final output will be the optimal solutions as mentioned in both bi-level and sequential design frameworks.

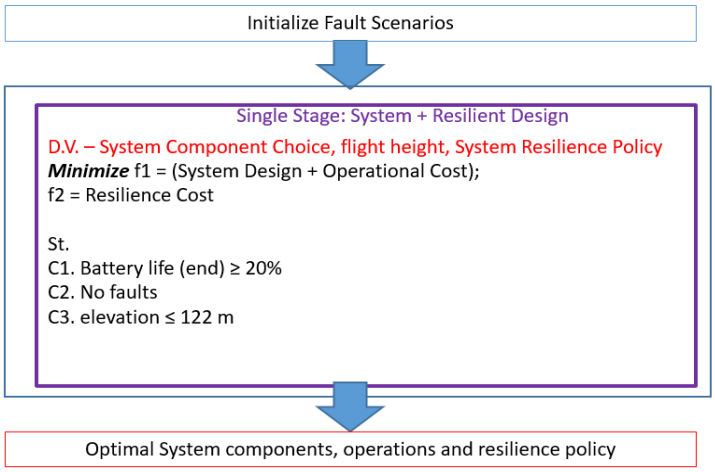


Fig. 2.6. Single-stage design architecture of the early drone resilient design problem**

### *2.4.4. Optimization algorithm and convergence criteria*

So far we have discussed how for each design architectures, different cost models like design, operational and resilience costs are coupled together with the common goal of optimizing towards a trade-off among the costs. Now, to solve this problem, we have considered two methods of optimization techniques. As $x_b$, $x_l$, $x_{bp}$ and $x_{lp}$ are discrete design variables whereas $x_h$ is a continuous design variable, we started with an exhaustive "brute force" search [74] where we first discretize $x_h$ to $n$ number of finite design values. With this brute force algorithm, all the finite design combinations are evaluated and thus result in a global convergence. However, we find a sub-optimal solution due to the discretization in case if the true $x_{h,opt}$ does not include with the discretized grid points: thus $x_{h,opt} \neq \bar{x}_{h,opt}$ where $\bar{x}_{h,opt}$ is the optimal solution among the discretized grid points. Also, this sub-optimal $\bar{x}_{h,opt}$ can affect the optimality of the other discrete design variables. However, it is to be noted, the way we structured the bi-level design, the lower level has only discrete design variables and thus always guarantees a global lower level convergence in this drone resilience design. This eliminates a common issue of convergence in bi-level design when the lower level problem fails to convergence (or does not have a guarantee in convergence). Once the

brute search algorithm is converged, we can run another optimization technique with the earlier optimal results as the initial or starting design values. This way we can polish the earlier solutions and aim for a better optimal solution. Given the nature and the constraints (e.g. computational time) of the problem, we can consider either a direct, heuristic or gradient-based search (if only the function is differentiable); however, in this problem we selected a *downward simplex method* or *Nelder-Mead simplex algorithm*, which only uses function values, not first or second derivatives. The convergence criteria are design and objective function tolerance limits which is set to $10^{-4}$. Attempts have been made to enhance performance Nelder-Mead algorithm for high dimensional problems [75], [76] and alternative approaches can be considered in future research.

## 2.5. Results**

As discussed in the problem description in Section 2.3, the drone design problem can be run in different design scenarios which each have different failure costs because of the mission of the drone. In this chapter, we consider two extreme flight scenarios: rural and congested scenarios. The Python function used for the brute search optimization algorithm is *scipy.optimize.brute*, and to polish the solution with another Nelder-Mead algorithm, we put the function *optimizie.fmin* as one of the arguments in *scipy.optimize.brute.* The results are obtained from running on a machine with configuration of Windows 10, Intel Processor 3.4 GHz and 16 GB RAM.

### *2.5.1. Trade-Space Analysis*

Figures 2.7 and 2.8 are the trade-space analysis of the set of design variables and the objective functions for rural and congested scenarios. The battery and rotor/line architecture options are coded in numbers as in Table 1. The resilience policies for both battery and line architectures are coded as continuing the mission (0), returning to base (1), flying to the closest safe landing point (2), or landing immediately (3). In both the scenarios, the design cost is comparatively much lower than the other operational and failure costs, and thus will not have much individual influence on the optimal solutions. Thus, we add the design and operational costs as the total nominal cost (in nominal

situation) whereas the resilience cost is the failure cost (in faulty situation). In the rural scenario, the landing (i.e. crashing) cost of the multi-rotor drone is low due to low risk of life loss. The resilience cost in the rural scenario mostly involves the repair or replacement cost which is much lower in magnitude than the operational cost or the nominal cost (fig. 2.7). In the congested scenario, on the other hand, the resilience or failure costs overwhelm the nominal cost, as now the consequences are very high due to high risk of life loss (fig. 2.8).

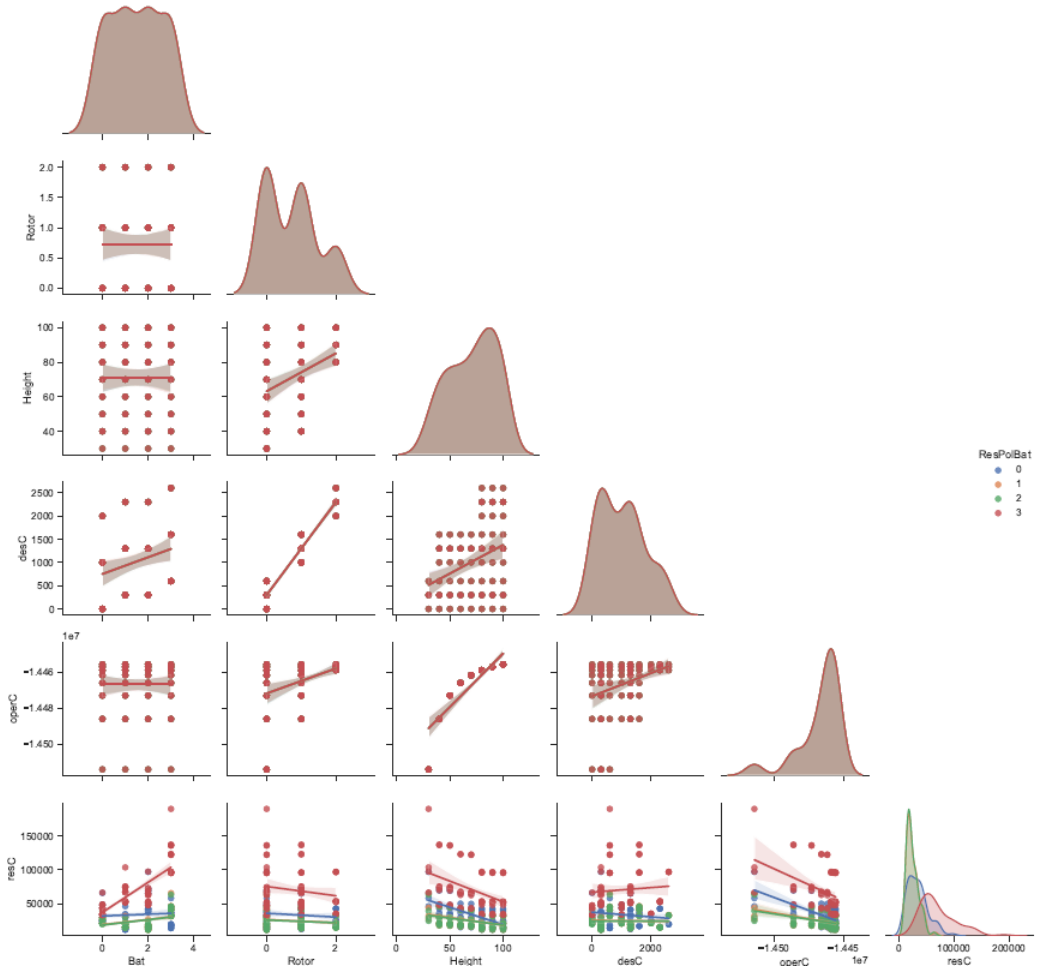


Fig. 2.7. Trade-space analysis of the early drone resilient design problem for rural flight scenario**

As shown in the trade-space analysis of both scenarios, while there is a clear dependency between variables in the design and operational models with positive association between design and operational costs, the resilience policy also has an

effect (negative association) on the operational costs. Additionally, the resilience policies for any faults on the drone systems (battery or rotor/line architectures) also have an interactive effect where the policy 1 (to base) and 2 (to closest safe landing point) have minimal mean and variability of the resilience cost. Due to this complex trade-off among the different cost models, the system architecture, operations and resilience policy should be considered together when exploring the design space in order to find the optimal trade-offs. These properties make it a difficult problem to optimize, since the optimal choices of design, operations, and resilience policies are coupled but take place in different models. After conducting this preliminary analysis over the design space, in the next section, we analyze the solutions from different optimization architectures.

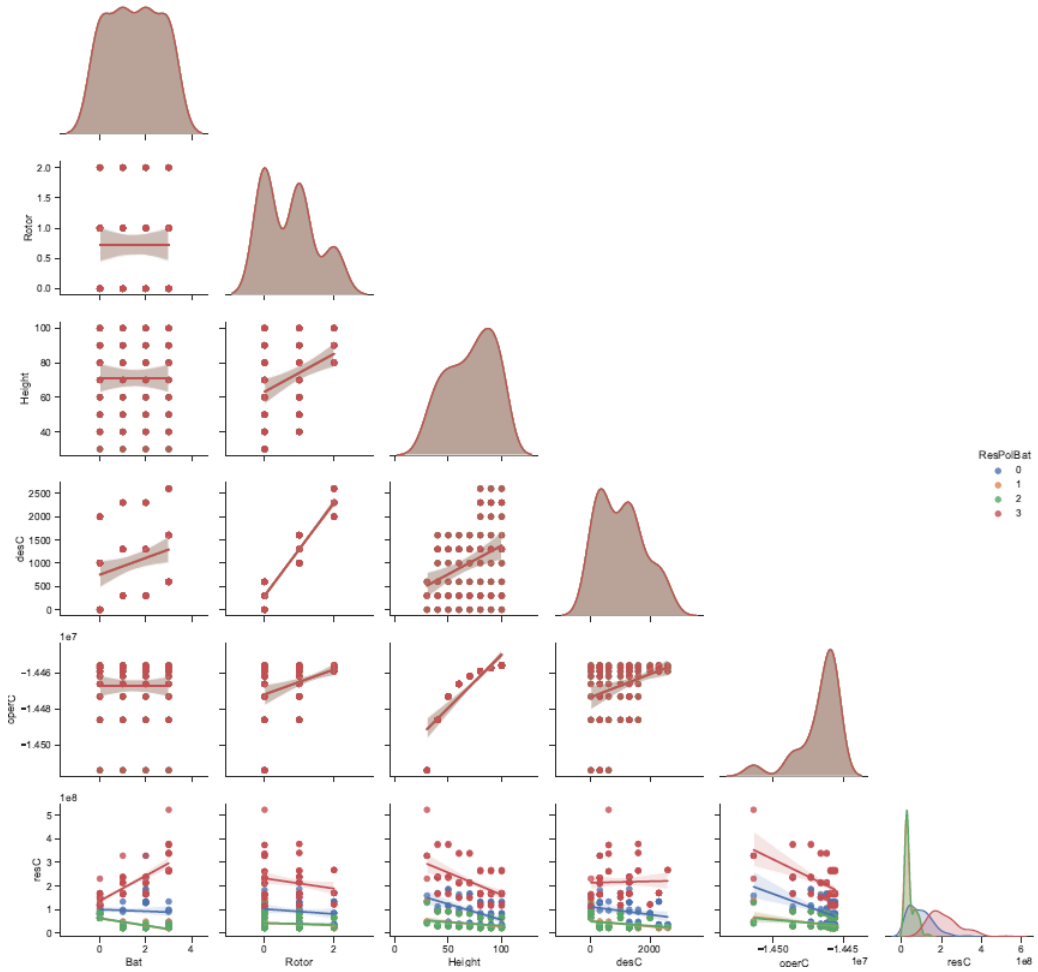


Fig. 2.8. Trade-space analysis of the early drone resilient design problem for congested flight scenario**

### *2.5.2. Comparison of the design architectures in early resilient design*

In this comparative study, the research interest is to look at the trade-off between the nominal cost (design + operational cost) and the resilience or failure cost as we want to obtain a low-risk design for both the scenarios. Considering both the rural (low-risk) or congested (high-risk) scenarios, we are interested in the magnitude we are increasing the design and operational cost to minimize failure costs, by optimizing with different design architectures to ultimately conclude the appropriate design architecture which has a better likelihood to balance the combined cost for two extreme scenarios. Table 2.2 and 2.3 are the optimal solutions and the respective design costs, operational revenue, resilience cost and the total revenue for single-stage, sequential and nested bi-level design architectures. As mentioned, the operational revenue is the negative of the operational cost, thus high values are better for operational revenue. The total revenue is defined as the difference between operational revenue and the sum of design and failure or resilience cost; thus higher total revenue is better. As we focused on preferring low-risk designs, in the single-stage architecture, we considered three values of weighting the resilience cost objective: $w_2 = 0.5, 0.7, 0.9$. Similarly, in the bi-level architecture, we considered three values of penalization $\mathcal{M}_r = 1, 10, 100$ which represents increasing preference on the objective of resilience cost. $\mathcal{M}_r = 1$ means equal preference between objective 1: nominal cost and objective 2: resilience or failure cost. Unlike these two design architectures, where the designers can control the preferences of the objectives, the sequential architecture does not consider this trade-off due to the independent nature of optimizing these two objectives. To avoid the optimization algorithm influencing only one objectives due to differences in objective magitudes, we normalize the cost values during the optimization. However, with the final solution transformed into the real values, we can see a clear picture of the trade-off of increasing the design and operational costs (decreasing operational revenue) in lowering the resilience cost at these two flight scenarios. The different single stage and bi-level architectures with varying preference of resilience objective are named in Table 2.2 and 2.3 as below:

| Architecture | $\boldsymbol{x_{opt}}$ | $C_D(\$)$ | $R_O(10^3\ \$)$ | $C_R(10^3\ \$)$ | Total Revenue $(R_O - C_D - C_R)$ $(10^3\ \$)$ | Time (0m : 0s) |
|---|---|---|---|---|---|---|
| Sequential | [0, 0, 23, 1, 2] | 0 | 14559.1 | 39.72 | 14519.4 | 0m : 39s |
| Single-stage A | [0, 0, 26, 0, 0] | 0 | 14535.4 | 66.15 | 14469.3 | 15m: 0s |
| Single-stage B | [0, 0, 29, 1, 0] | 0 | 14518.6 | 44.10 | 14474.5 | 15m: 0s |
| Single-stage C | [2, 0, 29, 1, 2] | 300 | 14518.6 | 24.82 | 14493.5 | 16m: 10s |
| Bi-level A | [0, 0, 23, 1, 2] | 0 | 14559.1 | 39.72 | 14519.4 | 35m: 55s |
| Bi-level B | [1, 0, 80, 0, 1] | 300 | 14459 | 10.25 | 14448.5 | 44m: 59s |
| Bi-level C | [1, 0, 98, 0, 1] | 300 | 14456 | 10.21 | 14445.5 | 42m: 43s |

Table 2.2. Comparison of the optimal solutions of multi-rotor drone problem from the design architectures at rural flight scenario**.

| Architecture | $\boldsymbol{x_{opt}}$ | $C_D(\$)$ | $R_O(10^3\ \$)$ | $C_R(10^3\ \$)$ | Total Revenue $(R_O - C_D - C_R)$ $(10^3\ \$)$ | Time (0m : 0s) |
|---|---|---|---|---|---|---|
| Sequential | [0, 0, 23, 1, 2] | 0 | 14559.1 | 128195 | -113636 | 0m : 44s |
| Single-stage A | [0, 0, 29, 0, 0] | 0 | 14518.6 | 230704 | -216185 | 15m : 4s |
| Single-stage B | [0, 0, 29, 2, 2] | 0 | 14518.6 | 128195 | -113676 | 16m :0s |
| Single-stage C | [1, 0, 27, 1, 0] | 300 | 14529.2 | 48797.7 | -34268.5 | 16m :0s |
| Bi-level A | [2, 0, 23, 1, 2] | 300 | 14559.1 | 39499.9 | -24941 | 41m :20s |
| Bi-level B | [2, 0, 23, 1, 2] | 300 | 14559.1 | 39499.9 | -24941 | 41m :59s |
| Bi-level C | [2, 0, 80, 1, 1] | 300 | 14559 | 21182.6 | -6624 | 49m :18s |

Table 2.3. Comparison of the optimal solutions of multi-rotor drone problem from the design architectures at congested flight scenario**.

Note: $\boldsymbol{x_{opt}} = [x_b, x_l, x_h, x_{bp}, x_{lp}]_{opt}$ and the $C_D$ is in dollars where the other cost columns are in 1K dollars; $R_O = -C_O$ is the operational revenue.

- Single-stage A: equal preference $w_1 = w_2 = 0.5$.
- Single-stage B: unequal preference $w_1 = 0.3, w_2 = 0.7$.
- Single-stage C: unequal preference $w_1 = 0.1, w_2 = 0.9$.
- Bi-level A: equal preference $\mathcal{M}_r = 1$.
- Bi-level B: unequal preference $\mathcal{M}_r = 10$.
- Bi-level C: unequal preference $\mathcal{M}_r = 100$.

As expected, we can clearly see the computational cost is highest for the bi-level architectures in both the flight scenarios. However, the cost values at the optimal solutions among these architectures at both flight scenarios differ among architectures. Starting with the rural scenario (table 2.2), the operation revenue is the highest for sequential and the bi-level A, but the lowest for the bi-level C. Interestingly, the resilience cost is the lowest for the bi-level C. This is because in the rural scenario the failure costs are much lower, and when we consider higher preference to minimize the failure cost, we add substantial redundancy to the design and add significant operational cost, thus lowering the operational revenue. Thus, we see the total revenue is the worst in bi-level C. But, as the bi-level architecture has the control to adjust the preference, we see the same architecture also attained the best total revenue as in bi-level A when equal preferences of objectives are considered, thus avoiding substantial redundancy in design. The single-stage architecture, however, provides excess resilience cost even at the equal preference of the objectives (single-stage A), and thus does not have the best total revenue. Similar to bi-level design, the total revenue decreases (adding redundancy) as we increase the preference of minimizing resilience costs. Thus, we see that when the failure cost is much lower in the early resilience system design (for e.g. no or minimal crashing cost), the sequential and the bi-level stage work best when avoiding excess redundant design in attaining a better (maximize) resiliency in design. However, this scenario can be only restricted for planned actions when failure cost is low. In a real scenario (e.g. full aircraft flight), the fault occurrence is unknown and therefore the flight scenario will be unknown during the fault (crashing in rural or congested areas), and ultimately the failure cost is likely unknown (low or high). This uncertainty of the magnitude of risk in the early resilience design, leads us to compare

the design architectures for the congested flight scenarios (table 2.3), when the resilience cost is much higher.

The operational revenue is the highest for the sequential and all the bi-level architectures; however, with a slight increase in design cost, the bi-level design architectures attain significant decreases in the resilience costs over the sequential architecture. Like the rural scenario, as we increase the preference to minimize risk, the resilience cost decreases. Now, due to having high failure cost in the congested flight scenario, adding the preference of resiliency in optimization does not add redundancy and we obtain a low-risk design in a high-risk scenario. Thus, the total revenue is best in the bi-level architectures. The negative total revenue in table 2.3 denotes the loss incurred; thus we are looking for the design solution with minimal loss. The negative total revenue or the loss for the optimal solution in sequential architecture is the second worst with almost five times higher loss than the bi-level A solution. Single-stage architectures re inefficient with all the highest costs and lowest revenue in single-stage A. Thus, we see that when the failure cost is much higher in the early resilience system design due to high risk to failure consequences, the bi-level stage works better than the other architectures in attaining a better resiliency in design without any significant increase of other costs due to excessive redundancy in the design.

## 2.6. Conclusion**

When optimizing the value of a system, resilience often must be traded with design and operational considerations to find the best solution. Because the design and operational profile usually affect the resilience of a system, it is necessary to optimize the design, operational, and resilience policy in an integrated approach. When structuring this optimization problem, it is prudent to choose an architecture which effectively finds the optimum design at a satisfactory computational cost. This chapter introduced the integrated resilience optimization formulation of the early resilience-based design problem and presented different optimization architectures to leverage this framework. These architectures were then compared on a drone design problem where one must choose an appropriate design architecture which minimizes design and operational

costs while maximizing the resilience (minimizing resilience cost) of the contingency management of the drone over a set of fault scenarios. The result in this problem shows a trade-off of any redundant costs in achieving higher resiliency, depending on the flight scenarios. Two extreme scenarios have been considered in this chapter—1. Rural scenario (low-risk) where the failure cost is negligible and 2. Congested scenario (high-risk) where the failure cost is very high. It has been found, for a low-risk scenario, as the design redundancy cost is much higher comparing to design resilience cost, the preference over minimizing the failure cost increases significantly the operation costs. Here the bi-level architecture attains one of the best, only when we avoid any preferences on the high resilient or low risk design. On the other hand, for a high-risk scenario, as the design redundant cost is much lower comparing to design resilient cost, the preference over minimizing the failure cost has negligible adverse effect on the operation costs. Here, the bi-level architecture outperformed the others, with or without any preference on the design resiliency in the optimization. Thus, as overall, the bi-level design architectures did the best performance irrespective of two extreme scenarios to attain the best solutions. This results shows the general potential of the bi-level architecture in the domain of early resilience complex engineered system design to attain the efficient design solutions in terms of redundancy and resiliency at any risk-level scenarios, with proper tuning of preference level of resiliency. However, as a limitation, the convergence and computational issue still need future investigation for extending to any large scale early resilient design problem, while having mixture of discrete and continuous design variables in both upper and lower level. The ultimate choice of architecture depends on the nature of the problem considered, including the computational cost at each level, the interacting design constraints, and the size, scope, and form of the problem.

**Acknowledgment**

This research was funded in part by NASA Grant 80NSSC18M0106. The opinions, findings, conclusions, and recommendations expressed are those of the authors and do not necessarily reflect the views of the sponsor.

# CHAPTER 3

## An Approach to Bayesian Optimization for Design Feasibility Check on Discontinuous Black-Box Functions

**Authors:**

**Arpan Biswas**
Department of Mechanical Engineering
Oregon State University
Corvallis, Oregon 97331
biswasar@oregonstate.edu

**Christopher Hoyle**
Department of Mechanical Engineering
Oregon State University
Corvallis, Oregon 97331
chris.hoyle@oregonstate.edu

Chapter 3 manuscript is issued in below conference and journal:

**Proceedings of the ASME 2020 International Design Engineering Technical Conferences & Computers and Information in Engineering Conference**
**IDETC/CIE 2020**
**August 17-19, 2020**
**Status: Published**

**Journal of Mechanical Design, ASME**
**Paper No. MD-20-1404**
**Status: Accepted with Revision**

**ABSTRACT**

*The chapter presents a novel approach to applying Bayesian Optimization (BO) in predicting an unknown constraint boundary, also representing the discontinuity of an unknown function, for a feasibility check on the design space, thereby representing a classification tool to discern between a feasible and infeasible region. Bayesian optimization is a low-cost black-box global optimization tool in the Sequential Design Methods where we learn and update our knowledge from prior evaluated designs, and proceed to the selection of new designs for future evaluation. However, BO is mostly suited to problems with the assumption of a continuous objective function, and does not guarantee true convergence when having discontinuous design space. This is because of the insufficient knowledge of the BO about the nature of the discontinuity of the unknown true function. Therefore, in this chapter, we have proposed to predict the location of the discontinuity using a BO algorithm on the artificially projected continuous design space from the original discontinuous design space. The proposed approach has been implemented in a thin tube design with the risk of creep-fatigue failure under constant loading of temperature and pressure. The stated risk depends on the location of the designs in terms of safe and unsafe regions, where the discontinuities lie at the transitions between those regions; therefore, the discontinuity has also been treated as an unknown creep-fatigue failure constraint. The proposed BO algorithm has been trained to maximize sampling towards the unknown transition region, finally to act as a high accuracy classifier between safe and unsafe designs with minimal training cost. The converged solution has been validated for different design parameters with classification error rate and function evaluations at an average of <1% and ~150, respectively. Finally, the performance of our proposed approach in terms of training cost and classification accuracy of thin tube design is also shown to be better than the existing ML algorithms like SVM, Random Forest and Boosting.*

## 3.1. Introduction

In the early design phase, it is very important for the designers to be able to identify the feasible regions in a large design space while the design cost is low. This knowledge

guides can help guide the designers to eliminate inferior designs and avoid investing in the high cost manufacturing and testing of those designs at the later design phase. With efficient knowledge of the feasible space, the designers can also avoid falsely selecting infeasible designs as optimal which can result in high risk to failure consequences. In design practice, most of the design problems are too complex to be handled by simple optimization frameworks due to having constraints on cost, time, formulation, etc. Also, approximating a complex design problem into much simpler problems can lead to the negligence of the original complex constraints; thus the design may violate those constraints and not provide a useful choice for practical decisions. Some practical design problems have been investigated where complex optimization frameworks have been modeled [1], [2], [77]. However, in many design problems, it is difficult to numerically formulate an objective function or constraint boundaries and therefore we consider those as black-box problems with high function evaluation cost due to limited resources [78], [79]. Thus, a trade-off between learning and expense is present, and a low fidelity surrogate model is often implemented to reduce cost. When we have no/limited knowledge on the expensive true unknown functions, we cannot guarantee the maximization of our learning towards optimizing the functions without proper guidance or expertise. Also, due to the mentioned high function evaluation cost, exhaustive search is not a valid option. In such problems, a Bayesian Optimization technique (BO), which eliminates the need of standard formulation of the black-box functions, is widely applied in sequential learning and provides better guidance in sampling the designs for expensive experiments or function evaluations in order to find the optimal region of that unknown function at minimal cost of experiments. In the BO approach, we first build a posterior surrogate model, given the data from the current evaluations. We then use this model to strategically select the best design locations for future evaluations by maximizing the Acquisition functions, defined from the posterior model. BO can be used in optimizing any black-box functions in a design problem, either to emulate the unknown objective functions when the goal is to locate the optimal solutions, or to emulate the unknown constraints when the goal is the classification and preservation of only potential good designs [80]. This chapter is focused on BO

framework to emulate the unknown constraint boundary as a classification problem for design feasibility check. However, the motivation behind this classification problem comes from the ultimate goal of design optimization under the complex design space which has been described in the next section.

### *3.1.1. Research motivation*

Although BO is a powerful method, it works on the assumption that the true function is continuous [7] and generally fails to converge to the solution if the objective function has a discontinuity. This is because of insufficient knowledge of the BO about the nature of the discontinuity of the unknown true function. Figures 3.1- 3.2 provide an example where a BO model fails to converge to the true discontinuous function even after excessive sampling. Figure 3.1 shows the true response function in terms of design variables $x_1, x_2$where there is jump discontinuity at $x_1, x_2 = 1$. Figure 3.2 shows how inefficiently the BO model emulated the true function even after 500 sampling for function evaluations, denoted by black dots, and produces a very non-smooth surface with many peaks near the discontinuity. Now, with this limitation of BO for the discontinuous design space, we will next talk about a research example problem to highlight our motivation behind the design feasibility check classification problem.

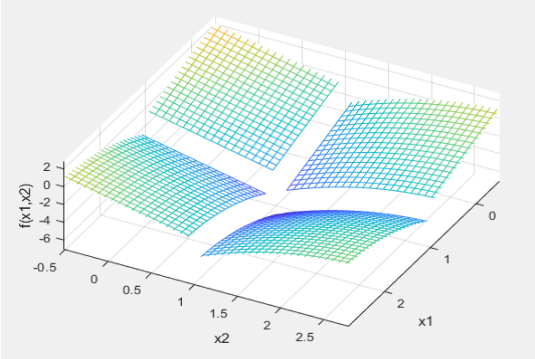


Fig 3.1. True discontinuous response function

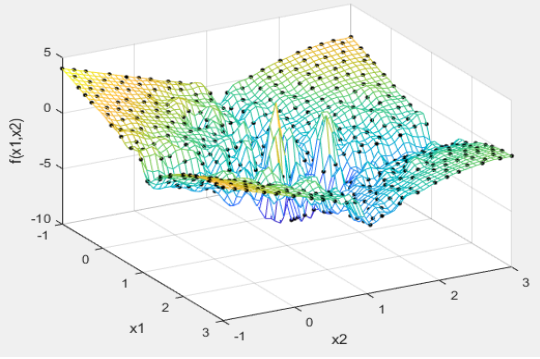


Fig 3.2. Discontinuous Response function from BO model after 500 function evaluations at design location denoted by black dots.

#### *3.1.1.1. Compact heat exchanger design example*

In this chapter, we consider the design of a diffusion bonded Compact Heat Exchanger (CHX) as a motivating example. In the design of a diffusion bonded CHX, the ultimate

goal is to find the optimal design geometries which minimizes the risk of creep-fatigue failure under constant loading of temperature and pressure. The stated risk depends on the location of the design in regions such as Elastic, Shakedown, Plastic or Ratchetting. A similar example has been provided for thin tubes where the location of the designs can be numerically represented from a Bree Diagram [81] (Figure in Appendix A.3.1) in terms of pressure and thermal stresses. Under cyclic loading, the *Elastic* and *Shakedown* region in the Bree diagram are considered as the *safe* region where no strain accumulation occurs or the growth of residual strain is practically diminishing when sufficient loading cycles are applied. However, *Plastic* and *Ratchetting* in the Bree diagram are *unsafe* designs where the plastic strain accumulates until failure. When the complexity of the design increases like in diffusion bonded CHX [82] (Figure in Appendix A.3.2), we cannot provide a numerical representation of the function which defines the location of designs; thus it can be considered as black-box problem. However, the transition between Shakedown and Plastic or Ratchetting creates a jump discontinuity at the transition line due to different formulation in strain analysis in each region. This is the limitation of the application of BO as we have demonstrated earlier in section 3.1.1, and thus the convergence of the model to find the optimal solution cannot be trusted when the design space has discontinuity, as it has high likelihood to lead to non-optimal solutions. Also, since we have no knowledge of the true function, it is evident that we have no knowledge on the location of discontinuous transition region as well, representing the black-box unknown constraint boundary between the safe and unsafe region. Thus, ignoring the constraint boundary can lead to preserving infeasible solutions, which can lead to very high design failure costs, such as accidents, economic disasters etc. This motivates us to believe that it is necessary first to understand the discontinuity of the unknown function, build the constraint boundary to classify between safe and unsafe design in terms of creep-fatigue failure as a design pre-stage before attempting to find the optimal design.

### *3.1.2. Research contribution*

To address the issues of sections 3.1.1 and 3.1.1.1, this chapter proposes an approach to Bayesian Optimization in solving the stated classification problem, to predict the

location of the discontinuous transition region as a constraint boundary between safe and unsafe regions, by strategically sampling designs and minimizing the cost of expensive function evaluations and maximizing classification accuracy towards predicting the true boundary. Focusing on these challenges on a discontinuous black-box design problem with unknown constraint, this research contributes in tackling these with adopting a design space partitioning approach. Here, the original discontinuous design space is first transformed into a pseudo continuous design space by building a heuristic, then optimize the location of the unknown constraint or the discontinuity with the BO on this artificially created continuous design space. This new function helps us to develop the acquisition function in the proposed BO model, which when maximized, guide our sampling towards the desired unknown constraint boundary (transition region), which ultimately maximize the classification accuracy. Thus, a sequential Bayesian optimization is developed as a design classifier in locating and partitioning the discontinuous design space along the discontinuity to mitigate the performance issue of BO by optimizing on two separate continuous design spaces or by eliminating the infeasible designs during optimization for finding the efficient or optimal design solutions. The impact of this research is to finally provide a design methodology or classification tool to classify the creep-fatigue failure feasibility of any new designs in the specified design space, without conducting any further expensive function evaluations once the model is fully trained (converged). The content of this chapter focuses on the proof of concept and therefore we have simplified the large scale complex design of the diffusion bonded CHX into a simple thin tube where we will be able to compare the results obtained from the proposed model with the known true solution. The proposed approach can be considered as the pre-stage for the optimization of the design geometry of diffusion bonded CHX to minimize the risk of failure with manufacturing and experimental cost, subject to constraints for creep-fatigue failure (from proposed pre-stage) and other manufacturing constraints, which is considered as future research.

The roadmap of this chapter is as follows. Section 3.2 provides an overview on Bayesian Optimization and machine learning to solve classification problem. Section

3.3 talks more on the thin tube problem and the formulation, projecting the original discontinuous design space to the artificial continuous design space, from knowledge gained by actual function evaluations or experiments. Section 3.4 provides the detail description of the design methodology in fast and adaptive sampling towards predicting the constraint boundary (transition region) and minimizing error rate in the classification problem. Section 3.5 shows the results of the proposed approach under different design parameters. Section 3.6 concludes the chapter 3 with final thoughts.

## 3.2.Background

### *3.2.1. Classification problem*

Classification problem, in general, is a subset of machine learning problems where the main idea is to subset a region of interest or design space into labels or clusters through proper training of a machine learning tool with existing data. After the designer is satisfied with the training the model, then for any new design data, without going for expensive evaluations, can be classified as which label the design has the maximum probability to belong to. Classification problems can be subdivided into Binary Classification and Multi-Label Classification problems. To solve this, different machine learning tools has been used like Support Vector Machine (SVM), Random Forest, Boosting [83]–[85]. Recently advanced method like neural network has been widely used in both binary and multi-label classification problems [86], [87]. Inan et. al. [88] proposed a robust neural network based classification method for premature ventricular contractions whereas Li et. al. [89] attempted a hyperspectral image reconstruction method using convoluted neural network to enhance classification accuracy. Similarly, clustering approaches has been taken, especially for multi-label classification problem with large number of labels [90]. Barros et. al. [91] proposed a probabilistic clustering approach for hierarchical multi-label classification of Protein Functions. Solving a design classification problem with standard machine learning classifier methods is dependent on the quality or amount of training data and always raise the question on how much data is enough to get the maximum learning [8], [9], thus can be very critical to the sampling cost and methods. Therefore, in order to apply

these machine learning algorithms, we need to assume we already have a lot of existing data, which is not true in our classification problem. Considering a black-box problem where these sampled designs undergo expensive evaluations, training data is limited due to very high cost. As mentioned earlier, the research objective in this chapter is not only to identify an appropriate classifier tool, but also an efficient sampling strategy for training the classifier sequentially towards the desired goal of fast and adaptive learning (minimizing expensive evaluations). With this BO as a design classifier, we attempt to first optimize the location (discontinuity or constraint boundary) with the existing technique of minimizing expensive sampling (data) for fast and adaptive learning (data sampling suggested where there is more likelihood of achieving user-defined good solutions), then classify any new designs (either side of the discontinuity or constraint boundary) by the trained posterior surrogate model of the converged (maximized learning) BO. Thus, this research also contributes in integrating the classification technique into the existing efficient sampling method of BO, without having to worry about pre-existing data.

### *3.2.2. Bayesian optimization*

Bayesian optimization [7] (BO) is an emerging field of study in the Sequential Design Methods. It has been considered as a low-cost global optimization tool for design problems having expensive black-box objective functions. The general idea of BO is to emulate an expensive unknown design space and find the local and global optimal locations while reducing the cost of function evaluation from expensive high-fidelity models. As discussed in [7], the reason it is called Bayesian is that it follows the ideology of Bayes theorem, which states that "*posterior* probability of a model (or parameters) $M$ given evidence (or data, or observations) $E$ is proportional to the *likelihood* of $E$ given $M$, multiplied by the *prior* probability of $E$."

In mathematical notation it can be stated as below:

$$p(M|E) \propto \ell(E|M)p(M) \tag{3.1}$$

In the BO setting, the prior represents the belief of the unknown function $f$, assuming there exists a prior knowledge about the function (e.g. smoothness, noisy or noise-free etc.). Given our prior belief, the likelihood represents how likely the data, $D$, we have

observed. These data are the sampled data where we know the true function value from expensive evaluations and can be viewed as the realizations from the unknown function. Finally, given the data we sampled, we can get the posterior distribution in the BO as a posterior surrogate model (e.g. Gaussian process model): $\Delta = p(f|(D))$ is developed from these sampled data. Thus, eqn. 1.3 in the Bayesian optimization setting, can be modified as below:

$$p(f|(D_{1:k})) \propto \ell((D_{1:k})|f)p(f) \tag{3.2}$$

where $D_{1:k} = [x_{1:k},\ f(x_{1:k})]$ is the augmentation of the observation or sampled data till $k^{th}$ iteration of BO. This augmentation of data at each iteration combines the prior distribution with the likelihood function.

This approach has been widely used in many machine learning problems [92]–[96]. However, attempts have been made when the response is discrete such as in consumer modeling problems where the responses are in terms of user preference [7], [97]. The idea is to approximate the user preference discrete response function into continuous latent functions using Binomial-Probit model for two choices [98], [99] and polychotomous regression model for more than two choices where the user can state no preference [100]. BO has also been implemented in multi-objective [101] and high dimensional [102], [103] engineering design problems.

BO adopts a Bayesian perspective and assumes that there is a prior on the function; typically, we use a Gaussian process prior. The prior is represented from the experiment or training data which is assumed as the realizations of the true function. The overall Bayesian Optimization Approach has two major components: A predictor or *Gaussian Process Model (GPM)* and an *Acquisition Function (AF)*. As shown in Figure 3.3, in this approach, we first build a posterior GPM, given the data from the current experiments. The surrogate GPM then predicts the objective or response of the samples generated from a DOE based sampling method within the design space. We then use this model to strategically select the best design locations for future experimentation by maximizing the acquisition functions, defined from the posterior simulations which is obtained from the GPM. However, we need to assume that the objective or response is Lipschitz continuous [7]. As an alternative to a GPM, random forest regression has

been proposed as an expressive and flexible surrogate model in the context of sequential model-based algorithm configuration [104]. Although random forests are good interpolators in the sense that they output good predictions in the neighborhood of training data, they are very poor extrapolators where the training data are far away [105]. This can lead to selecting redundant exploration (more experiments) in the non-interesting region as suggested by the acquisition function in the early iterations of the optimization, due to having additional prediction error of the region far away from the training data. This motivates us to consider the GPM in a Bayesian framework while extending the application to discontinuous design response surfaces, which can be represented as complex practical problems in the domain of experimental design. We next describe the GPM and AF.

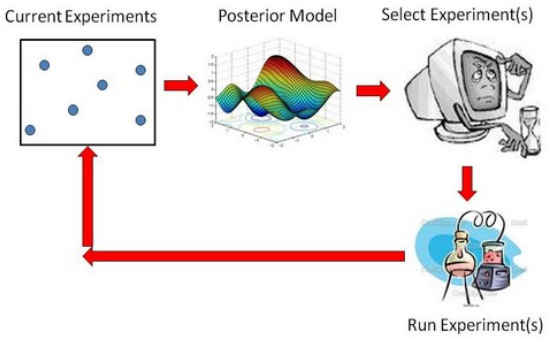


Figure 3.3. Bayesian Optimization Framework [106]

*3.2.2.1.Gaussian process model (GPM)*

Figure 3.4 shows a simple 1D *Gaussian Process Model* with one design variable $x$ and one response variable $z = f(x)$. The dots are the experimental design variables and the dotted and solid lines are the true and the predictor mean functions or responses in the design space, given the observations. The shaded area along the solid line shows the measure of uncertainty over the surrogate GPM prediction. We can clearly see that the variance near the observations is small and increases as the design samples are farther away from the observational data, thereby related to kriging models where the errors are not independent. Much research has been ongoing regarding incorporating and quantifying uncertainty of the experimental or training data by using a nugget term in the predictor GPM. It has been found that the nugget provides better solution and

computational stability framework [107], [108]. Furthermore, GPM has also been implemented in high dimensional design space exploration [109] and BIG DATA problems [110], as an attempt to increase computational efficiency. A survey of implementation of different GP packages has been provided in different coding languages such as MATLAB, R, Python [111].

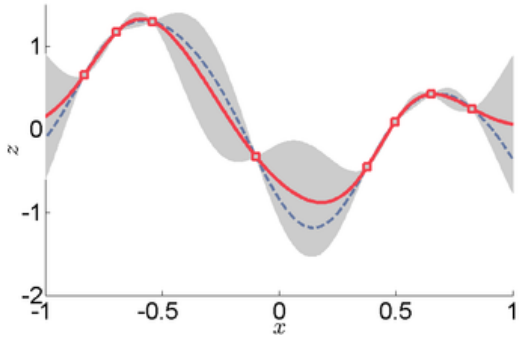


Figure 3.4. 1D Gaussian Process (from Wikipedia)

*3.2.2.2. Acquisition function (AF)*

The second major component in Bayesian optimization is the Acquisition Function whose goal is to guide the search for future experiments towards the desired goal and thereby bring the sequential design into the BO. The AF predicts an improvement metric for each sample. The improvement metric depends on *exploration* (unexplored design spaces) and *exploitation* (region near high responses). Thus, the acquisition function gives high value of improvement to the samples whose mean prediction is high, variance is high, or a combination of both. Thus, by maximizing the acquisition function, we select the best samples to find the optimum solution and reduce the uncertainty of the unknown expensive design space. Throughout the years, various formulations have been applied to define the acquisition functions. One such method is the Probability of Improvement, PI [112] which is improvement based acquisition function. Jones in [113] notes that the performance of PI(·) "is truly impressive;… however, the difficulty is that the PI(·) method is extremely sensitive to the choice of the target. If the desired improvement is too small, the search will be highly local and will only move on to search globally after searching nearly exhaustively around the current best point. On the other hand, if the small-valued tolerance parameter $\xi$ in PI(.)

equation is set too high (see [113]), the search will be excessively global, and the algorithm will be slow to fine-tune any promising solutions." Thus, the Expected Improvement acquisition function, EI [7], is widely used over PI which is a trade-off between exploration and exploitation. Another Acquisition function is the Confidence bound criteria, CB, introduced by Cox and John [114], where the selection of points is based on the upper or lower confidence bound of the predicted design surface for maximization or minimization problem respectively.

## 3.3. Problem Description

In this section, we describe the thin tube design problem which represents the proof of concept for the large complex design of diffusion bonded Compact Heat Exchanger (CHX). As the tube is assumed to undergo constant loading of temperature and pressure, there will be risk of creep-fatigue failure which will vary with the design geometry. *Fatigue damage* is created when one cycles a test specimen at a fixed stress amplitude for enough cycles until it develops microstructural damage and eventually fails. *Creep damage* is created when one holds a test specimen at a fixed load for a long enough time that it eventually develops microstructural damage and fails. *Creep-fatigue damage* is therefore to do both of these things simultaneously (i.e. a stress controlled cycle with a hold) and the specimen will generally fail sooner than conducting the cycling and the hold individually. As mentioned previously, our goal is to predict the transition region between the safe and unsafe region as defined in section 3.1.2. For design variables for the CHX which will influence creep-fatigue behavior, we choose the radius (*rad*) and length (*l*) of the tube. Next we describe the experimentation and the formulation of the objective function which depends on the experimental results and the prior knowledge on the domain of solid mechanics.

### *3.3.1. Model experiments*

In this section, we provide the computation of the location of any design in terms of Elastic, Plastic, Shakedown and Ratchetting, and the respective strain accumulation. We represent these outputs as the responses from the expensive experiments. In our problem of thin tube design, though these computations are not expensive and can be

done analytically, we still represent these as expensive function evaluations which will be true for our future problem of considering the actual diffusion bonded CHX geometry where expensive Finite Element Analysis is required. The computations have been done based on the formulation of a *Bree diagram* [81]. In this chapter, we considered the Bree diagram for a non-work-hardening material whose yield stress remains unchanged by changes in mean temperature, as provided in Appendix A.3.1. For the sake of simplicity, we have ignored the further division of Shakedown (S1, S2) and Ratchetting (R1, R2) as shown in the figure, and assumed a single region of Shakedown (S) and Ratchetting (R). This is because, for the purpose of our problem any design in Shakedown is considered safe, while in Ratchetting is considered unsafe.

Below are the steps for computation of the various stresses and strains for the thin tube required for our methodology:

Step 1: Calculate Pressure and Temperature Stress:

$$\sigma_p = P * rad/d \tag{3.3}$$

$$\sigma_t = (E * \alpha * \Delta T)/2(1-\rho) \tag{3.4}$$

Where,

$$\Delta T = \Delta T_{slop} * l + T_{in} \tag{3.5}$$

$$\Delta T_{slop} = -T_{in} + T_{out} * (\frac{rad - rad_{min}}{rad_{max} - rad_{min}}) \tag{3.6}$$

where $\sigma_p$ and $\sigma_t$ are the pressure and temperature stresses; $P$ is internal pressure subjected to the tube which is taken as 25MPa; *rad* is the radius; *d* is the wall thickness; $l$ is the length; E = 200GPa is the Young's Modulus; $\alpha = 16e-6$ is the thermal co-efficient of the linear expansion; $\rho = 0.27$ is the Poisson Ratio; $\Delta T$ is temperature drop across the wall with $T_{in}$ and $T_{out}$ are the inlet and outlet temperatures which are taken as 400ºC and 20ºC, respectively; $rad_{min}$ and $rad_{max}$ are the minimum and maximum radius.

Step 2: Determine the region of the design:

Case 1:

- If $\sigma_p \leq 0.5\sigma_y$ and $\sigma_t < 2\sigma_y$, ($\sigma_y = 205$MPa is the yield stress), the design is in the *Elastic* or *Shakedown* (Safe) region;

- else, if $\sigma_t > 2\sigma_y$, the design is in *Plastic* or *Ratchetting* region (Unsafe). For the design in Plastic or Ratchetting, if $\sigma_p * \sigma_t \leq \sigma_y^2$, the design is in *Plastic*.
- else, if $\sigma_t = 2\sigma_y$, the design is in at the transition line.

Case 2:

- If $\sigma_p > 0.5\sigma_y$ and $\sigma_p + 0.25\sigma_t < \sigma_y$, the design is in *Elastic* or *Shakedown* (Safe);
- else, if $\sigma_p + 0.25\sigma_t > \sigma_y$, the design is in *Ratchetting* region (Unsafe).
- else, if $\sigma_p + 0.25\sigma_t = \sigma_y$, the design is in at the transition line.

Step 3: Calculate the strain accumulation:

- If the design is in *Elastic*/*Shakedown*, strain $\varepsilon_s$ can be calculated as:

$$\varepsilon_s = \left(\frac{2}{E}\right) * \left(\sigma - \left(\frac{x}{d}\right) * \sigma_t\right) \tag{3.7}$$

where

$$\sigma = \sigma_p + 2\left(\frac{x}{d}\right) * \sigma_t \tag{3.8}$$

and $x$ is the section of the tube wall, which varies from 0 at the outer wall to $d$ at the inner wall. Since our problem is subjected to internal pressure, the maximum stress is at the inner wall of the tube. Thus, we consider the worst condition and focus on the stress at the inner wall at $x = d$.

- If the design is in *Plastic*, strain $\varepsilon_p$can be calculated as:

$$\varepsilon_p = \left(\sigma_t - 2\sigma_y\right) * n/E \tag{3.9}$$

- If the design is in *Ratchetting*, strain $\varepsilon_r$can be calculated as:

$$\varepsilon_r = \left(\frac{2n*\sigma_t}{E}\right) * (1 - 2\sqrt{(\sigma_y - \sigma_p)/\sigma_t}) \tag{3.10}$$

Where $n$ is the number of cycles. In this problem, we considered $n$ =50.

It is to be noted that when the design is at the transition line, as per Step 2, we avoid the Step 3 strain calculation for those designs as for those designs, equation 3.7, 3.9 or 3.10 are all justified which creates the jump discontinuity (refer Appendix Fig. A.3.3 for 1D example). In the next section, we have presented the formulation of the distance metric which mitigates this discontinuity issue, suitable for the BO framework.

### *3.3.2. Formulation of distance metric*

In this section, we provide the formulation of the distance metric. Although we can obtain the strain accumulation for a particular design from the model experiments, we do not have a good idea of strain accumulation for a design close to the transition region, where we do not know which equation (eq. 3.7, 3.9, 3.10) applies. Therefore, with the value of strain only, it is difficult to formulate an objective function where we can either maximize or minimize the strain accumulation in the BO model in order to maximize the accuracy and iteratively get closer to the unknown transition region. Also, the jump discontinuity still lies at the transition line between safe and unsafe region in the design space of strain accumulation. Therefore, we propose to formulate a new function with the help of the experimental results, which we have defined as a distance function, *Y*, by transforming the original discontinuous design space into artificially created continuous design space. The computation of the distance value for any designs is based on the heuristics that, given two designs that are in the Shakedown (Safe) region, the design having more strain accumulation is closer to the unknown transition region and therefore higher value will be assigned. The reverse occurs for any design in Plastic or Ratchetting (Unsafe) region where for any two designs in those regions, the design having lower strain accumulation is towards the unknown transition region and therefore lower value will be assigned. Thus, this prior knowledge helps us to build our distance function where we first separate the sampled designs (prior data) in terms of regions which can be evaluated from experiments (Step 2 in Section 3.3.1). It is worth noting that for the complex problem of diffusion bonded HCX, the determination of the region for a design must be conducted from FEA. After we separate all the sampled designs into regions as Elastic/Shakedown, Plastic and Ratchetting, next we assume a linear increment of strain accumulation with increasing the risk of creep-fatigue failure and build our formula for computing the distance value of the $i^{th}$ design at iteration k of BO model, $Y_{k,i}$ as below:

- For design *i*, in *Elastic/Shakedown*:

$$Y_{s,k,i} = YS_{min} + \frac{(\varepsilon_{s,i} - \min(\boldsymbol{\varepsilon_{s,k}}))}{\max(\boldsymbol{\varepsilon_{s,k}}) - \min(\boldsymbol{\varepsilon_{s,k}})} * (YS_{max} - YS_{min}) \tag{3.11}$$

- For design *i*, in *Plastic*:

$$Y_{p,k,i} = YP_{min} + \frac{(\varepsilon_{p,i} - \min(\boldsymbol{\varepsilon_{p,k}}))}{\max(\boldsymbol{\varepsilon_{p,k}}) - \min(\boldsymbol{\varepsilon_{p,k}})} * (YP_{max} - YP_{min}) \quad (3.12)$$

- For design *i*, in *Ratchetting*:

$$Y_{r,k,i} = YR_{min} + \frac{(\varepsilon_{r,i} - \min(\boldsymbol{\varepsilon_{r,k}}))}{\max(\boldsymbol{\varepsilon_{r,k}}) - \min(\boldsymbol{\varepsilon_{r,k}})} * (YR_{max} - YR_{min}) \quad (3.13)$$

where $\varepsilon_{s,i}, \varepsilon_{p,i}, \varepsilon_{r,i}$are the strain accumulation of design *i*, given the design falls into Elastic/ Shakedown, Plastic or Ratchetting respectively; $\min(\boldsymbol{\varepsilon_{s,k}})$, $\max(\boldsymbol{\varepsilon_{s,k}})$ are the minimum and the maximum strain accumulation among all the sampled designs (training data) in Shakedown at iteration *k*; $\min(\boldsymbol{\varepsilon_{p,k}})$, $\max(\boldsymbol{\varepsilon_{p,k}})$ are the minimum and the maximum strain accumulation among all the sampled designs (training data) in Plastic at iteration *k*; $\min(\boldsymbol{\varepsilon_{r,k}})$, $\max(\boldsymbol{\varepsilon_{r,k}})$ are the minimum and the maximum strain accumulation among all the sampled designs (training data) in Ratchetting at iteration *k*; $YS_{min}, YS_{max}$ are the minimum and maximum distance function bounds for the designs in Elastic/ Shakedown and are set as 0 and 0.45 respectively; $YP_{min}, YP_{max}$ are the minimum and maximum distance function bounds for the designs in Plastic and re set as 0.55 and 1 respectively; $YR_{min}, YR_{max}$ are the minimum and maximum distance function bounds for the designs in Ratchetting and re set as 0.51 and 1 respectively. With changing the values for $YS_{max}, YP_{min}, YR_{min}$, the efficiency of the model changes in terms of accuracy and cost of function evaluations and, therefore, a sensitivity analysis has been done within a recommended range of values which will be described later. However, the values given have been found to produce consistent performance in terms of accuracy.

The idea of the objective is that the design samples, at iteration k, in the Elastic/Shakedown region which are nearest to the predicted transition region will have $Y_{s,k,i}$= 0.45 and the design samples in the Elastic/Shakedown region which are farthest from the predicted transition region will have $Y_{s,k,i}$=0. All the other samples, or training data, in the Elastic/ Shakedown region will have values within the range of [0-0.45] based on the closeness to the predicted transition region. Similarly, at iteration k, the sample in the Plastic or Ratchetting region which is nearest to the predicted transition region will have $Y_{p,k,i}$ or $Y_{r,k,i}$= 0.55 and the sample in the Plastic or Ratchetting region

which is farthest from the predicted transition region will have $Y_{p,k,i}$ or $Y_{r,k,i}$=1. All the other samples or training data in the Elastic/ Shakedown region will have values within the range of [0.55-1] based on the closeness to the predicted transition region. The width of the transition region thus set in this case as [0.45-0.55], assuming the true transition or constraint boundary line is at $Y_{s,i} = Y_{p,i} = Y_{r,i}$ =0.5 for any iteration of the BO model. In our formulation, this setting of distance value of 0.5 for any design at the transition line build the continuity in the design space. It is to be noted that knowing the distance value at the transition line, we attempt to optimize the location of the unknown transition region, given the width of the region. Locating the exact transition line or constraint boundary will require exhaustive experiments or function evaluations and may occur overfitting issues in prediction to classify safe and unsafe designs; therefore, we assume that with sequential improvement of the prediction of the location of the transition region from BO increases accuracy in the location of transition line (constraint boundary line) as well.

To summarize, the reasons to construct the distance function are 1) an output as a discrete region is not useful in the BO framework: we need to transform region knowledge into a continuous metric, and 2) it allows us to define our objective in the BO framework in terms of finding the transition region between Elastic/Shakedown vs. Plastic and Ratchetting. It is to be noted that this is a sequential design approach and with more training data (increase prior knowledge), the values of distance function, $Y$ for all the training data, except at the transition line, changes and are re-computed per iteration.

### 3.4. Design Methodology

Figure 3.5 shows the detailed structure of the proposed Bayesian Optimization framework. Below is the algorithm with explanation of each steps of the proposed pre-stage Bayesian Optimization framework to predict the transition region between safe and unsafe region for the thin tube problem as describe in section 3.3.1; however, the

general algorithm is applicable to larger scale problems such as the diffusion bonded CHX.

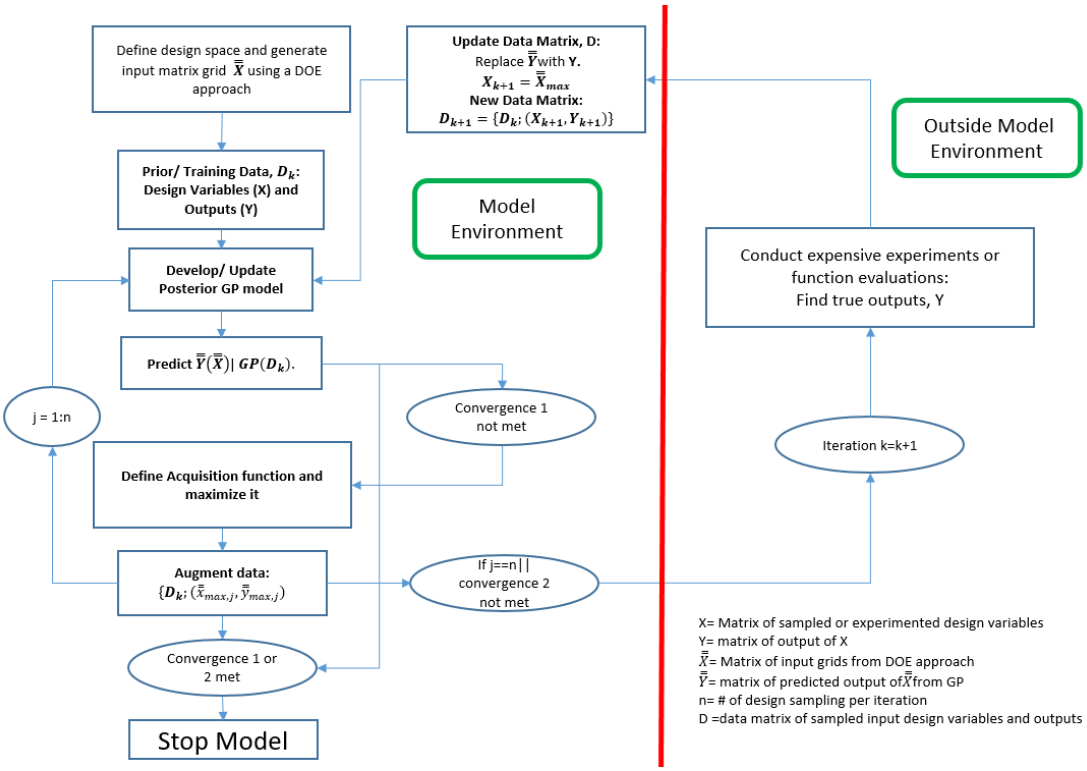


Figure 3.5. Overall flow-chart of the proposed Bayesian Optimization framework

***Step-by-Step description for proposed Bayesian Optimization to find the transition region between safe and unsafe designs of the thin tube***

<u>*Step 0 (Initialization):*</u> Define the design space or the region of interest for the given problem. From the defined design space, generate grid matrix $\bar{\bar{\boldsymbol{X}}}$ using a DOE approach. Conduct function evaluations or experiments of very limited randomly generated samples in the design space. In our thin tube problem, we choose 10 random selected designs as starting samples which are not included in $\bar{\bar{\boldsymbol{X}}}$.

<u>*Step 1: Build a training data matrix with the sampled designs:*</u> The data consist of **X** as design input variables and **Y** as output functions. In our problem, we define **X** as the matrix of design geometries as radius (*rad*) and length (*l*) of the thin tube and $\boldsymbol{Y}$ as the vector of distance values of the respective sampled designs as described in Section 3.3. Create the training data matrix, assuming at iteration k, $\boldsymbol{D_k} = \{\boldsymbol{X_k}, \boldsymbol{Y}(\boldsymbol{X_k})\}$. It is to be

noted $\boldsymbol{D_k}$ contains the distance values for all sampled designs from any region. Also, like in the Bree diagram, it is possible to choose the pressure and temperature stresses as the design variables. However, with design geometry as the design variables, it is more useful for a designer to directly visualize and understand the efficiency of the designs.

<u>*Step 2: GPM:*</u> Next, with the knowledge gained from previous experiments (prior knowledge), $\boldsymbol{D_k} = \{\boldsymbol{X_k}, \boldsymbol{Y}(\boldsymbol{X_k})\}$, we can *develop a single posterior Gaussian Process model*.

<u>*Step 3:*</u> Use the posterior GP model $\boldsymbol{\Delta_k}$, to conduct posterior predictive simulations of the non-sampled designs in the grid matrix $\bar{\bar{\boldsymbol{X}}}$ and predict respective mean and MSE of distance values, forming two vectors of $\boldsymbol{\mu}\left(\bar{\bar{\boldsymbol{Y}}}(\bar{\bar{\boldsymbol{X}}})\right)|\ \boldsymbol{\Delta_k}$ and $\boldsymbol{\sigma^2}\left(\bar{\bar{\boldsymbol{Y}}}(\bar{\bar{\boldsymbol{X}}})\right)|\ \boldsymbol{\Delta_k}$ respectively.

<u>*Step 4: Define objectives to sample designs towards unknown transition region:*</u> Now, we have the vector of predictive posterior means of all the non-sampled designs, we need to define our objective, for which the acquisition function will be formulated. In this classification problem between safe and unsafe designs, our goal is to therefore maximize sampling of designs towards the unknown transition boundary and thus train the BO model sequentially with higher accuracy towards the transition region. Thus, maximizing the distance function for the set of designs in Elastic or Shakedown (Safe) will create the optimal region towards the transition region as the design in Shakedown closest to the transition region will have higher distance values. Similarly, minimizing the distance function for the set of designs in Plastic and Ratchetting (Unsafe) will create the optimal region towards the transition region as the designs in those regions closest to the transition region will have lower distance function values.

To convert into a single-objective maximization problem, we did the elementwise transformation of the vector $\boldsymbol{\mu}\left(\bar{\bar{\boldsymbol{Y}}}(\bar{\bar{\boldsymbol{X}}})\right)|\ \boldsymbol{\Delta_k}$. Let us define the transformed mean vector as $\boldsymbol{\mu^T}\left(\bar{\bar{\boldsymbol{Y}}}(\bar{\bar{\boldsymbol{X}}})\right)$, after conducting the elementwise operation as follows:

$$\begin{cases} \mu(\bar{\bar{y}}(\bar{\bar{x}}))\ if\ \bar{\bar{x}}_{region} \in Elastic/Shakedown \\ 1-\mu(\bar{\bar{y}}(\bar{\bar{x}}))\ if\ \bar{\bar{x}}_{region} \in Plastic/Rachetting \end{cases} \tag{3.14}$$

where $\bar{\bar{y}}$ is the scalar posterior mean value of the non-sampled design $\bar{\bar{x}}$.

<u>*Ste*p 5: *Define the Acquisition Function and maximize the Acquisition function* $u(.)$:</u>
After the transformation as mentioned in Step 4, we calculated the acquisition function value elementwise as $u(\bar{\bar{y}}(\bar{\bar{x}})|\boldsymbol{\Delta_k})$, for each non-sampled designs, considering the respective mean and MSE values in vectors $\boldsymbol{\mu^T}\big(\bar{\bar{\boldsymbol{Y}}}(\bar{\bar{\boldsymbol{X}}})\big)$ and $\boldsymbol{\sigma^2}\big(\bar{\bar{\boldsymbol{Y}}}(\bar{\bar{\boldsymbol{X}}})\big)$. Thus, we develop the vector of the acquisition function values as $\boldsymbol{u}(\bar{\bar{\boldsymbol{Y}}}(\bar{\bar{\boldsymbol{X}}})|\boldsymbol{\Delta_k})$. A selection criterion is applied to choose new design location for future sampling, $\{\bar{\bar{x}}_{max}\}$; $\bar{\bar{x}}_{max} \in \bar{\bar{\boldsymbol{X}}}$, which will maximize the predicted improvement of the learning of the unknown design space (maximizing acquisition function). Thus we select the design with maximum acquisition function value as,

$$\bar{\bar{y}}_{max}(\bar{\bar{x}}_{max}) = \max(\boldsymbol{u}(\bar{\bar{\boldsymbol{Y}}}(\bar{\bar{\boldsymbol{X}}})|\boldsymbol{\Delta_k})) \tag{3.15}$$

Augment the Data, $\bar{\bar{\boldsymbol{D}}}_{\boldsymbol{k}} = \{\boldsymbol{D_k}; (\bar{\bar{x}}_{max}, \bar{\bar{y}}_{max})\}$. The methodology used to compute the acquisition function has been described in section 3.4.3.

<u>*Step 6:*</u> Check for convergence criteria 1. If not met, run *j*=1: *n* loops of Step 2 to 6; each loop takes one optimal design location $\{\bar{\bar{x}}_{max,j}\}$; to select the best *n* design locations $\bar{\bar{\boldsymbol{X}}}_{\boldsymbol{max}} = \{\bar{\bar{x}}_{max,1}, \dots, \bar{\bar{x}}_{max,n}\}$ to proceed to the next round of experiments. This step provides multiple experimental data in a single round of an experiment since it will be unrealistic and time consuming to provide one experiment at a time. The assumption behind this step is that we believe the GP prediction of $\{\bar{\bar{x}}_{max,j}\}$ is accurate and proceed to the next best location $\{\bar{\bar{x}}_{max,j+1}\}$ by minimizing the error in the current selected location$\{\bar{\bar{x}}_{max,j}\}$. We believe this is a fair assumption since with more knowledge, the GP prediction will be close to the actual experiment data. In the early round of experiments, although we might see deviations from the actual experiment results (not following the assumptions), with the knowledge from those experiments, eventually the GP will improve and provide predictions closer to the actual experiment results as the model convergences (following assumptions).

*Step 7: Expensive Function evaluations:* Conduct experiments for new design location $\boldsymbol{X_{k+1}} = \bar{\bar{\boldsymbol{X}}}_{\boldsymbol{max}}$. This step is outside the model environment as actual experiments will be conducted from the original high-fidelity model to generate required outputs (strain accumulation and the location of the designs), which ultimately used to compute distance metric (Eq. 3.9 - 3.11). Therefore, the new experiment data is: $\{\boldsymbol{X_{k+1}}, \boldsymbol{Y}(\boldsymbol{X_{k+1}})\}$.

*Step 8: Data Augmentation:* Update the prior knowledge for the next iteration of the model. Update training data matrix with current experimented data $\boldsymbol{D_{k+1}} = \{\boldsymbol{D_k}; (\boldsymbol{X_{k+1}}, \boldsymbol{Y}(\boldsymbol{X_{k+1}}))\}$. Repeat Steps 2 to 8 until convergence.

*Step 9:* If convergence criteria 2 is met, update the GP with the final training data $\boldsymbol{\Lambda}$, augmented with final sampled data and stop the model. Convergence criteria 1 and 2 will be explained later in this section.

*Step 10: Feasibility Check between safe and unsafe region:*

This step is after the optimization is completed and the proposed BO model is fully trained, satisfying convergence criteria. Now, instead of running expensive evaluations, to classify any new designs as safe or unsafe design, we check the feasibility using the trained low-cost BO model:

If the posterior predictive mean of the new design, $\mu((Y_{new}(X_{new}))| \boldsymbol{\Lambda}) \leq 0.5$, the new design is in safe region. Otherwise, the new design is in the unsafe region. The value 0.5 is the threshold as we set this distance value at the transition boundary line.

### *3.4.1. Gaussian process model formulation of the thin tube*

In this section, we present the GPM in our proposed BO model. The general form of the GPM is as follows:

$$y(x) = x^T\beta + z(x) \tag{3.16}$$

where $x^T\beta$ is the Polynomial Regression model. In our model, we have used 1st and 2nd order polynomial regression model. The polynomial regression model captures the global trend of the data. In general, 1st order polynomial regression is used, which is also known as universal kriging [115]; however, it has also been claimed that it is fine

to use a constant mean model [116]. $z(x)$ is a realization of a correlated Gaussian Process with mean $E[z(x)]$ and covariance $cov(x^i, x^j)$ functions defined as follows:

$$z(x) \sim GP\left(E[z(x)], cov(x^i, x^j)\right); \tag{3.17}$$

$$E[z(x)] = 0, cov(x^i, x^j) = \sigma^2 R(x^i, x^j) \tag{3.18}$$

$$R(x^i, x^j) = \exp\left(-\sum_{m=1}^{d} \theta_m (x_m^i - x_m^j)^2\right); \tag{3.19}$$

$$\theta_m = (\theta_1, \theta_2, \ldots., \theta_d)$$

where $\sigma^2$ is the overall scale parameter and $\theta_m$is the correlation length parameter in dimension $m$ of $d$ dimension of $x$. These are termed as the hyper-parameters of GP model. $R(x^i, x^j)$ is the spatial correlation function. In our model, we have used a Gaussian Spatial correlation function which is given by equation 3.13. The objective is to estimate (by MLE) the hyper-parameters $\sigma$, $\theta_m$ which creates the surrogate model that best explains the training data $\boldsymbol{D_k}$ at iteration k.

After we build the GP model, the next task of the GP model is to predict (Step 3) an arbitrary point drawn from the grid matrix in Step 0. Assume $\boldsymbol{D_k} = \{\boldsymbol{X_k}, \boldsymbol{Y(X_k)}\}$ is the prior information from previous experiments from high fidelity models, representing the realizations of prior belief of the unknown true functions, and $\bar{\bar{x}}_{k+1} \in \bar{\bar{\boldsymbol{X}}}$ is any new design. The predictive output distribution of $x_{k+1}$, given the posterior GP model, is given by equation 3.20.

$$P(\bar{\bar{y}}_{k+1} | \boldsymbol{D_k}, \bar{\bar{x}}_{k+1}, \sigma_k^2, \boldsymbol{\theta_k}) = \boldsymbol{N}(\mu(\bar{\bar{y}}_{k+1}(\bar{\bar{x}}_{k+1})), \sigma^2(\bar{\bar{y}}_{k+1}(\bar{\bar{x}}_{k+1}))) \tag{3.20}$$

where:

$$\mu\left(\bar{\bar{y}}_{k+1}(\bar{\bar{x}}_{k+1})\right) = \boldsymbol{cov_{k+1}^T COV_k^{-1} Y_k}; \tag{3.21}$$

$$\sigma^2\left(\bar{\bar{y}}_{k+1}(\bar{\bar{x}}_{k+1})\right) = cov(\bar{\bar{x}}_{k+1}, \bar{\bar{x}}_{k+1}) - \boldsymbol{cov_{k+1}^T COV_k^{-1} cov_{k+1}} \tag{3.22}$$

$\boldsymbol{COV_k}$ is the kernel matrix of already sampled designs $\boldsymbol{X_k}$ and $\boldsymbol{cov_{k+1}}$ is the covariance function of new design $\bar{\bar{x}}_{k+1}$ which is defined as follows:

$$\boldsymbol{COV_k} = \begin{bmatrix} cov(x_1, x_1) & \cdots & cov(x_1, x_k) \\ \vdots & \ddots & \vdots \\ cov(x_k, x_1) & \cdots & cov(x_k, x_k) \end{bmatrix}$$

$$\boldsymbol{cov_{k+1}} = [cov(\bar{\bar{x}}_{k+1}, x_1), cov(\bar{\bar{x}}_{k+1}, x_2), .., cov(\bar{\bar{x}}_{k+1}, x_k)]$$

### *3.4.2. Generating grid points from unknown design spaces of thin tube*

In this section, we discuss the generation of grid points within the specified design spaces, where the selected grid points by the acquisition function will be considered as samples for experiments. The goal of generating a grid using a rectangular grid or Latin hypercube is to use the space filling properties to cover the entire design space of the unknown design response surface. More details on the formulations and sampling strategies of these two methods has been referred in the paper [117]. However, the proposed model is not restricted to use these two methods and the user can select a preferred sampling strategy.

### *3.4.3. Acquisition function formulation of the thin tube*

In this section, we provide a detailed formulation of the acquisition function for Step 4 of the proposed model. Three types of acquisition functions have been studied in the model: *Probability of Improvement*, *Expected Improvement* and *Full Exploration* search. The first acquisition function considers the idea of pure exploitation (selecting design points where predicted mean is high); the second acquisition function develops on the idea of exploitation (selecting design points where predicted mean is high) and exploration (selecting design points where predicted variance is high). The final acquisition function is based on only exploration. The final acquisition function is very useful when the design space is very flat, and the global optimal solution is confined in a very small region. With the first two acquisition functions, it has been seen the model falls into false convergence since the design space is flat with limited samples in the early iterations. The acquisition function predicts very low probability/expected improvement as all the responses have similar values for all the experimented design inputs. Thus, when the design surface is unknown and could be very flat in most regions, it is important to use a full exploration acquisition function in the early iterations of the model to ensure that any potential optimal region is not missed. Once we find a sample within the confined interesting region, we can switch back to exploration-exploitation search to avoid unnecessary selection of samples for experiments in the non-optimal regions. In our model, we have set a switching criterion as follows:

*do Full Exploration search*

$$if\ \max(\boldsymbol{Y_k}) - \min(\boldsymbol{Y_k}) \leq \delta\ \ k = 1,2, \dots K$$

*else do Expected Improvement or Probability of Improvement*

where $\delta$ is a very small value which is set as 0.1. We can also set $\delta$ as the percentage (say 1%) of the mean $\boldsymbol{Y_k}$.

After selecting an appropriate acquisition function, we optimize over the GP to get the next design input location

$\{\bar{\bar{x}}_{max}\};\ \bar{\bar{x}}_{max}\ \in\ \bar{\bar{\boldsymbol{X}}}$ such as

$$\bar{\bar{x}}_{max} = \underset{x_i \in \bar{\bar{\boldsymbol{X}}}}{\operatorname{argmax}}\, \boldsymbol{u}\left(\bar{\bar{\boldsymbol{Y}}}(\bar{\bar{\boldsymbol{X}}}) \middle| \boldsymbol{\Delta_k}\right) \tag{3.23}$$

where $\boldsymbol{u}(\bar{\bar{\boldsymbol{Y}}}(\bar{\bar{\boldsymbol{X}}})|\boldsymbol{\Delta_k})$ is the vector of acquisition function values of all the elements of vector $\bar{\bar{\boldsymbol{Y}}}(\bar{\bar{\boldsymbol{X}}})$ given the posterior model at iteration k. Below are the equations for the acquisition functions, Probability of Improvement (Eq. 3.24), Expected Improvement (Eq. 3.25, 3.26) and Full Exploration (Eq. 3.27)

$$u(\bar{\bar{y}}(\bar{\bar{x}})|\boldsymbol{\Delta_k}) = PI(\bar{\bar{y}}(\bar{\bar{x}})) =$$
$$\begin{cases} \Phi\left(\frac{\mu(\bar{\bar{y}}(\bar{\bar{x}})) - y(x^+) - \xi}{\sigma(\bar{\bar{y}}(\bar{\bar{x}}))}, mean = 0, sd = 1\right)\ if\ \sigma(\bar{\bar{y}}(\bar{\bar{x}})) > 0 \\ 0\ if\ \sigma(\bar{\bar{y}}(\bar{\bar{x}})) = 0 \end{cases} \tag{3.24}$$

$$u(\bar{\bar{y}}(\bar{\bar{x}})|\boldsymbol{\Delta_k}) = EI(\bar{\bar{y}}(\bar{\bar{x}})) =$$
$$\begin{cases} (\mu(\bar{\bar{y}}(\bar{\bar{x}})) - y(x^+) - \xi) * \Phi(\mathrm{Z}, 0, 1) + \sigma(\bar{\bar{y}}(\bar{\bar{x}})) * \phi(Z)\ \ if\ \sigma(\bar{\bar{y}}(\bar{\bar{x}})) > 0 \\ 0\ if\ \sigma(\bar{\bar{y}}(\bar{\bar{x}})) = 0 \end{cases} \tag{3.25}$$

$$Z = \begin{cases} \frac{\mu(\bar{\bar{y}}(\bar{\bar{x}})) - y(x^+) - \xi}{\sigma(\bar{\bar{y}}(\bar{\bar{x}}))}\ \ if\ \sigma(\bar{\bar{y}}(\bar{\bar{x}})) > 0 \\ 0\ \ if\ \sigma(\bar{\bar{y}}(\bar{\bar{x}})) = 0 \end{cases} \tag{3.26}$$

$$u(\bar{\bar{y}}(\bar{\bar{x}})|\boldsymbol{\Delta_k}) = \sigma^2(\bar{\bar{y}}(\bar{\bar{x}})) \tag{3.27}$$

where $y(x^+)$is the maximum actual response among all the experimented data until the current stage which is at $x = x^+$ ; $\mu(\bar{\bar{y}})$ and $\sigma^2(\bar{\bar{y}})$ are the predicted mean and MSE from GPM for the non-sampled design $\bar{\bar{x}} \in \bar{\bar{\boldsymbol{X}}}$ ; $\Phi(.)$ is the cdf; $\phi(.)$ is the pdf; $\xi \geq 0$

is a small value which is recommended to be 0.01 [93] as this works well in most cases whereas the cooling function of $\xi$ did not. Jones [113] notes that the performance of PI(·) is highly sensitive to the value of ξ, with non-ideal values leading to poor performance.

### *3.4.4. Convergence criteria*

In this section, we have discussed on the convergence criteria established into the model. From the steps of the proposed BO model, there are two checks for convergence in the model in Step 5 and in Step 8 in Section 3.4. The convergence criteria in Step 5 is Convergence 1 and the convergence criteria in Step 8 is Convergence 2. If either of the convergence checks succeed, the model stops and return the final solution. Below is the list of Convergence criteria which can be implemented into the models.

Convergence 1:

a. The maximum improvement value of the acquisition function in selecting the first design sample (1st iteration in Step 5) after conducting actual experiments is less than α=0.001. Mathematically, it can be stated as

If $j == 1$

$$\max\{u(\overline{\overline{\boldsymbol{Y}}}(\overline{\overline{\boldsymbol{X}}}|\boldsymbol{\Delta_k})\} \leq \alpha \quad (3.28)$$

Convergence 2:

a. The absolute difference in the total mean MSE of the predicted responses in m successive iterations is less than $\alpha_1$.

$$|\mu\left(\sigma^2(\overline{\overline{\boldsymbol{Y}}}_{\boldsymbol{k}})\right) - \mu\left(\sigma^2(\overline{\overline{\boldsymbol{Y}}}_{\boldsymbol{k+m}})\right)| \leq \alpha_1 \quad (3.29)$$

Where, $\overline{\overline{\boldsymbol{Y}}}_{\boldsymbol{k}}$ is the column vector of all the predicted value of matrix $\overline{\overline{\boldsymbol{X}}}$ at iteration $k$.

b. Stopping the model after limiting the budget in terms of maximum number of experiments or function evaluations, i.e $\sum n_k \geq S$ where $S$ is the maximum number of function evaluations possible; $n_k$ is the number of samples selected for experiments at k[th] iteration.

## 3.5.Results

In this section, we will show the results of the proposed Bayesian Optimization framework on the design of the tube in terms of the performance of finding the transition region between safe and unsafe region. We used the DACE package [117] in MATLAB to fit the GP model in the Bayesian Optimization. With radius and length of the tube as decision variables, two test scenarios have been considered with different values of thickness of the tube given as 1.7mm and 1.2mm. The feasible bounds for radius and length are [4 – 6.55] mm and [0.1-1] m, respectively. Figures 3.6 - 3.9 shows the results after the model satisfies convergence criteria 1, considering two different thickness of tube (thickness =1.7mm and 1.2mm).

### *3.5.1. Predicted transition region of converged model*

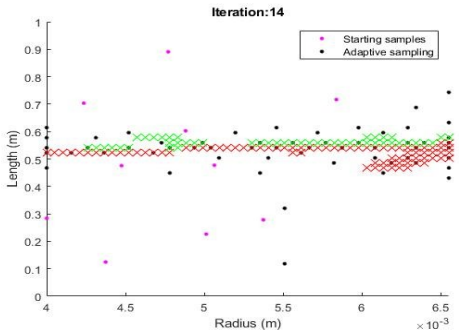


Figure 3.6. Transition region between Safe and Unsafe region for Thickness = 1.7mm (Convergence 1 satisfied)

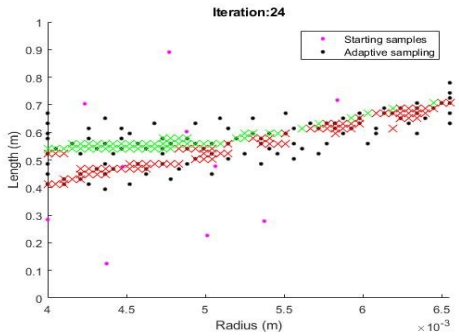


Figure 3.7. Transition region between Safe and Unsafe region for Thickness = 1.2mm (Convergence 1 satisfied)

The pink and black dots in the Figures 3.6 and 3.7 represent the randomly starting samples and the BO guided adaptive sample design locations that have been trained from actual function evaluations as described in section 3.3.1. The final posterior predicted transition region, representing also the discontinuity or the constraint boundary region, has been developed based on those prior training data only and, therefore, the designers can provide decisions about the feasibility of any new designs in the specified design space based on the small sample of data, instead of undergoing further experiments. The green and red highlighted region represent the final transition region which is defined as the predicted distance function value $Y$, ranges between 0.4 to 0.5 and 0.5 to 0.6 respectively, given the prior training data. The green highlighted region represents the area in the Shakedown region (safe), but very close to transition

region near the constraint boundary line. The red dots represent the area in the Plastic or Ratchetting region (unsafe), but very close to transition region near the constraint boundary line.

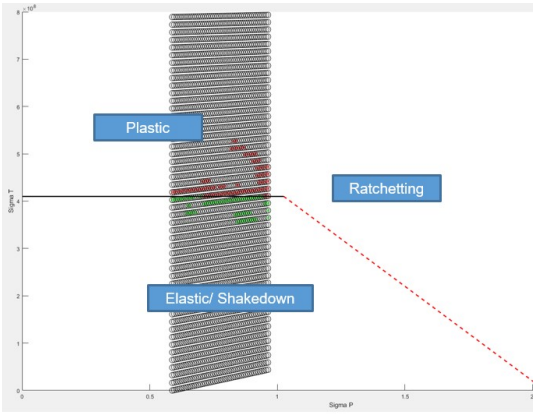


Figure 3.8. Comparison with Bree diagram of thin tube for Thickness = 1.7mm

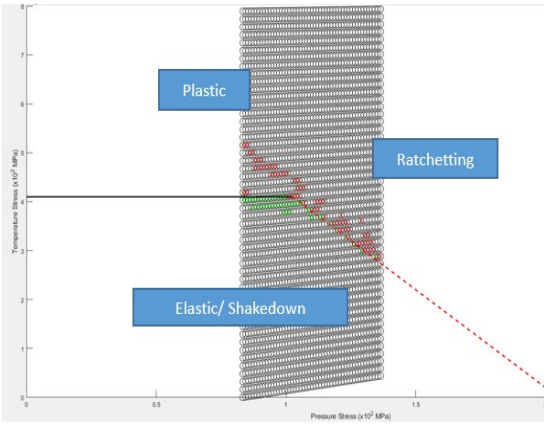


Figure 3.9. Comparison with Bree diagram of thin tube for Thickness = 1.2mm

From visualization, we can see that a that design falls *above* the green region is most likely to be safe and a good design. A design that falls *within* the green or red region is very close to the transition region and therefore recommended for further analysis. Any design that falls *below* the red region is most likely not a safe design, susceptible to creep-fatigue failure. The converged results of both scenarios from the proposed BO framework have been compared with the true solution (Bree Diagram of thin tube) in terms of pressure and temperature stresses in Figures 3.8 and 3.9. The grey shadowed part is the region of interest of our test cases where we show our predicted transition region (denoted by red and green) centered about the true transition line. We know from the Bree diagram that below the solid black and dashed red line is the Elastic/Shakedown (safe) region and above those are the Plastic and Ratchetting region (unsafe), respectively. The region of interest in Figure 3.8 does not cover the Ratchetting region; thus, we see the red region above the solid black line (towards the plastic region) and the green region below the solid black line (towards the elastic region). The region of interest is more complicated in Figure 3.9, since the region covers Elastic/Shakedown (below black and red dashed line), Plastic (above black line) and Ratchetting region (above red dashed line). It can be understood that due to a more

complex design response surface, the model took more training data (black dots) for the 1.2mm vs. the 1.7mm thickness to reach model convergence.

### *3.5.2. Classification error*

Next, we consider a randomly selected 100k new designs (test data) from Latin Hypercube sampling in the same design space for validation to classify between safe and unsafe region (Step 9 in Section 3.4). Tables 3.1 and 3.2 provide the confusion matrices for both the test scenarios with a classification error rate of 0.42% when $YS_{max}$= 0.45 and $YP_{min} = YR_{min}$= 0.55. We found some incorrect classifications as the BO model optimizes for a transition region rather than the true line. However, our assumption appears reasonable, as optimizing the model to locate the transition region provides efficient learning and high accuracy (error rate < 1%) in locating the true constraint boundary line.

Table 3.3 provides a summarization of the sensitivity analysis of the values of $YS_{max}, YP_{min}, YR_{min}$ in eqs. 3.11 – 3.13 in terms of the number of training data sampled and the accuracy of the model in terms of the classification of the new designs, considering the equivalent 100k test data and both values of thickness parameter of the thin tube after model convergence (Convergence 1). In this case study, from the sensitivity analysis, we can see best consistent accuracy of classification for both scenarios of thickness values when $YS_{max}$= 0.45 and $YP_{min} = YR_{min}$= 0.55 having a mean error rate of 0.55 and 0.52, respectively. However, considering the amount of training data sampled, a range of $YS_{max}$ between 0.45 to 0.48 and $YP_{min}, YR_{min}$ between 0.55 and 0.52 is good in terms of tradeoff between cost of training data and the accuracy of classification. However, beyond that range, we can see that either we have significant error rate (mean approx. 5.3%) or significant cost of training data (mean approx. 150-200) to reach the minimal error rate. Thus, when we attempt to locate the exact transition line (last two rows of Table 3.3) vs. a region, the model has the highest error rate (~ 5.3%) and requires much more sampling to reduce error, making the model inefficient.

| | *Safe (Actual)* | *Unsafe (Actual)* |
|---|---|---|
| *Safe (Model Estimated)* | 50328 | 359 |
| *Unsafe (Model Estimated)* | 58 | 49255 |

Table 3.1. Confusion matrix to classify between safe and unsafe region for Thickness = 1.7mm

| | *Safe (Actual)* | *Unsafe (Actual)* |
|---|---|---|
| *Safe (Model Estimated)* | 44603 | 352 |
| *Unsafe (Model Estimated)* | 64 | 54981 |

Table 3.2. Confusion matrix to classify between safe and unsafe region for Thickness = 1.2mm.

| $YS_{max}$ | $YP_{min}$ | **Thickness (mm)** | **# design samples (training data)** | **Error rate (%)** | **Mean Error Rate (%)** |
|---|---|---|---|---|---|
| 0.4 | 0.6 | 1.7 | 113 | 0.53 | 0.495 |
| 0.4 | 0.6 | 1.2 | 158 | 0.46 | |
| 0.43 | 0.57 | 1.7 | 78 | 0.47 | 0.485 |
| 0.43 | 0.57 | 1.2 | 134 | 0.5 | |
| 0.44 | 0.56 | 1.7 | 60 | 0.5 | 0.48 |
| 0.44 | 0.56 | 1.2 | 253 | 0.46 | |
| 0.45[a] | 0.55[a] | 1.7[a] | 67 | 0.42 | 0.42 |
| 0.45[a] | 0.55[a] | 1.2[a] | 120 | 0.42 | |
| 0.46 | 0.54 | 1.7 | 63 | 0.48 | 0.5 |
| 0.46 | 0.54 | 1.2 | 96 | 0.51 | |
| 0.47 | 0.53 | 1.7 | 31 | 0.58 | 0.52 |
| 0.47 | 0.53 | 1.2 | 120 | 0.46 | |
| 0.48 | 0.52 | 1.7 | 45 | 0.38 | 0.53 |
| 0.48 | 0.52 | 1.2 | 99 | 0.68 | |
| 0.49 | 0.51 | 1.7 | 31 | 1.39 | 0.935 |
| 0.49 | 0.51 | 1.2 | 99 | 0.48 | |
| 0.5 | 0.5 | 1.7 | 218 | 7.27 | 5.3 |
| 0.5 | 0.5 | 1.2 | 18 | 3.33 | |

Table 3.3. Summarization of the performance of the proposed BO model at different values of $YS_{max}, YP_{min}, YR_{min}$

*Note[a]: The results shown in Fig 3.8-3.13 consider use this region.*

Sensitive analysis has been presented in this chapter as preliminary study to see the effect of gap width (Table 3.3, col 2- col 1) on the model performance. Though we have seen some changes in the model classification accuracy, but that has mostly been overall <1% error rate. This shows the performance is not extremely sensitive to the

gap width and therefore, in general application, we can think of a standard value (not too wide or thin gap width) as the values provided in the sensitivity analysis. However, this chapter was focused on understanding the sensitivity and further research on the strategy to optimize the band width as a trade-off between model performance and cost has been considered in future scope.

### *3.5.3. Comparison to existing classification methods*

| **Methods** | **Thick-ness (mm)** | **Error rate (# Training data 2500, 2500)** [b] | **Mean Error Rate (%)** | **Error rate (# Training data 67, 120)** [c] | **Mean Error Rate (%)** |
|---|---|---|---|---|---|
| Proposed BO | 1.7 | NA | NA | 0.42 | 0.42 |
| | 1.2 | NA | NA | 0.42 | |
| SVM | 1.7 | 0.24 | 0.325 | 0.65 | 1.49 |
| | 1.2 | 0.41 | | 2.32 | |
| Random Forest | 1.7 | 0.56 | 0.56 | 0.57 | 0.72 |
| | 1.2 | 0.56 | | 0.86 | |
| Ada-Boosting | 1.7 | 0.85 | 3.39 | 0.85 | 9.15 |
| | 1.2 | 5.92 | | 17.45 | |

Table 3.4. Comparison of proposed BO with Existing Classification Methods

*Note[b]: Full matrix of 2500 samples used to train the SVM, RF and ADA for both scenarios of thickness parameter*

*Note[c]: Out of 2500 designs, only the 67 and 120 selected designs sampled from the proposed BO model are used to train the SVM, RF and ADA for both scenarios of thickness parameter respectively.*

Finally, Table 3.4 shows a comparison of our proposed method with other methods, such as a Support Vector Machine (SVM), Random Forest (RF) and Ada Boosting (ADA) [83]–[85], for classification between safe and unsafe designs among 100k randomly selected new thin tube designs, considering both thickness values. These existing methods were implemented using inbuilt function in R packages [118]–[120], with a radial kernel in SVM and 2000 trees (iterations) for ADA; the responses are provided as standard binary values (0-unsafe and 1-safe). At first, we use Latin Hypercube sampling to generate a full matrix, $\bar{\bar{\boldsymbol{X}}}$ (refer Section 3.4, Step 0), over the

design space as the training data (2500 samples) for the SVM, RF and ADA models. From results in Table 4, we can see in classification, SVM gives the best performance (err rate = 0.325) and ADA gives worst performance (err rate =3.39). Though SVM has lower error rate than our proposed BO method, it took much more sampling to train the models (2500 samples vs. 67 and 120 samples), thus causing a significant increase in experimental or function evaluation cost. Thus, we did another comparison where we used *only* the training data used, until convergence, of the proposed BO models to train the SVM, RF and ADA models. Using the minimal BO training data, our proposed method provides the best performance (err. rate = 0.42), while SVM gives much higher error rate of 1.5%, and ADA is the worst (err. rate = 9.15%). The detailed confusion matrices for classification using SVM, RF and ADA are provided in Appendix Table A.3.1-A.3.4. In this problem, as our main objective is to classify the design between safe and unsafe region, the BO model guides us to do more sampling towards the unknown transition region so that the surrogate GP model predict the output for a design with high accuracy close to the transition boundary than the designs which are far away from the transition boundary. This is because the designs closer to the boundary are more critical for mis-classification, thus higher prediction accuracy is required from GP model, thus higher sampling over that region has been recommended by the BO model. This is not true for the designs farther away from the transition boundary, since even with lower prediction accuracy, the designs still have lower likelihood to jump the threshold (refer Section 3.4, Step 10), and thus still have higher likelihood to fall under the true classification. Therefore, more sampling in such non-interesting region would be redundant considering the trade-off between experimental cost and model classification accuracy. Thus, with the strategic and adaptive sampling from BO model, we could see a minimal error rate with minimal training design samples (Table 3.4). Now, given the designs are safe, the goal for predicting the respective output with higher accuracy from the surrogate model in that safe design space towards finding the optimal design will be addressed in future research.

### 3.6. Conclusion and Future Research Scope

In this chapter, we have proposed the application of the Bayesian Optimization to locate the constraint boundary of at the transition region between safe and unsafe region for thin tube in terms of risk of creep fatigue failure under constant application of pressure and temperature stresses, and thereby use as a classification tool for evaluation of new designs as good or bad designs. As we have discussed, the constraint boundary in this problem also represents the discontinuity of the function (discontinuous transition region); the proposed strategy provides a way to tackle the discontinuous design space by projecting to an artificial continuous design space for better convergence of BO model. However, it is worthy to mention that once we obtain the required data (region and strain accumulation) for the design, the formulation of the distance function is not dependent upon the scale or complex design geometry as in 316SS DB-CHX (Figure A.3.2). The complexity arises on how those required data is obtained in complex design (eg. Finite element analysis). At each iteration, the model with prior knowledge of training data sampled from previous iterations updates the posterior predictive model. This informs the acquisition function to choose the design for sampling in the next iteration to maximize learning of the optimal region of the unknown function. However, unlike the standard BO model for maximization or minimization problems, our objective is to locate the unknown constraint boundary. Therefore, we reformulate our objective function as a distance function which helps us to recast our objective as a maximization problem where the maximum objective function value, or the new optimal region, is towards the true constraint boundary.

Our proposed BO approach does not have dependencies of having pre-existing training data as incorporating Bayesian knowledge into the optimization framework allows us to strategically select design samples to maximize the learning iteratively and minimize the overall cost for sampling for expensive function evaluations (training data) to achieve the desired level of accuracy. With the resulting small error rate, we have high likelihood that the model emulates the true constraint boundary and this will help us to continue our problem to the next stage (future research) to find the optimal design as we have higher confidence to preserve only feasible designs in term of Creep-fatigue failure. The next stage of research will be focused on the full framework will

be implemented in a complex high-dimensional 316SS DB-CHX (Figure A.3.2) design. In this problem, we use the results of the classification as an optimization pre-stage, where the design optimization problem considers application and manufacturing constraints.

## ACKNOWLEDGMENTS

This research was funded in part by DOE NEUP DE-NE0008533. The opinions, findings, conclusions, and recommendations expressed are those of the authors and do not necessarily reflect the views of the sponsor.

# APPENDIX A OF CHAPTER 3
FIGURES

A.1. Bree Diagram

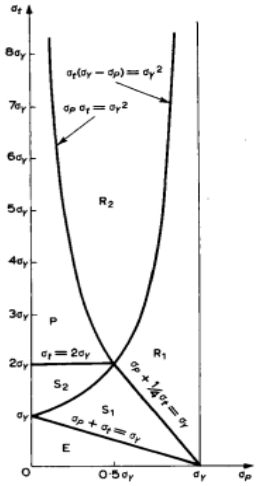


| Stress régime | Can behaviour |
|---|---|
| $R_1$ and $R_2$ | Ratchetting |
| $S_1$ and $S_2$ | Shakedown after first half-cycle |
| P | Plastic cycling |
| E | Elastic |

Figure A.3.1. Bree diagram of non-work-hardening material whose yield stress remain unchanged by the change in mean temperature [81]

A.2. 316 SS diffusion bonded Hybrid Compact Heat Exchanger

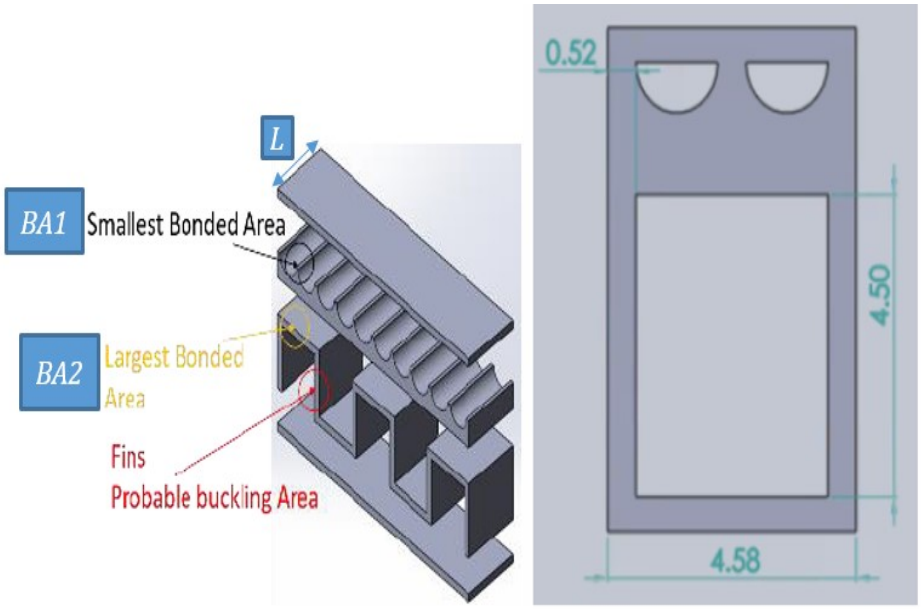


Figure A.3.2. (left) Hybrid Compact Heat Exchangers (H-CHX); (right) unit cell 2D view [82]

A.3. An example of discontinuity at the strain calculation of the thin tube (Numerically calculated from Bree diagram)

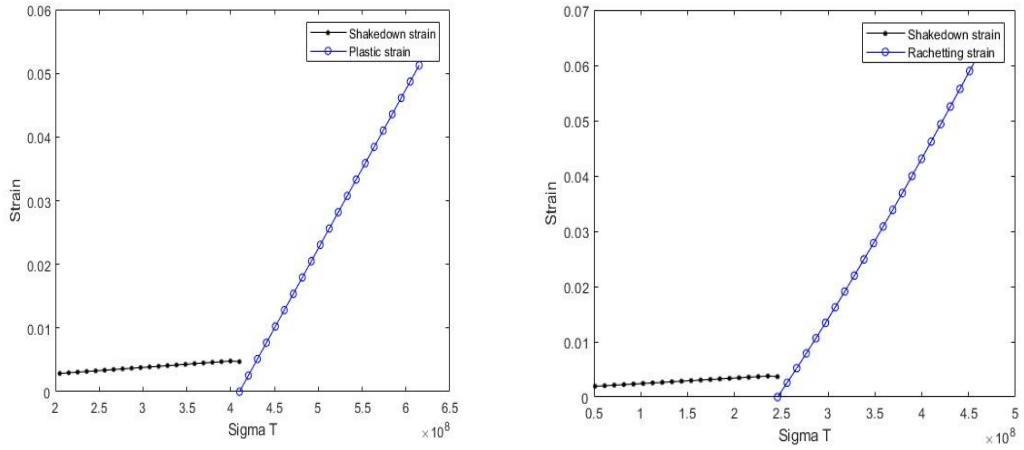


Figure A.3.3. 1D representation of the jump discontinuity at the strain level, considering constant $\sigma_p$ and variable $\sigma_t$; (left) at the transition between Shakedown and Plastic region for $\sigma_p = 82MPa$ where the discontinuity observed at $\sigma_t = 410\ MPa$; (right) at the transition between Shakedown and Ratchetting region for $\sigma_p = 143.5MPa$ where the discontinuity observed at $\sigma_t = 246\ MPa$

TABLES

Existing Method for Classification: Support Vector Machine(SVM), Random Forest and Ada-Boosting

Full Data Matrix in Step 1, used as Training Data (2500 samples)

| *Methods* | *SVM* | | *Random Forest* | | *Boosting* | |
|---|---|---|---|---|---|---|
| | *Safe (Actual)* | *Unsafe (Actual)* | *Safe (Actual)* | *Unsafe (Actual)* | *Safe (Actual)* | *Unsafe (Actual)* |
| *Safe (Model Estimated)* | 50370 | 222 | 50210 | 384 | 49768 | 618 |
| *Unsafe (Model Estimated)* | 16 | 49392 | 176 | 49230 | 232 | 49382 |

Table A.3.1 Confusion matrix to classify between safe and unsafe region for Thickness = 1.7mm (err rate = 0.24%, 0.56%, 0.85%)

| *Methods* | *SVM* | | *Random Forest* | | *Boosting* | |
|---|---|---|---|---|---|---|
| | *Safe (Actual)* | *Unsafe (Actual)* | *Safe (Actual)* | *Unsafe (Actual)* | *Safe (Actual)* | *Unsafe (Actual)* |
| *Safe (Model Estimated)* | 44471 | 213 | 44428 | 320 | 43354 | 1313 |
| *Unsafe (Model Estimated)* | 196 | 55120 | 239 | 55013 | 4605 | 50728 |

Table A.3.2. Confusion matrix to classify between safe and unsafe region for Thickness = 1.2mm (err rate = 0.41%, 0.56%, 5.92%)

Training Data are ONLY sampled from proposed BO till convergence, where $YS_{max}$= 0.45 and $YP_{min} = YR_{min}$= 0.55 (refer Table 3)

| *Methods* | *SVM* | | *Random Forest* | | *Boosting* | |
|---|---|---|---|---|---|---|
| | *Safe (Actual)* | *Unsafe (Actual)* | *Safe (Actual)* | *Unsafe (Actual)* | *Safe (Actual)* | *Unsafe (Actual)* |
| *Safe (Model Estimated)* | 49950 | 210 | 50241 | 427 | 49768 | 618 |
| *Unsafe (Model Estimated)* | 436 | 49404 | 145 | 49187 | 232 | 49382 |

Table A.3.3. Confusion matrix to classify between safe and unsafe region for Thickness = 1.7mm (err rate = 0.65%, 0.57%, 0.85%)

| *Methods* | *SVM* | | *Random Forest* | | *Boosting* | |
|---|---|---|---|---|---|---|
| | *Safe (Actual)* | *Unsafe (Actual)* | *Safe (Actual)* | *Unsafe (Actual)* | *Safe (Actual)* | *Unsafe (Actual)* |
| *Safe (Model Estimated)* | 42611 | 263 | 44259 | 447 | 27680 | 16987 |
| *Unsafe (Model Estimated)* | 2056 | 55070 | 408 | 54886 | 467 | 54866 |

Table A.3.4. Confusion matrix to classify between safe and unsafe region for Thickness = 1.2mm (err rate = 2.32%, 0.86%, 17.45%)

# CHAPTER 4

## A MO-Bayesian Optimization Approach Using the Weighted Tchebycheff Method

**Authors:**

**Arpan Biswas**

Department of Mechanical Engineering

Oregon State University

Corvallis, Oregon 97331

biswasar@oregonstate.edu

**Claudio Fuentes**

Department of Statistics

Oregon State University

Corvallis, Oregon 97331

fuentesc@oregonstate.edu

**Christopher Hoyle**

Department of Mechanical Engineering

Oregon State University

Corvallis, Oregon 97331

chris.hoyle@oregonstate.edu

Chapter 4 manuscript is issued in below conference and journal:

**Proceedings of the ASME 2020**

**ASME International Mechanical Engineering Congress and Exposition**

**IMECE2020**

**November 16-19, 2020**

**Status: Published**

**Journal of Engineering Design, ASME**

**Paper No. MD-20-1759**

**Status: In Review**

**ABSTRACT**

*Bayesian optimization (BO) is a low-cost global optimization tool for expensive black-box objective functions, where we learn from prior evaluated designs, update a posterior surrogate Gaussian process model, and select new designs for future evaluation using an acquisition function. This research focuses upon developing a BO model with multiple black-box objective functions. In the standard Multi-Objective optimization (MOO) problem, the weighted Tchebycheff method is efficiently used to find both convex and non-convex Pareto frontiers. This approach requires knowledge of utopia values before we start optimization. However, in the BO framework, since the functions are expensive to evaluate, it is very expensive to obtain the utopia values as a prior knowledge. Therefore, in this chapter, we develop a MO-BO framework where we calibrate with multiple linear regression (MLR) models to estimate the utopia value for each objective as a function of design input variables; the models are updated iteratively with sampled training data from the proposed multi-objective BO. This iteratively estimated mean utopia values is used to formulate the weighted Tchebycheff multi-objective acquisition function. The proposed approach is implemented in optimizing thin tube geometries under constant loading of temperature and pressure, with minimizing the risk of creep-fatigue failure and design cost, along with risk-based and manufacturing constraints. Finally, the model accuracy with frequentist, Bayesian and without MLR-based calibration are compared to true Pareto solutions.*

## 4.1. Introduction

In the early design phase, it is very important for the designers to be able to identify potential good design decisions in the large design space while the design cost is low. This helps the designers to easily eliminate the undesirable designs and avoid investing in high cost manufacturing and testing of those designs at the later design phase. In practice, most of the design problems are too complex to be handled by simple optimization frameworks due to having constraints in cost, time, formulation, etc. Also, approximating a complex design problem into much simpler problems can lead to the disregard of original complex constraints; thus it can violate such constraints and not

be a useful approach for practical decisions. Some practical design problems have been investigated where complex optimization frameworks have been modeled [1], [2], [77]. However, in many design optimization problems, it is difficult to numerically formulate an objective function and therefore we consider those problems having a *black box* objective function with high function evaluation cost due to limited resources, tools, time, etc. Thus, a trade-off between learning and expense is likely; therefore, a low-fidelity surrogate model is developed to reduce the cost. When we have no/limited knowledge on the expensive true objective function, we cannot guarantee the maximization of our learning towards an optimal solution without proper guidance or expertise. Also, due to the mentioned high function evaluation cost, exhaustive search is not a valid option. In such black box engineering design problems, a Bayesian Optimization technique (BO), which eliminates the need of standard formulation of objective functions [101]–[103], is widely applied in sequential learning to provide better guidance in sampling the designs for expensive experiments or function evaluations in order to find the optimal region of the unknown function at minimal cost of experiments. In this approach, we first build a posterior surrogate model, given the data from the current evaluations. We then use this model to strategically select the best design locations for future evaluations by maximizing the acquisition functions, defined from the posterior model.

#### *4.1.1. Research motivation*

In the design of mechanical components under temperature and pressure cycling, such as heat exchangers, the design decisions are defined as optimal geometries which focuses on multiple objectives, such as minimizing the risk of creep-fatigue failure and the design cost under continuous cycling of temperature and pressure. The stated risk depends on the location of the design material state, such as within the Elastic, Shakedown, Plastic or Ratchetting region. An example has been provided for thin tubes where the location of the design can be numerically represented from a Bree Diagram [81] (Figure in Appendix A.4.1) in terms of pressure and thermal stresses. Under cyclic loading, the Elastic and Shakedown region in the Bree diagram are considered as the safe region where no strain accumulation occurs or the growth of residual strain is

practically diminishing when sufficient loading cycles are applied. However, Plastic and Ratchetting in the Bree diagram are unsafe designs where the plastic strain accumulates until failure. The cost of the design involves the total cost in the entire design process and thus can be based on material, component, manufacturing, assembly and quality checking. When the complexity of the design increases like in compact heat exchangers [82], we cannot provide a numerical representation of the function which defines the location of designs. Also, considering different costs in the design process makes the cost function hard to formulate. This makes both the objectives such as risk and cost functions to be black-box functions, representing the problem as black-box multi-objective design problem.

In the standard multi-objective problem, the *Weighted Tchebycheff* method [71], [73], a global criterion method, is used to find the Pareto frontier to identify every Pareto-optimal solution from both convex and non-convex regions of the frontier. In a minimization problem, a point $x^*$ in the feasible design space S is Pareto Optimal if and only if there does not exist another point $x$ in the set S that gives a lower minimum objective function for at least one of the objectives $f_i(x) < f_i(x^*)$ without sacrificing the others $f_j(x) \leq f_j(x^*)$. However, this approach requires knowledge of utopia values, i.e., optimal values of each objective independently, before we start optimization. Thus, for a multi-objective optimization problem having two objectives, we need to solve three optimization problems with three different objective functions: one problem with objective function 1 (finding utopia 1); one problem with objective function 2 (finding utopia 2); and finally the multi-objective function. It is obvious that with $n$ objectives, the number of optimization problems increases to $n$+1. In the BO framework, since the objective functions are black-box and expensive to evaluate, it is very expensive to conduct so many optimizations to obtain the utopia values as a priori knowledge. One way we can mitigate this issue is by providing a rough approximation of global minimum or maximum values of the single objective problems [121], [122]. For example, the global minimum values of risk and cost could be zero. However, the value might not be feasible due to different manufacturing and design constraints and therefore are not the true utopia values. As in figure 4.1, we can see as we deviate from

true utopia values (u`) in the X or Y directions, we cannot find the true optimal solution (C) for a specific weighting factor (w) and fall into a different location at C`, further minimizing one objective function at the expense of the other. Thus, providing an incorrect utopia values can lead to a deviation from the true Pareto-optimal solutions and will not represent the desired trade-off between the objectives. This motivates us to predict the utopia values using low-cost statistical regression models instead of guessing. This helps to have better prediction of utopia values, thereby increasing the accuracy to fall into at least a better local optimal solution at negligible computational cost

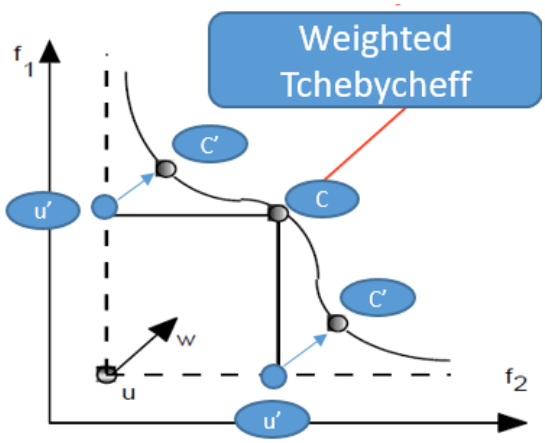


Figure 4.1. Incorrect utopia values leading to deviate from true pareto-optimal solution

### *4.1.2. Research contribution*

The main goal in this chapter is to propose an approach to properly utilize the existing BO training data to predict the utopia values, rather than using a fixed educated guess (global solution). In this chapter, we focus on linear regression models to predict the utopia values; however, the proposed approach can be extended to implement any linear or non-linear regression models based on the complexity of the problem. To better illustrate the approach, we have simplified the large scale complex design of a heat exchanger into a simple thin tube where we will be able to compare the results obtained from the proposed model with the known true solutions. The road-map of this chapter is as follows. Section 4.2 provides an overview on Bayesian optimization, multi-objective optimization, and linear regression modeling using frequentist and

Bayesian approaches, and model calibration and validation. Section 4.3 talks more on the thin tube problem and the formulation of the objectives and constraint functions along with the detailed description of the multiple linear regression modelling. Section 4.4 provides the algorithm of the proposed MO-BO framework. Section 4.5 shows the results of the proposed approach with detailed comparison. Section 4.6 concludes the chapter 4 with final thoughts.

## 4.2. Background

In this section, we provide literature reviews on Bayesian optimization (BO) in single and multi-objective settings, different methods for formulating multi-objective functions, and developing multiple linear regression models in frequentist and Bayesian approaches.

### *4.2.1. Bayesian optimization*

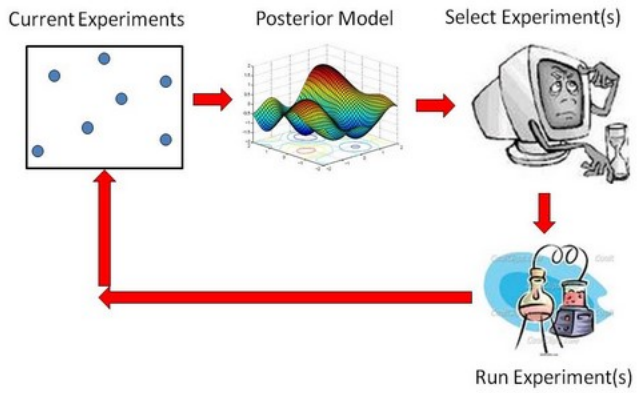


Figure 4.2. Bayesian Optimization Framework [106]

Bayesian optimization [7] (BO) is an emerging field of study in the Sequential Design Methods. It has been considered as a low-cost global optimization tool for design problems having expensive black-box objective functions. The general idea of BO is to emulate an expensive unknown design space and find the local and global optimal locations while reducing the cost of function evaluation from expensive high-fidelity models. This approach has been widely used in many machine learning problems [92]–[96]. However, attempts have been made when the response is discrete such as in

consumer modeling problems where the responses are in terms of user preference [7], [97]. The idea is to approximate the user preference discrete response function into continuous latent functions using Binomial-Probit model for two choices [98], [99] and polychotomous regression model for more than two choices where the user can state no preference [100]. BO has also been implemented in multi-objective [101] and high dimensional [102], [103] engineering design problems.

BO adopts a Bayesian perspective and assumes that there is a prior on the function; typically, we use a Gaussian process prior. The prior is represented from the experiment or training data which is assumed as the realizations of the true function. The overall Bayesian Optimization Approach has two major components: A predictor or *Gaussian Process Model (GPM)* and an *Acquisition Function (AF)*. As shown in figure 4.2, in this approach, we first build a posterior GPM, given the data from the current experiments. The surrogate GPM then predicts the objective or response of the samples generated from a DOE based sampling method within the design space. We then use this model to strategically select the best design locations for future experimentation by maximizing the acquisition functions, defined from the posterior simulations which is obtained from the GPM. However, we need to assume that the objective or response is Lipschitz continuous [7]. As an alternative to a GPM, random forest regression has been proposed as an expressive and flexible surrogate model in the context of sequential model-based algorithm configuration [104]. Although random forests are good interpolators in the sense that they output good predictions in the neighborhood of training data, they are very poor extrapolators where the training data are far away [105]. This can lead to selecting redundant exploration (more experiments) in the non-interesting region as suggested by the acquisition function in the early iterations of the optimization, due to having additional prediction error of the region far away from the training data. This motivates us to consider the GPM in a Bayesian framework while extending the application to discontinuous design response surfaces, which can be represented as complex practical problems in the domain of experimental design. We next describe the GPM and AF.

*4.2.1.1.Gaussian process model (GPM)*

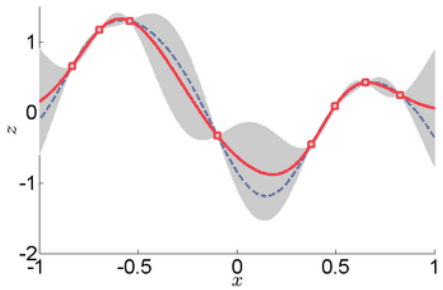


Figure 4.3. 1D Gaussian Process (from Wikipedia)

Figure 4.3 shows a simple 1D *Gaussian Process Model* with one design variable $x$ and one response variable $z = f(x)$. The dots are the experimental design variables and the dotted and solid lines are the true and the predictor mean functions or responses in the design space, given the observations. The shaded area along the solid line shows the measure of uncertainty over the surrogate GPM prediction. We can clearly see that the variance near the observations is small and increases as the design samples are farther away from the observational data, thereby related to kriging models where the errors are not independent. Much research has been ongoing regarding incorporating and quantifying uncertainty of the experimental or training data by using a nugget term in the predictor GPM. It has been found that the nugget provides better solution and computational stability framework [107], [108]. Furthermore, GPM has also been implemented in high dimensional design space exploration [109] and BIG DATA problems [110], as an attempt to increase computational efficiency. A survey of implementation of different GP packages has been provided in different coding languages such as MATLAB, R, Python [111].

*4.2.1.2.Acquisition function (AF)*

The second major component in Bayesian optimization is the Acquisition Function whose goal is to guide the search for future experiments towards the desired goal and thereby bring the sequential design into the BO. The AF predicts an improvement metric for each sample. The improvement metric depends on *exploration* (unexplored design spaces) and *exploitation* (region near high responses). Thus, the acquisition

function gives high value of improvement to the samples whose mean prediction is high, variance is high, or a combination of both. Thus, by maximizing the acquisition function, we select the best samples to find the optimum solution and reduce the uncertainty of the unknown expensive design space. Throughout the years, various formulations have been applied to define the acquisition functions. One such method is the *Probability of Improvement*, PI [112] which is improvement based acquisition function. Jones in [113] notes that the performance of PI(·) "is truly impressive;… however, the difficulty is that the PI(·) method is extremely sensitive to the choice of the target. If the desired improvement is too small, the search will be highly local and will only move on to search globally after searching nearly exhaustively around the current best point. On the other hand, if the small-valued tolerance parameter $\xi$ in PI(.) equation is set too high (see [113]), the search will be excessively global, and the algorithm will be slow to fine-tune any promising solutions." Thus, the *Expected Improvement* acquisition function, EI [7], is widely used over PI which is a trade-off between exploration and exploitation. Another Acquisition function is the *Confidence bound criteria*, CB, introduced by Cox and John [114], where the selection of points is based on the upper or lower confidence bound of the predicted design surface for maximization or minimization problem respectively. In multi-objective BO problems, *Expected Improvement Hyper-volume* (EIHV) acquisition functions have been modeled to provide better performance [10], [11]. However, to increase the computational efficiency, Yang et al. [123] modified the EIHV acquisition function into the *Expected Hyper volume gradient-based* (EIHVG) acquisition function and proposed an efficient algorithm to calculate it. To reduce the computational cost, other acquisition functions like the *Max-value Entropy Search* (MESMO) [124] and *Predictive Entropy Search* (PESMO) [125] have been formulated. Abdolshah et. al. [126] proposed a multi-objective BO framework with preference over objectives on the basis of stability and attempting to focus on the Pareto front where preferred objectives are more stable.

#### *4.2.2. Multi-objective optimization*

The numerical optimization problems can be classified on the basis of number of objective functions as Single (SOO) and Multi-Objective Optimization problems (MOO). MOO is the extension of SOO with having more than one objectives as equation 4.1.

$$\min f(\boldsymbol{X}) = [\min f_1(\boldsymbol{X}), \min f_2(\boldsymbol{X}), \ldots . \min f_n(\boldsymbol{X})] \; s.t \; X \in \mathbb{R} \tag{4.1}$$

It is obvious that SOO is relatively simpler with lower computational cost; however, in practical problems it may be a challenge to formulate a single objective problem and therefore, much focus has been given on Multi-Objective Optimization methods (MOO). The question we want to solve in any MOO is the optimal design decisions under user defined preferences of objectives; optimal solutions at different trade-offs of objectives are represented by a *Pareto frontier*. The methods to solve MOO problems can be classified into *a priori* and *a posteriori* Methods. The most fundamental *a priori* method is the *Weighted Sum Method* (WS) [127] where we transform all the objectives into a single objective of weighted objectives. The method though simple and fast, is inefficient to find the true pareto-optimal points, mainly in the non-convex region. To increase the performance, a global criterion method, the *Weighted Tchebycheff method* (WTB) [71]–[73] is introduced where the multi-objectives are combined into a weighted distance metric that guarantees finding all the Pareto-optimal solution. Another a priori method is the *$\epsilon$-Constraint method* where the most critical objective is picked and treated as a single objective problem where the other objectives treat as constraints [128]. Another a priori method is the *Lexicographic method* where the objective functions are organized sequentially in order of preferences [129]. Some posterior methods used in MOO problems are *Vector Evaluated Genetic Algorithm* (VEGA) [130], *Niche Methods* [131], *Particle Swarm Algorithm* (PSO) [132], *NGSA 2* [133], etc. Readers can view [127], [134] for the application in practical multi-objectives design problems using the above mentioned priori and posteriori methods, as well as ref. [135] for additional methods. It is a challenging task to pick a best method, as the performance of the methods depend on the problems and its constraints on dimension, formulation, computational cost, uncertainty in design etc. In this chapter, we choose to focus on *Weighted Tchebycheff* method in formulating the

proposed multi-objective BO framework. Details of the method will be provided in the later section 4.3.

### *4.2.3. Multiple linear regression modelling*

In this section, we provide some background on Multiple linear regression (MLR) which can be defined as the dependent response or objective variables as the linear function of the independent explanatory or design input variables. It is a statistical procedure to predict the values of a response variable from a collection of explanatory variable values, given the experimental data of another collection of explanatory variable. Thereby, the statistical model reduces the cost of extensive real experiments, and therefore, can also be thought of as surrogate modeling and helps in large scale studies at much cheaper cost. The general formulation of MLR is given below as equation 4.2.

$$\mu(Y|\boldsymbol{X}) = \beta_0 + \beta_1 X_1 + \cdots + \beta_p X_p \tag{4.2}$$

where $\mu(Y|\boldsymbol{X})$ denotes the mean of the response variable Y in terms of the set of p explanatory variables $\boldsymbol{X} = [X_1, \ldots X_p]$. If a linear model is used, the following assumptions should be met: the response variables should be linearly dependent (linearity assumption) and normally distributed (normality assumption) to each explanatory variable; the variance of the residual error should be constant throughout the values of explanatory variables; lastly, the observations or the experiments should be independent. The response variables should be continuous whereas the explanatory variables can be both discrete and continuous. Kuiper [136] applied multiple regression models to predict the car values based on mileage, make, model, engine size, interior style, and cruise control. Timothy [137] presented a research on multiple regression analysis to identify the impact of length of superintendent longevity, continuity, and tenure in New Jersey School Districts on student achievement. Regression modelling has also been researched on machine learning problems [138], experimental design [139], observational studies in medical science [140]. Not only in prediction, but also the model is extensively used in making inferences [141] on the relationship between response and explanatory variables. The general model in equation 4.2 corresponds to the frequentist approach, however, a different version of the MLR model is the

Bayesian Multiple Linear Regression (BMLR) model. Unlike in MLR, BMLR has a prior distribution of $\boldsymbol{\beta}$ co-efficient, generally a normal or Gaussian prior distribution $p(\boldsymbol{\beta})$, a likelihood function $\ell(Y|\boldsymbol{X},\boldsymbol{\beta})$ which is the regression model, and a posterior distribution, $p(\boldsymbol{\beta}|Y,\boldsymbol{X})$. The posterior distribution can be formulated as equation 4.3.

$$p(\boldsymbol{\beta}|Y,\boldsymbol{X}) \propto \ell(Y|\boldsymbol{X},\boldsymbol{\beta})p(\boldsymbol{\beta}) \tag{4.3}$$

O. Seidou et. al [142] presented a Bayesian Linear Regression model in the study of hydrology and climate science for better performance in sudden change of relationship between key variables due to sudden climatic or environmental changes. Tao and Elaine [143] presented a Bayesian linear regression in Spectroscopic calibration. Bayesian framework has also been attempted in experimental design [144] and multi-scale regression problems [145]. Likewise, in MLR, BMLR models can also be used for making Bayesian inferences [146]. In this chapter, have investigated and implemented both MLR and BMLR models in formulating the proposed multi-objective BO framework. Details of the formulation and implementation of MLR into MO-BO will be provided in the later section 4.3, 4.4.

#### *4.2.4. Model calibration and validation*

In the data-driven modeling approach, the performance of the model can be improved by tuning the unknown model parameters based on how closely they represent the real complex expensive designs. This tuning of model parameters is *model calibration* while the measurement of the performance of the model after calibration, by comparing the model solution with the true solution, is the *model validation*. Adequate true data is desired for model calibration and validation; however, getting true data can be very expensive and sometimes not possible in complex design problems. Due to the use of true data in model calibration and validation, it is necessary for the designer to know which parameters are likely to be more sensitive to the model before they start collecting true data. Calibrating and validating a model for any insensitive (minimal sensitive) model parameters will multiply the cost of true data collection. Thus, a sensitivity analysis should be done between the model parameters to observe the relationship between input and output functions [147], [148] by conducting a study with limited existing true data, or approximated model data, or solely on the knowledge

of the designers. Regression analysis is one of the low-cost statistical tools for sensitivity analysis which gives the variation of the output to the inputs. Finally, assuming true data from expensive evaluations, model calibration and validation can be done iteratively until designers find the best model parameter values, satisfying the model overall performance in terms of the trade-off between model accuracy and cost of data sampling. Model calibration and validation becomes further challenging when we have uncertainty on the model parameters and/or the true output values [149]. In such cases, a distribution of the model parameter is considered instead and distribution of the model output is validated with true values (if the true outputs are known and fixed) or the true distribution of the outputs (if the true outputs are known but uncertain). When we do not know the true distribution of the uncertain outputs, model validation is challenging and expert knowledge is required. Reviews of different techniques for model calibration and validation, considering the availability of true data and the model input-output uncertainty is provided in these papers [150].

### 4.3. Problem Description

In this section, we describe the thin tube design problem which provides the proof of concept for a larger complex design problem, such as a compact heat exchanger. As the tube is assumed to undergo constant loading of temperature and pressure, there will be risk of creep-fatigue failure which will vary with the design geometry. Fatigue damage is defined as cycling a test specimen at some fixed stress amplitude for enough cycles that it will develop micro-structural damage and eventually fail. Creep damage is defined as holding a test specimen at a fixed load for a long enough time that eventually it will develop micro-structural damage and fail. Creep-fatigue damage is therefore to do both of these simultaneously (e.g. a stress controlled cycle with a hold) such that the specimen will generally fail sooner than doing the cycling or holding individually. In our problem, we choose the design variables as radius (R), length (L), and thickness (t) of the tube. Next we overview the experimentation, the regression modeling and the formulation of the multi-objective function and the constraints which depend on the experimental results and the regression models.

### *4.3.1. Experiments*

In this section, we provide a short overview of the experimental procedure. To formulate the objective of risk of creep-fatigue failure, we need to find the location of any design in terms of Elastic, Plastic, Shakedown and Ratchetting, and the respective strain accumulation. We represent these outputs as the responses from the expensive experiments. In this chapter, we considered the Bree diagram for a non-work-hardening material whose yield stress remains unchanged by changes in mean temperature as provided in Appendix A.4.1. For the sake of simplicity, we have ignored the further division of Shakedown (S1, S2) and Ratchetting (R1, R2) as shown in the figure, and assumed a single region of Shakedown (S) and Ratchetting (R), because the design risks are equivalent in the S1 and S2, and R1 and R2 regions, respectively. The three major steps we follow in the procedure are 1) Calculate Pressure and Temperature Stress of the design point, 2) Determine the region of the design in terms of Elastic, Plastic, Shakedown and Ratchetting and 3) Calculate the strain accumulation based on the location of the design. The detailed computation of the whole process for the thin tube can be found in our earlier chapter [Section 3.3.1, chapter 3]. In thin tube design, though these computations are not expensive and can be done analytically, we still represent these as expensive function evaluations which will be true in our future problem of considering a compact heat exchanger where expensive *Finite Element Analysis* (FEA) is required.

### *4.3.2. Formulation of objective function and constraints*

In this section, we provide the formulation of the proposed multi-objective objective function and the manufacturing and other design constraints.

#### *4.3.2.1.Multiple objectives for the thin tube problem*

In this section, we discuss the objectives considered in the problems. The first objective is the distance function, $Y_1$, which is defined on the location of the design and the respective strain values. The quantification of the distance function was the scope of chapter 3, and therefore, we provided a short overview in this chapter to help the reader to understand. We would encourage the readers to look into [Section 3.3.2, chapter 3] for detailed computation and explanation. The general idea is to create a distance metric

which gives a higher value (towards 1) as the designs moves toward the unsafe region (Plastic and Ratchetting), posing a higher risk of creep fatigue failure under constant loading of temperature and pressure. Alternatively, the distance metric gives a lower value (towards 0) as the designs moves toward safe region (Elastic and Shakedown) and the distance metric, $Y_1 \approx 0.5$ gives an indication that the design is close to the transition between the *safe* and *unsafe* region. Since our goal is to minimize the risk of creep-fatigue failure, we minimize the distance function. Thus, our objective 1 is defined as below:

$$\min_{R,L,t} Y_1 = \min_{R,L,t} f(\psi, \xi, k) \tag{4.4}$$

Equation (4.4) is the distance function which measures the risk of creep-fatigue failure where $\psi \in \Psi$ is the region (elastic, shakedown, plastic and ratchetting) within the design space $\Psi$; $\xi$ is the total strain accumulation; $k$ is the $k^{th}$ iteration of the BO model. It is to be noted that in each iteration, with more experimental or training data (increase prior knowledge), the distance value for all the training data is re-evaluated.

The next objective is the cost function, $Y_2$, which is defined in our problem as the material cost of the tube. For the sake of simplicity and he numerical computation, we focus upon the material cost only. Another reason to include the material cost is that intuitively, we can think of having more material in the tube generally leads to stronger design and minimizes the risk of creep-fatigue failure but increase the cost of the design. Thus, we have a trade-off between risk and material cost. It is to be noted, our proposed MO-BO model has the flexibility to add any other cost as part of our objectives, which can be a black box function in the complex design. Thus, our objective 2 is defined as below:

$$\min_{R,L,t} Y_2 = \min_{R,L,t} P\rho V = \min_{R,L,t} P\rho\pi tL(2R - t) \tag{4.5}$$

$P$ is the material cost per $kg$, $\rho$ is the density of the material, $V$ is the total volume of the tube.

*4.3.2.2. Linear regression models for the thin tube problem*

In this section, we provide the formulation of multiple linear regression models with both frequentist and Bayesian approaches, and the prediction of utopia values. These

models are used for calibration to get the estimate of the utopia for better representation of the true solutions. As we have already discussed earlier (fig. 4.1) how the utopia values affect the accuracy of the weighted Tchebycheff Pareto-optimal solutions and we proceed to approximate the unknown utopia values for our black-box problem. Thus, after we complete the experimental procedure and formulate both objectives, the next step is to find the utopia values for both objectives. The utopia values of an objective function are the optimal value of the objective, if each objective function is optimized independently of the other objectives. Thus, in our problem, to start the multi-objective optimization, we need to run two separate optimizations to find the utopia values. However, as we mentioned, this is not desirable if we have black-box functions as we cannot run expensive experiments based on three BO models. Also, predicting the utopia from the surrogate GP model of proposed MO-BO is not ideal since the data is sampled based upon finding the optimal region of the different trade-offs of the multi-objective function, not for finding the optimal region of the individual objectives. Thus, the proposed MO-BO model, with iterations, does not provide a guarantee of sampling designs towards the independent optimal region (utopia) of each objective. In such cases when there are limited samples at the individual optimal region of the objective functions, since the error in GP is not independent, there is a likelihood of bad and/or no improvement in estimating utopia. Thus, in this section, we propose the formulation of error independent linear regression models in order to predict the utopia values, given the same experimental data we sampled from the multi-objective BO model. Since the objectives are assumed independent with each other during the computation of utopia, we defined two independent models, one for each objective. We considered a full additive model per Eqn. (4.6) and (4.7), where both the objectives are a function of all predictor design variables (R, L and t). It is also to be noted that the models do not need to have the same predictor design variables and the decision of one regression model selection should be independent of the other models.

$$\widehat{\mu_k}(Y_1|R,L,t) = \hat{\beta}_{0,1,k} + \hat{\beta}_{1,1,k}R + \hat{\beta}_{2,1,k}L + \hat{\beta}_{3,1,k}t \tag{4.6}$$

$$\widehat{\mu_k}(Y_2|R,L,t) = \hat{\beta}_{0,2,k} + \hat{\beta}_{1,2,k}R + \hat{\beta}_{2,2,k}L + \hat{\beta}_{3,2,k}t \tag{4.7}$$

where $\widehat{\boldsymbol{\beta}}_{.,\mathbf{1},\boldsymbol{k}} = \left(\hat{\beta}_{0,1,k},\ \hat{\beta}_{1,1,k},\ \hat{\beta}_{2,1,k},\ \hat{\beta}_{3,1,k}\right)^T$ ; $\widehat{\boldsymbol{\beta}}_{.,\mathbf{2},\boldsymbol{k}} = (\hat{\beta}_{0,2,k},\ \hat{\beta}_{1,2,k},\ \hat{\beta}_{2,2,k},\ \hat{\beta}_{3,2,k})^T$ are the vectors of estimated regression co-efficient for objective Eqn. (4.6) and (4.7) respectively at iteration k of the MO-BO model; $\hat{\mu}(.|R, L, t)$ is the mean of the estimated objective function.

In the Bayesian approach, the estimation of regression coefficients for $i^{th}$ objectives and $k^{th}$ iteration of the MO-BO model, $\widehat{\boldsymbol{\beta}}_{.,\boldsymbol{i},\boldsymbol{k}} = \left(\hat{\beta}_{0,i,k},\ \hat{\beta}_{1,i,k},\ \hat{\beta}_{2,i,k},\ \hat{\beta}_{3,i,k}\right)^T$ are complex as we need to formulate the prior $p(\boldsymbol{\beta})$, likelihood function $\ell(Y|\boldsymbol{X}, \boldsymbol{\beta})$, and posterior distribution $p(\boldsymbol{\beta}|\boldsymbol{X}, Y)$. For BMLR, we set Gaussian (or normal) priors in eqns. 4.8, 4.9:

$$p\left(\boldsymbol{\beta}_{.,1,k}\right) \sim \boldsymbol{MVN}\left(\widehat{\boldsymbol{\mu}}_{\boldsymbol{\beta}_{.,1,k-1}}, \widehat{\boldsymbol{cov}}^{\mathbf{2}}_{\boldsymbol{\beta}_{.,1,k-1}} \boldsymbol{I_{p+1}}\right) \tag{4.8}$$

$$p\left(\boldsymbol{\beta}_{.,2,k}\right) \sim \boldsymbol{MVN}\left(\widehat{\boldsymbol{\mu}}_{\boldsymbol{\beta}_{.,2,k-1}}, \widehat{\boldsymbol{cov}}^{\mathbf{2}}_{\boldsymbol{\beta}_{.,2,k-1}} \boldsymbol{I_{p+1}}\right) \tag{4.9}$$

Therefore, the posterior distribution is defined as equations 5.18, 5.19:

$$p\left(\boldsymbol{\beta}_{.,1,k}\middle|Y_1, R, L, t\right) \propto l_k\left(Y_1\middle|R, L, t, \boldsymbol{\beta}_{.,1,k}\right)\ p\left(\boldsymbol{\beta}_{.,1,k}\right) \tag{4.10}$$

$$p\left(\boldsymbol{\beta}_{.,2,k}\middle|Y_2, R, L, t\right) \propto l_k\left(Y_2\middle|R, L, t, \boldsymbol{\beta}_{.,2,k}\right)\ p\left(\boldsymbol{\beta}_{.,2,k}\right) \tag{4.11}$$

where $\widehat{\boldsymbol{\mu}}_{\boldsymbol{\beta}_{.,1,k-1}}, \widehat{\boldsymbol{\mu}}_{\boldsymbol{\beta}_{.,2,k-1}}, \widehat{\boldsymbol{cov}}^{\mathbf{2}}_{\boldsymbol{\beta}_{.,1,k-1}} \boldsymbol{I_{p+1}},\ \widehat{\boldsymbol{cov}}^{\mathbf{2}}_{\boldsymbol{\beta}_{.,2,k-1}} \boldsymbol{I_{p+1}}$ are the estimated means and the variances, respectively, of the beta parameters for objectives 1 and 2 at iteration $k-1$ of the MO-BO model. $\boldsymbol{I_{p+1}}$ is the $(p+1)$ identity matrix where $p$ is the number of input design variables. Thus, the general idea is to compute the posterior distribution of the regression coefficients at the current iteration of MO-BO model; the respective prior distribution is taken as the posterior distribution of the regression coefficients at the previous iteration. Thus unlike the frequentist approach, in the Bayesian framework we consider both the knowledge of experimental or training data and the prior knowledge of the estimate of regression coefficients parameters. More details on the workflow of the proposed MO-BO model will be explained in Section 4.4.

Now, once the regression models are developed with the sampled training data, the next step is to predict the objectives, given a new set of unsampled design data (say $R_f, L_f, t_f$) which are not sampled from expensive experiments or function evaluations. As we want to minimize the objectives (Eqn. 4.4, 4.5), therefore, the estimated utopia

values at iteration $k$, will be the minimum predicted mean values per Eqn. (4.12) and (4.13).

$$\hat{\mu}_k(u_1) = \min(\widehat{\mu_k}(Y_1|R_f, L_f, t_f)) \quad (4.12)$$

$$\hat{\mu}_k(u_2) = \min(\widehat{\mu_k}(Y_2|R_f, L_f, t_f)) \quad (4.13)$$

These estimated utopia values will be input as the fixed unknown parameters in the weighted Tchebycheff multi-objective function of the MO-BO model which will be described in the later section. The prediction error or the uncertainty of the outputs (utopia) of regression models will be addressed in future. Thus, we calibrate the MO-BO model from the results of regression analysis and using the sequentially sampled data (true data) from the proposed MO-BO model.

*4.3.2.3. Weighted Tchebycheff multi-objective function*

In this section, now we have defined the multiple objectives and the prediction of utopia for each objective, we can start formulating the multi-objective objective function using Weighted Tchebycheff method. It is to be noted, though our focus in this chapter is the Tchebycheff method, we can apply the proposed approach to any multi-objective methods where we need the prior knowledge of utopia. The idea is to select the objective functions which are farther away from the respective utopia values. Therefore, the weighted Tchebycheff multi-objective black-box function is defined as eqn. 4.14. We define this as black-box function since $Y_i$ are assumed as black-box objective function, which is true for the complex design.

$$Y_{multi} = \max_{i=1,2,..,N} \{w_i|\hat{\mu}(Y_i|\mathbf{\Delta_k}) - \widehat{\mu_k}(u_i)|\} \quad (4.14)$$

where $w_i$ is the weighting factor of $i^{th}$ objective; $N = 2$ is the total number of objectives; $\hat{\mu}(Y_i|\mathbf{\Delta_k})$ is the estimated posterior mean of the $i^{th}$ objective function, given the posterior Gaussian process model $\mathbf{\Delta_k}$, at iteration $k$ of the MO-BO; $\widehat{\mu_k}(u_i)$ is the estimated mean utopia value of the $i^{th}$ objective function, which has been calibrated from the selected regression model. Minimizing the maximum weighted distance from the utopia, among the objective functions will provide the non-dominated solutions or pareto-optimal solutions.

*4.3.2.4. Design and manufacturing constraints for the Thin Tube Problem*

Below are some of the manufacturing and design constraints which have been considered in this problem to ensure the safe and realistic design solutions.

a. Creep-Fatigue failure

Though one of our objectives is to minimize the risk of creep fatigue failure, the minimization of the other objective increases the risk of creep fatigue failure. Thus, in the trade-off between risk and cost, it is acceptable to have a design which falls in the domain of safe region (Elastic, Shakedown) but closer to the transition to the unsafe region (Plastic, Ratchetting), thus minimizing the cost at the expense of risk of failure. However, in the similar trade-off, it is not acceptable to have a design which is likely to fall into unsafe region, irrespective of the reduction of cost. We termed that design as an unsafe design and therefore not a feasible solution. Thus, we formulate the constraint to bound the objective 1 and ensure we do not have a trade-off where the design will fail. Since the transition boundary will not be known exactly when the objectives are black-box, we can only predict the transition boundary. The approach to predict the transition boundary between safe and unsafe region was done by another Bayesian optimization model, which was the major focus of chapter 3. In this chapter, we assumed that we have already identified the transition region. Thus, to account for the uncertainty of the prediction of the transition region, we define the Probabilistic constraint as Eqn. (4.15)

$$P\big((\hat{\mu}(Y_1(R,L,t)|\boldsymbol{\Lambda})) \leq 0.5\big) \geq Rel \tag{4.15}$$

where $(\hat{\mu}(Y_1(R,L,t)|\boldsymbol{\Lambda})$ is the predicted value of the response distance function, $Y_1$, for the input design variables, given the converged GP model of the BO framework in the pre-stage [Section 3.4, chapter 3]. This converged model maximizes the accuracy of the predicted location of the transition boundary between safe and unsafe regions to classify a new design at a minimal error rate. This error rate is taken into account as the Probabilistic constraint 10 where $Rel = 0.99$ is the reliability factor. The value 0.5 is the threshold since we set this distance value at the transition boundary line.

b. Normal Stress

The normal stress should not exceed the yield stress. Therefore, constraint eqn. (4.16) is defined as

$$\frac{L_D}{2\pi Rt} - \sigma_y \leq 0 \tag{4.16}$$

where $L_D = 1KN$ is the load exerted on the wall of the thin tube, $t$ is the thickness, $\sigma_y = 205MPa$ is the yield stress.

c. Buckling Load

The tube should not buckle. Therefore, the constraint eqn. (4.17) is defined as

$$L_D - \frac{\pi^3 ER^3 t}{4L^2} \leq 0 \tag{4.17}$$

where $E = 207\ GPa$ is Young Modulus.

d. Aspect Ratio

This constraint eqn. (4.18) ensures to avoid any unrealistic design solutions with L>>R.

$$\frac{R}{L} \leq \delta \tag{4.18}$$

Where $\delta = 0.025$ in this problem.

## 4.4. Design Methodology

Figure 4 shows the detailed structure of the proposed weighted Tchebycheff multi-objective Bayesian Optimization framework with the implementation (highlighted in red) of the regression models (MLR or BMLR). Below is the algorithm with explanation of each step of the proposed MO-BO framework in order to find the optimal geometry of the thin tube problem which minimizes two objectives such as risk and cost. It is noted that the algorithm will be applicable for a large-scale problem, such as a compact heat exchanger, with $> 2$ objectives.

### *4.4.1. Step-by-Step Explanation for Proposed Weighted-Tchebycheff MOBO*

*Step 0 (Initialization):* Define the design space or the region of interest for the given problem. From the defined design space, generate a grid matrix $\overline{\overline{\boldsymbol{X}}}$ using a DOE approach. These grid designs are unsampled, meaning we don't know the true output function values for these designs. Load all the experimental data sampled during a pre-stage optimization. As explained before, the pre-stage optimization is assumed to be

done before starting this optimization process. It is to be noted, when there is no requirement to conduct the pre-stage optimization, this algorithm can be initialized with limited randomly selected experimental data. Calculate the objectives and normalize the values. Normalizing each objective is preferred to avoid any discrepancies due to inconsistent magnitude between the objectives.

*Step 1: Build a training data matrix with the sampled designs*: We build a training data matrix with the sampled data. We define X as design input variables and Y as output functions. In our problem, we define $\boldsymbol{X} = [\boldsymbol{R}, \boldsymbol{L}, \boldsymbol{t}]$ as the matrix of design geometry containing radius, length and thickness of the thin tube and $\boldsymbol{Y} = [\boldsymbol{Y_1}, \boldsymbol{Y_2}]$ as the matrix of the distance and cost functions of the respective sampled designs (as described in Section 4.3). Create the training data matrix, assuming at iteration $k$, $\boldsymbol{D_k} = [\boldsymbol{X_k}, \boldsymbol{Y}(\boldsymbol{X_k})]$.

*Step 2: Constraint Validation*: Next, we validate the generated design grid matrix $\bar{\bar{\boldsymbol{X}}}$ and the available sampled data with the constraints eqs. 13-16. We select only the designs which do not violate the constraints. Also, we filter the feasible sampled data from the data sampled in our pre-optimization problem. This is optional in general as when pre-optimization is not conducted and the starting sampling can be selected randomly over the feasible design space. Let, $\boldsymbol{X_f} = \{\boldsymbol{R_f}, \boldsymbol{L_f}\}$ be the feasible unsampled grid matrix and $\boldsymbol{D_{f,k}}$ be the filtered feasible sampled data matrix with $\boldsymbol{D_{f,k}} \in \boldsymbol{D_k}$.

*Step 3: Predicting the utopia from Regression Analysis*: Conduct linear regression modeling, either frequentist or Bayesian approach, using the feasible sampled data, $\boldsymbol{D_{f,k}}$, as explained in Section 4.3.2.2. The reasons for not including any infeasible data for our regression modelling is to avoid any influential observations outside the feasible design space. For Bayesian MLR, at iteration $k = 1$, we start with non-informative prior as $p(\boldsymbol{\beta}_{.,.,1}) \sim \boldsymbol{N}(\boldsymbol{0}, \boldsymbol{10^6})$. For iteration, $k > 1$, we update the prior as explained in

equation 8, 9. Calculate the mean utopia values for both objectives, $\hat{\mu}_k(\boldsymbol{u}) = [\hat{\mu}_k(u_1), \hat{\mu}_k(u_2)]$. These values, at iteration $k$, is used in Step 6.

*Step 4: GPM*: Next with the full available sampled data (prior knowledge), $\boldsymbol{D_k}$, we can develop posterior surrogate Gaussian Process models for each objectives independently, $\boldsymbol{\Delta_k}$. Thus, we develop a Bayesian framework. It is to be noted to build the GP model, unlike in Step 3 regression modeling, we have also used the infeasible data, sampled during pre-optimization stage. This is because with more data, GP model reduces uncertainty in the overall design space and provides better prediction where more data are sampled.

*Step 5:* Use the posterior GP model to conduct posterior predictive simulations of the unsampled feasible designs in the grid matrix $\boldsymbol{X_f}$ and predict respective mean and MSE of the objective outputs, forming two matrices of $\widehat{\boldsymbol{\mu}}(\boldsymbol{Y_f}(\boldsymbol{X_f}))|\ \boldsymbol{\Delta_k}$ and $\widehat{\boldsymbol{\sigma}}^{\boldsymbol{2}}(\boldsymbol{Y_f}(\boldsymbol{X_f}))|\ \boldsymbol{\Delta_k}$ respectively.

*Step 6: Define the Acquisition Function and maximize the Acquisition function* $\boldsymbol{U}(.)$:

Define the weighted Tchebycheff multi-objective Acquisition Function and maximize the Acquisition function, $\boldsymbol{U}(.|\boldsymbol{\Delta_k})$. Minimizing the maximum weighted distance from the utopia, among the objective functions will provide the non-dominated solutions or pareto-optimal solutions. Equation 4.14 has been accounted to below maximization problem, thereby selecting samples for expensive function evaluations from the set of feasible unsampled grid matrix, $\boldsymbol{X_f}$ with higher likelihood of being a pareto-optimal solution:

$$\max_{R_f, L_f, t_f} U(-\max_{i=1,2}\{w_i|\hat{\mu}(y_{f,i}(R_f, L_f, t_f)|\boldsymbol{\Delta_k}) - \widehat{\mu_k}(u_i)|\}) \tag{4.19}$$

We calculated the acquisition function value for each feasible non-sampled designs individually, considering the respective mean and MSE values in matrices generated in Step 5. Thus, we develop the vector of the acquisition function values as $\boldsymbol{U}(-\boldsymbol{Y_{multi}}(\boldsymbol{X_f})|\boldsymbol{\Delta_k})$. It is to be noted that we transformed the multiple objectives into a single multi-objective function using the Tchebycheff method, thus we can treat eqn.

(4.19) as single objective acquisition function. Since the general setting in BO is the maximization the acquisition function and our goal is to minimize the objectives like risk and cost, we added a negative sign before the weighted Tchebycheff multi-objective function. In this chapter, we applied an Expected Improvement (EI) acquisition function. In the computation of EI for all the unsampled designs, the vectors of the predicted MSE of the respective weighted Tchebycheff multi-objective function, $\widehat{\boldsymbol{\sigma}}^{\boldsymbol{2}}(\boldsymbol{Y_{multi}}(\boldsymbol{X_f}))$, is the predicted MSE of the individual objective (from GP in Stage 5) which has maximum weighted Tchebycheff distance. Thus, for a design $x_f$,

$$\hat{\sigma}^2\left(y_{multi}(x_f)\right) = \sigma^2_{y_{f,i}}\left(\max_{i=1,2}\{w_i\left|\hat{\mu}\left(y_{f,i}(R_f, L_f, t_f)\right|\boldsymbol{\Delta_k}\right) - \widehat{\mu_k}(u_i)\}\right) \tag{4.20}$$

Finally, the Expected-Improvement Acquisition function is formulated as below Eqn. (4.21) and (4.22):

$$u(y_{multi}(x_f)|\boldsymbol{\Delta_k}) = EI\left(y_{multi}(x_f)\right) =$$

$$\begin{cases}\left(\hat{\mu}\left(y_{multi}(x_f)\right) - y_{multi}(x^+) - \xi\right) * \Phi(\mathrm{Z}, 0, 1) + \hat{\sigma}\left(y_{multi}(x_f)\right) * \phi(Z) & if\ \hat{\sigma}\left(y_{multi}(x_f)\right) > 0 \\ 0 & if\ \hat{\sigma}\left(y_{multi}(x_f)\right) = 0\end{cases} \tag{4.21}$$

$$Z = \begin{cases}\frac{\left(\hat{\mu}\left(y_{multi}(x_f)\right) - y_{multi}(x^+) - \xi\right)}{\sigma\left(y_{multi}(x_f)\right)} & if\ \hat{\sigma}\left(y_{multi}(x_f)\right) > 0 \\ 0 & if\ \hat{\sigma}\left(y_{multi}(x_f)\right) = 0\end{cases} \tag{4.22}$$

where $y_{multi}(x^+)$ is the maximum of the negative actual responses (for minimization problem) among all the sampled data until the current stage which is at $x = x^+$; $\hat{\mu}\left(y_{multi}(x_f)\right)$ and $\hat{\sigma}\left(y_{multi}(x_f)\right)$ are the predicted mean and MSE from GPM for the non-sampled design $x_f \in \boldsymbol{X_f}$; $\Phi(.)$ is the cdf; $\phi(.)$ is the pdf; $\xi \geq 0$ which is recommended to be 0.01 [15].

A selection criterion is applied to choose new optimal design locations, $\{x_{f,max}\}$; $x_{f,max} \in \boldsymbol{X_f}$ which will maximize the predicted improvement of the learning of the unknown design space (maximizing acquisition function). Thus we select the design with maximum acquisition function value as,

$$y_{f,max}(x_{f,max}) = \max(\boldsymbol{U}(-\boldsymbol{Y_{multi}}(\boldsymbol{X_f})|\boldsymbol{\Delta_k})) \tag{4.23}$$

Augment the Data, $\boldsymbol{\mathcal{D}_k} = [\boldsymbol{D_k}; (x_{f,max}, y_{f,max})]$.

<u>*Step 7*</u>: Check for convergence criteria 1. If not met, run *j*=1: *n* loops of Step 4 to 7; each loop takes one optimal design location $\{x_{f,max,j}\}$; to select the best *n* design locations $\boldsymbol{X_{f,max}} = \{x_{f,max,1}, \dots, x_{f,max,n}\}$ to proceed to the next round of experiments. The reason for this step to provide multiple experimental data in a single round of an experiment as it will be time consuming to provide one experiment at a time. The assumption behind this step is that we believe the GP prediction of $\{x_{f,max,j}\}$ is accurate and proceed to the next best location $\{x_{f,max,j+1}\}$ by minimizing the error in the current selected location$\{x_{f,max,j}\}$. We believe this is a fair assumption since with more knowledge GP prediction will be close to the actual experimented data. Therefore, in the early round of experiments, though we might see deviations from the actual experimented results (not following the assumptions), with the knowledge from those experiments, eventually the GP will improve and provide predictions closer to the actual experimented results as the model goes to convergence.

<u>*Step 8: Expensive function evaluations*</u>: Conduct experiments for new design locations $\boldsymbol{X_{k+1}} = \boldsymbol{X_{f,max}}$. This step is outside the model environment as actual experiments will be conducted from the original high-fidelity model. As described earlier, the outputs from the actual experiments like strain accumulation and the location of the designs in terms of Elastic, Shakedown, Plastic and Ratcheting from the function evaluation will be modified into the distance function. Likewise, the cost function is also assumed to be evaluated from actual experiments, thereby increasing the flexibility of the proposed model when the cost cannot be numerically computed in large complex scenarios. Therefore, new experimented data is: $\{\boldsymbol{X_{k+1}}, \boldsymbol{Y}(\boldsymbol{X_{k+1}})\}$

<u>*Step 9: Data augmentation*</u>: Update the prior knowledge for the next iteration of the model. Update training data matrix of both the regression (Step 3) and the GP models (Step 4) with current sampled data as $\boldsymbol{D_{f,k+1}} = \{\boldsymbol{D_{f,k}}; (\boldsymbol{X_{k+1}}, \boldsymbol{Y}(\boldsymbol{X_{k+1}}))\}$ $\boldsymbol{D_{k+1}} =$

$\{\boldsymbol{D_k}; (\boldsymbol{X_{k+1}}, \boldsymbol{Y}(\boldsymbol{X_{k+1}}))\}$. Repeat Step 3 to 9 until convergence. Repeat Step 3 to 9 until convergence.

*Step 10*: If convergence criteria 2 met, update the GP with the final training data $\boldsymbol{\Lambda}$, augmented with final sampled data and stop the model. After convergence, note the optimal solution, $\boldsymbol{X_{opt}} = \{R_{opt}, L_{opt}, t_{opt}\}$ and $\boldsymbol{Y_{opt}} = \{Y_1(\boldsymbol{X_{opt}}), Y_2(\boldsymbol{X_{opt}})\}$. Convergence criteria 1 and 2 will be explained in the next section.

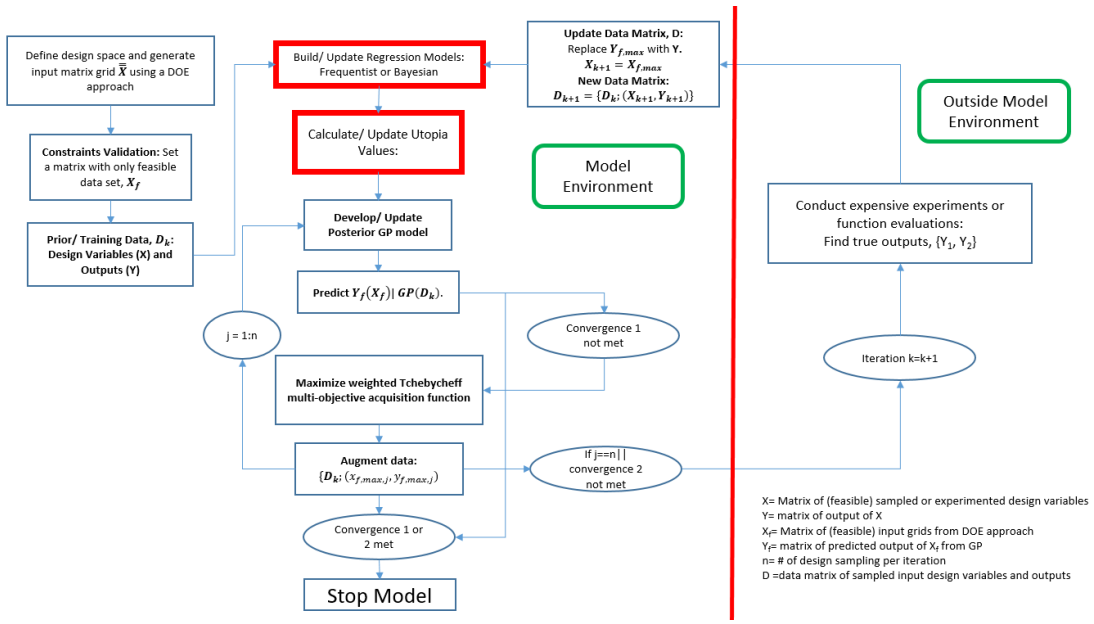


Figure 4.4. Overall flow-chart of the proposed MO-BO framework with regression-based model calibration

### *4.4.2. Convergence criteria*

In this section, we have discussed on the convergence criteria established into the model. From the steps of the proposed MO-BO model, there are two checks for convergence in the model in Step 7 and in Step 10. Label the convergence criteria in Step 7 Convergence 1 and the convergence criteria in Step 10 Convergence 2. If either of the convergence checks succeed, the model stops and returns the final solution. Below is the list of Convergence criteria which can be implemented into the models.

Convergence 1.

The maximum improvement value of the acquisition function in selecting the first design sample (1st iteration in Step 7) after conducting actual experiments is less than α. In this problem, $\alpha = 10^{-6}$. Mathematically, it can be stated as

If $j == 1$

$$\max\{U(-\boldsymbol{Y_{multi}}(\boldsymbol{X_f})|\boldsymbol{D_k})\} \leq \alpha \quad (4.24)$$

Convergence 2.

Stop the model after limiting the budget in terms of maximum number or experiments or function evaluations, i.e. $\sum n_k \geq S$ where $S$ is the maximum number of function evaluations possible; $n_k$ is the number of samples selected for experiments at k[th] iteration.

### 4.5. Results

In this section, we will show the results of the proposed *weighted Tchebycheff multi-objective Bayesian optimization* framework on the design of the tube in terms of the performance in finding optimal solutions by minimizing the risk of creep-fatigue failure at constant loading of temperature and pressure, and the material cost of the design, considering design and manufacturing constraints. With radius, length and thickness of the tube as decision variables, referring to Step 0-Algorithm 4.1, the pre-stage optimization is done to locate and optimize the transition boundary (see constraint eqn. 4.15) between safe and unsafe designs in terms of Creep-fatigue failure. The feasible bounds for radius, length and thickness are [4 – 6.55]mm, [0.1 - 1]m and [0.8 – 1.7]mm respectively and this defines our region of interest. Considering the convergence criteria 1 (Eq. 4.24), where $\alpha = 10^{-3}$, table 4.1 shows the confusion table for mis-classification which gives a low error rate of 1.1 %.

| | *Safe (Actual)* | *Unsafe (Actual)* |
|---|---|---|
| *Safe (Model Estimated)* | 41956 | 867 |
| *Unsafe (Model Estimated)* | 236 | 56941 |

Table 4.1. Confusion matrix to classify between safe and unsafe region of thin tube design.

### *4.5.1. Data Analysis*

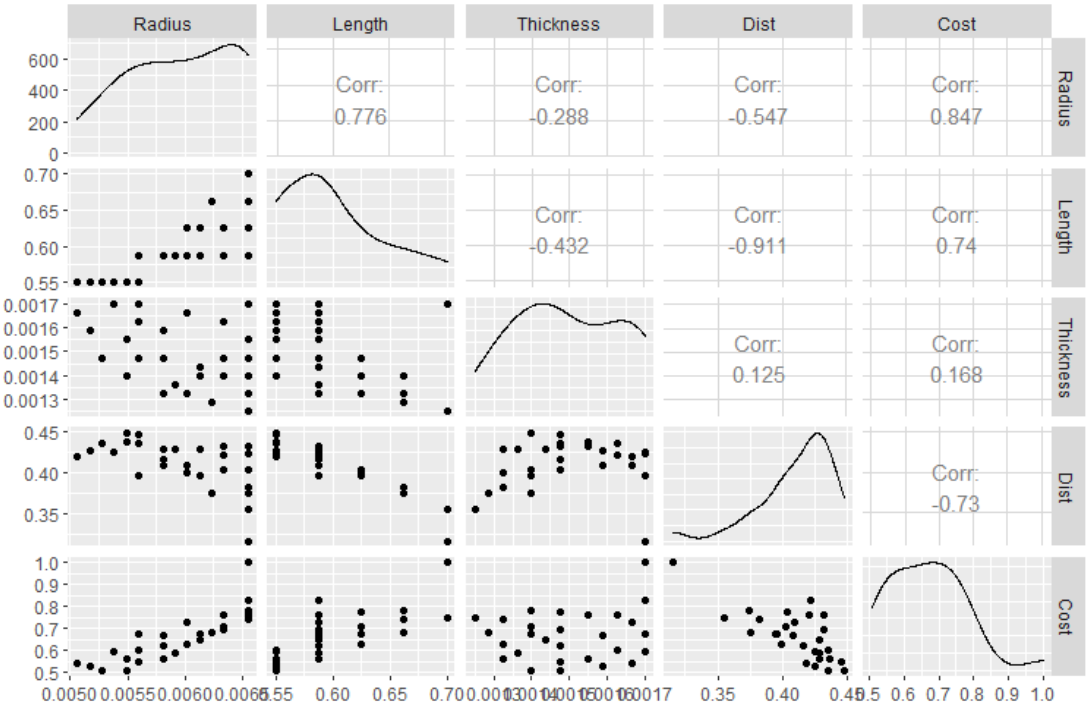


Figure 4.5. Scatter plots with correlation matrix among design variables and obj. functions.

Before running the MO-BO problem, we conduct some statistical data analysis to visualize the relationship among the design variables and objective functions. It is to be noted that the data sampled from the pre-optimization problem is first filtered to get only the feasible data for this multi-objective optimization problem. Any data which is infeasible for this problem is discarded since those can affect our analysis and the proposed data-driven MO-BO model by acting as an influential observations or outliers. This is because, in the current MO-BO model, sampling will be only done within the feasible design space and will not be explored in the infeasible region. Figure 4.5 shows the scatter plots with correlation matrix among the design variables (Radius, Length and Thickness) and objectives (Distance and Cost). From the correlation matrix we can clearly see the negative association (corr. coeff. = -0.73) between both objectives, which signifies the trade-offs in our optimization problem. We can see the design variables are all positively correlated (0.847, 0.74 and 0.168 respectively) with

cost function, which agrees with the intuition that with the increase of radius, length and thickness, the material cost of the tube increases. Similarly, we see radius and length are negatively correlated (-0.547 and -0.911) with distance function, which shows the risk of creep fatigue failure increases with the decrease of these variables. Interestingly, thickness is weakly positively correlated (0.125) with distance function, which is a discrepancy with our intuition. However, we believe this is due to the current data set as we see thickness is negatively correlated (-0.288 and -0.432 respectively) with both radius and length. This shows that with increase of thickness, the designs have lower radius and length which increases the distance function. However, since the relationship of radius and length with the objective functions are much stronger than thickness, those variables will primarily drive the trade-offs in our MO-BO problem. Looking at the scatter-plots of the design variables with the objective functions, we see some variables better meet linearity assumptions than the others. Similar conclusions can be drawn from the residuals plots as in figures 4.6 and 4.7, where we see some patterns. However, none of the plots show a strong violation of linearity or the constant variance assumption; therefore, we have focused in this chapter with linear models. However further improvement can be achieved considering more complex models, including non-linear terms and that study is left for future research.

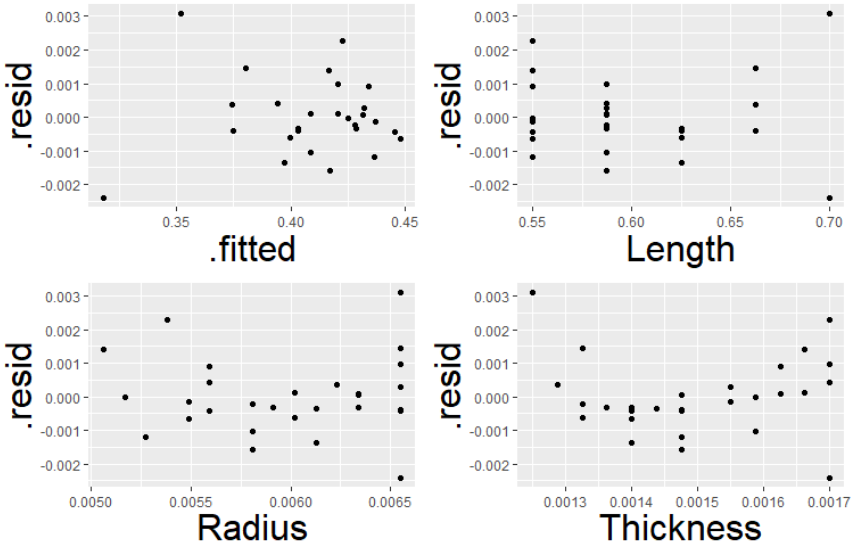


Figure 4.6. Residuals vs fitted and Design Variables for MLR model for Distance function


Figure 4.7. Residuals vs fitted and Design Variables for MLR model for Cost function

### *4.5.2. Comparison between MLR-based calibrated and non-calibrated MO-BO model*

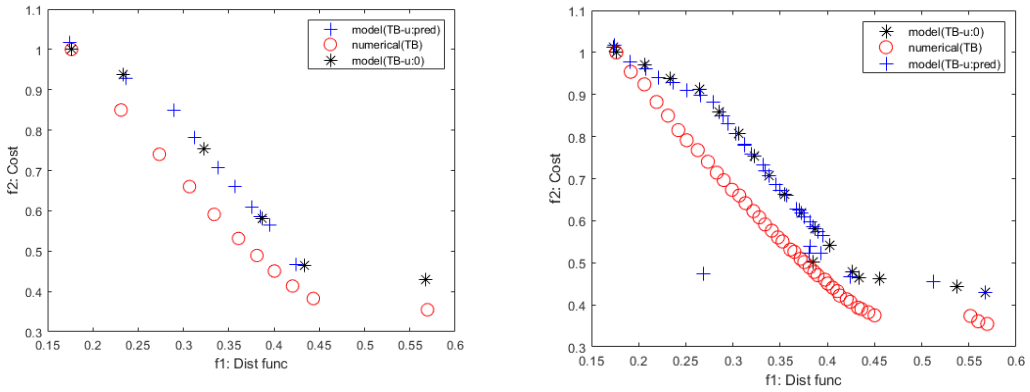


Figure 4.8. Pareto-optimal solutions at Obj. Criterion Space for (left) weighting factors $w_{11}$ and $w_{21}$; (right) weighting factors $w_{12}$ and $w_{22}$

Next, we run the proposed MO-BO model using two scenarios of weighting factors on objectives distance and cost functions, $\boldsymbol{w_{11}} = [0,0.1, \dots,1]$ and $\boldsymbol{w_{21}} = 1 - \boldsymbol{w_{11}}$; $\boldsymbol{w_{12}} = [0,0.025, \dots,1]$ and $\boldsymbol{w_{22}} = 1 - \boldsymbol{w_{12}}$, and considering the convergence criteria 1 (eqn. 4.24) with $\alpha = 10^{-5}$. We used the DACE function in MATLAB for GP model. The MO-BO model along with the MLR models has been coded in MATLAB 2018. Figure 4.8 show the comparison among Pareto optimal solutions at those weights using

different optimization methods and different strategies (calibrating vs non-calibrating) for providing utopia values in the objective criteria space. The red circles in both the figures are the Pareto-frontiers obtained numerically from the exhaustive search using the weighted Tchebycheff method, where the true utopia values [0.1764, 0.3545] are known. Thus, all the red circles can be considered as the true Pareto-optimal solutions, which are well spread with the weighting factors (trade-offs) of the objectives, likely giving unique solutions at different weights. This shows the efficiency of the weighted Tchebycheff method in solving MOO problems. Next, assuming the utopia values are unknown and the objectives are black-box, we conduct the weighted Tchebycheff MO-BO model with model calibration where utopia values are iteratively predicted from MLR models (denoted by blue +); and without model calibration by considering constant global optimal values [0, 0] as suggested in [121], [122], (denoted by black *). We can see the earlier (blue +) are more spread and closely aligned with true Pareto solutions (red circles) than the former (black *).

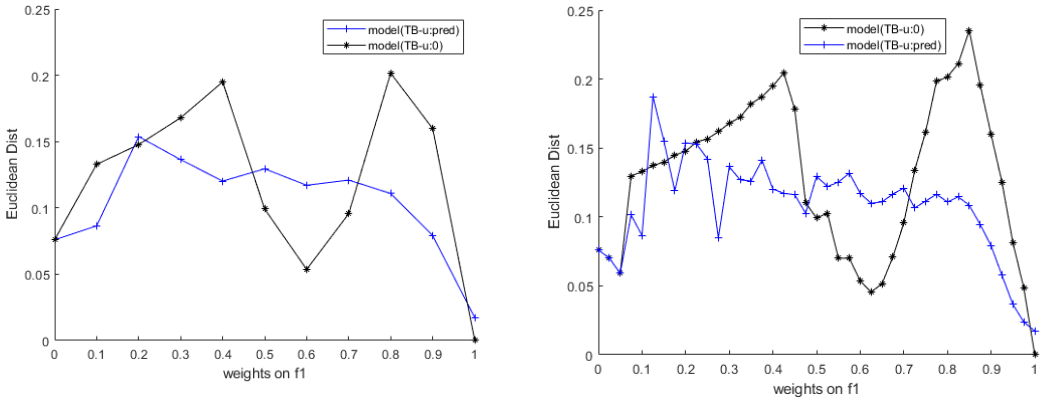


Figure 4.9. Euclidean norm distance for (left) weighting factors $w_{11}$ and $w_{21}$; (right) weighting factors $w_{12}$ and $w_{22}$

For better visualizations, we calculated and compared the Euclidean norms of the Pareto-optimal solutions, from calibrated and non-calibrated MO-BO at different weights, using the origins as the respective true Pareto-optimal solutions (red circles in fig. 4.8). The better method should have minimum Euclidean norms and the values should have minimum variability (insensitive) to different weighting parameter values. From fig. 4.9 (left figure), we can see, the results (blue line) from the proposed

calibrated MO-BO approach where the Pareto-optimal solutions are much more accurate and the solution accuracy is less variable across the weights or trade-offs between objectives (mean Euclidean norm = 0.1043; std. dev= 0.0377) than the results (black line) from using non-calibrated model with utopia values of global solutions [0, 0] (mean Euclidean norm = 0.1209; std. dev= 0.0623). Similar conclusions can be drawn from fig. 4.9 (right figure) where Euclidean norms are compared across 41 weights in $\boldsymbol{w_{12}}$ and $\boldsymbol{w_{22}}$, where we see minimum mean and std. dev of the norm for the proposed model as 0.1082 and 0.0349 respectively, when compared the models without calibration as 0.1297 and 0.0537 respectively. Although, we see the proposed approach has relatively higher norm values in the range of weights in $\boldsymbol{w_{12}}$ as [0.15-0.25], it is much better overall in comparison (following minimum norm and variability to weights).

### *4.5.3. Comparison between frequentist and Bayesian MLR-based calibrated MO-BO model*

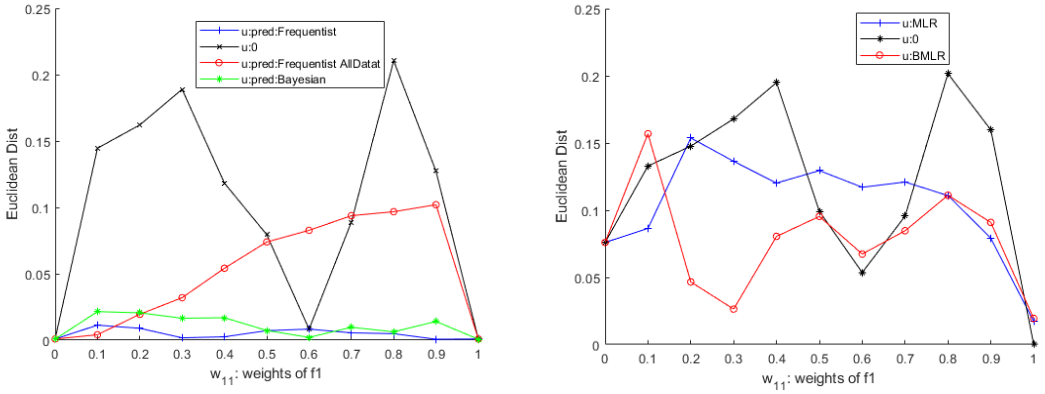


Figure 4.10. Euclidean norm distance with weighting factors $w_{11}$ and $w_{21}$ for (left) thin tube problem with 2 design vars: R and L; (right) thin tube problem with 3 design vars: R, L and t

Finally, we made a comparison of the proposed MO-BO model using frequentist MLR and Bayesian MLR in terms of accuracy (minimum Euclidean norm) and the variability towards the true Pareto-optimal solutions as shown in fig. 4.10. We considered the weighting factor, $\boldsymbol{w_{11}} = [0,0.1, \dots ,1]$ and $\boldsymbol{w_{21}} = 1 - \boldsymbol{w_{11}}$, with two case studies. The

first case study (left figure of 4.10) is the 2D problem where the radius (R) and length (L) of the tube are considered as decision variables, while the thickness (t) of the tube is kept as a constant value at 1.7mm. The second case study (right figure of 4.10) is the 3D problem with radius (R), length (L) and thickness (t) are all design variables. The Bayesian MLR model has been implemented in STAN using a *Markov Chain Monte Carlo* (MCMC) approach (no. of Markov chain =4, no. of warmup iter/chain =1000, max. iter/chain =4000) and considering *Metropolis–Hastings* (MH) sampling algorithm to approximate posterior distribution of regression co-efficient. From the comparison in 2D problem, we can interestingly see better accuracy and less variability to different weights in frequentist MLR-based calibrated MO-BO model (denoted by blue line) than in Bayesian MLR-based calibrated MO-BO model (denoted by green line) where the mean Euclidean norm and the standard deviation in frequentist approach are 0.0048 and 0.0037 respectively compared to those in Bayesian approach of 0.011 and 0.0078, respectively. However, both these approaches clearly surpass the performance of a model with non-calibrated fixed utopia values (black line) and a model with using the infeasible data for calibration (red line). Next, moving to the 3D problem (right figure of 4.10), we see the Bayesian MLR-based calibrated MO-BO model (denoted by red line) performs better than frequentist MLR-based calibrated MO-BO model (denoted by blue line) with mean and standard deviation of the Euclidean norm are 0.078 and 0.039; 0.104 and 0.038 respectively. Similarly, the model without calibration performs the worst. We know that one of the criteria for efficiency of the MO-BO models is how accurate we predict the utopia values. We think the Bayesian linear regression model performs better than the frequentist method in reducing the overall residual errors as expected, but not necessarily minimizing the residual error near the utopia region which gives lower accuracy to predict the utopia values. This is why we see MO-BO model calibrated with the Bayesian MLR provided lower accuracy for the 2D case study problem. However, both approaches show good performance overall. The further improvement will be addressed in future where we will add some trade-off and flexibility in selecting regression models to minimize the

residual error near the utopia region along with the overall reduction in the entire feasible design space.

### 4.6. Conclusion

In this chapter, we have proposed the application of Bayesian optimization to account for multiple objectives, formulating the acquisition function of weighted Tchebycheff method and calibrating the MO-BO model in which the prior knowledge of utopia values of each objective (optimal values of each objective independently) are iteratively predicted using frequentist or Bayesian MLR models. This proposed weighted Tchebycheff multi-objective Bayesian Optimization model (weighted Tchebycheff MO-BO) is applied to thin tube design, as a proof of concept to find the optimal geometry (radius, length and thickness), considering two objectives such as distance (risk of failure) and cost function, with manufacturing and design constraints. The data used in the prediction of the utopia point in each iteration is the sampled data from expensive experiments or function evaluations, suggested by maximizing the weighted Tchebycheff multi-objective acquisition function. Thus, in the calibration of the proposed MO-BO model, the MLR models utilizes the existing sampled experiment data, while providing at least better local optimal solutions than the non-calibrated model in terms of an overall accuracy and its variability at different trade-offs, as shown in the results. Our approach incorporates a Bayesian framework (using a Gaussian prior) into the optimization, where we strategically select design samples in order to maximize the learning (locating optimal designs) iteratively and reduce the overall cost of training data to achieve the desired level of accuracy, without the need of numerical formulations and having potential to consider for practical design problems. This proof of concept also shows potential broader impacts to optimize any number of black-box expensive objective functions, with no/minimal increment of complexity as the number of objectives increases, unlike in previous work where the complexity of the formulation (hyper-volume) of multi-objective acquisition function rises significantly with increasing the number of objectives. Though the focus of this chapter is on one multi-objective optimization technique (weighted Tchebycheff), the method is

applicable to any other global criterion multi-objective optimization methods where prior knowledge of utopia is required.

### *4.6.1. Limitations and future research*

There are few directions that we can proceed in this research as future tasks. As stated earlier, we started our work in this chapter with implementing linear regression models and thereby obtained better model accuracy. The future research scope is to add flexibility and further increase the proposed MO-BO model accuracy, where we develop a model selection (linear or non-linear) criteria based on the measure of cost, complexity, and trade-off in minimizing errors in fitting any complex black-box objective function at the overall feasible design space or in specific regions (optimal region), thereby broadening the utility of the proposed approach. Over the years, multi-objective BO has been handled by formulating the acquisition functions which consider mean vectors of objectives, obtained from independent runs of GP models for each objective. Finally, the full framework will be implemented in the complex high-dimensional design of a diffusion bonded heat exchanger while addressing the scalability issues.

**Acknowledgment**

This research was funded in part by DOE NEUP DE-NE0008533. The opinions, findings, conclusions, and recommendations expressed are those of the authors and do not necessarily reflect the views of the sponsor.

# APPENDIX A OF CHAPTER 4
FIGURES

A.1. Bree Diagram

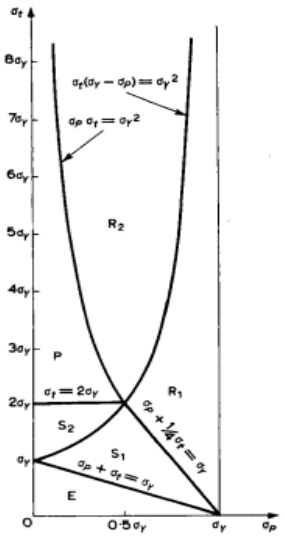


| Stress régime | Can behaviour |
|---|---|
| $R_1$ and $R_2$ | Ratchetting |
| $S_1$ and $S_2$ | Shakedown after first half-cycle |
| P | Plastic cycling |
| E | Elastic |

Figure A.4.1. Bree diagram of non-work-hardening material whose yield stress remain unchanged by the change in mean temperature [81]

# CHAPTER 5

## A Nested Weighted Tchebycheff MO-Bayesian Optimization Approach for Flexibility in Utopia Point Estimation

**Authors:**

**Arpan Biswas**
Department of Mechanical Engineering
Oregon State University
Corvallis, Oregon 97331
biswasar@oregonstate.edu

**Claudio Fuentes**
Department of Statistics
Oregon State University
Corvallis, Oregon 97331
fuentesc@oregonstate.edu

**Christopher Hoyle**
Department of Mechanical Engineering
Oregon State University
Corvallis, Oregon 97331
chris.hoyle@oregonstate.edu

Chapter 5 manuscript is issued in below journal:

**Journal of Engineering Design**

**Status: Submitted**

**ABSTRACT**

*In this work, we propose a nested Multi-objective Bayesian optimization MO-BO framework where we investigate a regression model selection procedure to estimate the utopia values for a global criterion method, such as the Weighted-Tchebycheff method, as the function of design input variables. In chapter 4, we have demonstrated a Weighted-Tchebycheff MO-BO approach which attempts to increase the model performance by estimating the model parameters (utopia) in formulating acquisition function of the weighted Tchebycheff multi-objective black-box functions, through calibration using regression analysis. However, the existing MO-BO model lacks flexibility in selecting the appropriate regression models given the guided sampled data and therefore, can under-fit or over-fit as the iterations of the MO-BO progress. This ultimately can reduce the model performance. The proposed approach is implemented in optimizing a multi-modal benchmark problem and a thin tube design under constant loading of temperature and pressure, with minimizing the risk of creep-fatigue failure and design cost. In this case study, different user-defined simple-to-complex regression models have been fitted with currently sampled training data from the MO-BO and the best model is selected following a prediction root mean square error approach. The utopia is estimated or updated given the iteratively selected regression models, which are used to formulate the weighted Tchebycheff multi-objective acquisition function. Finally, the nested weighted Tchebycheff MO-BO model performance is compared with different MO-BO frameworks with respect to parameter estimation, solution accuracy and function evaluation cost.*

## 5.1. Introduction

In the early design phase, it is very important for the designers to be able to identify potential good design decisions in a large design space while the design cost is low. In practice, most of the design problems are too complex to be handled by simple optimization frameworks due to having constraints in cost, time, formulation, etc. In many design optimization problems, it is difficult to numerically formulate an objective function and therefore we consider those problems as having black box objective

functions with high function evaluation cost. When we have no or limited knowledge on the expensive true objective function, we cannot guarantee the maximization of our learning towards an optimal solution without proper guidance or expertise. Furthermore, due to the mentioned high function evaluation cost, exhaustive search is not a feasible option. In such black box engineering design problems, a Bayesian Optimization technique (BO), which eliminates the need of standard formulation of objective functions [101]–[103], is widely applied in sequential learning to provide better guided design sampling to minimize expensive function evaluations in finding the optimal region of the unknown design space.

### *5.1.1. Research motivation*

In our previous chapter, we presented a *weighted Tchebycheff multi-objective Bayesian optimization* (MO-BO) where the prior utopia values are estimated iteratively using multiple linear regression model (MLR). The utopia point is the optimum of each objective individually and is needed for global criterion multi-objective methods such as the weighted Tchebycheff. The stated framework reduces the model complexities in formulating an acquisition function for a problem with increasing number of objectives, and increases the overall Pareto-optimal solution accuracy from estimating utopia instead of considering an educative guess [121], [122]. However, this existing model lacks flexibility where a simple linear regression model has been pre-defined for utopia estimation at each iteration of the MO-BO. Obviously, the simple regression model will under-fit if the unknown objective function is complex (non-linear). To avoid this, predefining a complex regression model can lead to overfitting if the unknown objective function is truly linear. In both the cases, the error in the utopia estimation increases. As shown in figure 5.1, we can see as we deviate from true utopia values (u`) in the X or Y directions, we cannot find the true optimal solution (C) for a specific weighting factor (w) and will fall into a different location at C`, further minimizing one objective function at the expense of the other. As the error in estimating utopia value increases, for instance due to inappropriate selection of regression models, we can observe an increase in deviation from the desired trade-off between the objectives, thereby, the MO-BO model may perform poorly. For obvious reasons, it is hard to

know a priori what could be the true nature of the black-box objective functions. Also in MO-BO, as the data sampling is done sequentially towards finding the multi-objective optimal region, the performance of different simple to complex regression models can vary iteratively depending on the available data at each iteration.

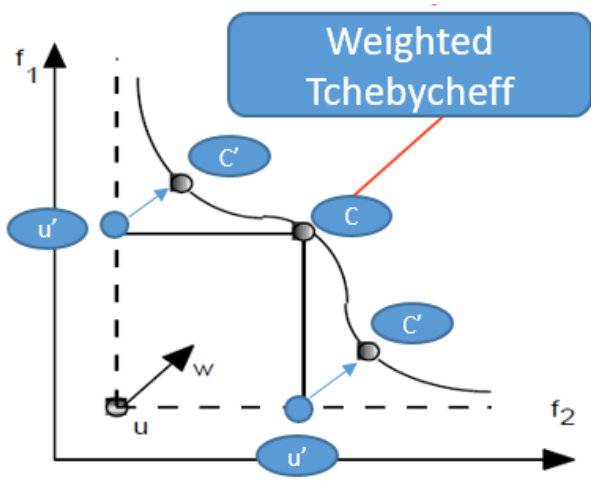


Figure 5.1. Incorrect utopia values leading to deviate from true pareto-optimal solution

### *5.1.2. Research contribution*

Attempting to increase the model performance, we introduce a *regression model selection approach* nested into the existing weighted Tchebycheff MO-BO. This iteratively selected regression model estimates the utopia values as a function of design input variables. Our main goal is to propose a design architecture for multi-objective black box problems in which one properly utilizes the existing sampled training data during model calibration and improves in predicting the utopia rather than having a fixed pre-defined regression model, by adding flexibility to choose a regression model. To illustrate the approach, we consider the same case study problem as in the previous chapters: *cyclic pressure-temperature loaded thin tube design* as we will be able to compare the results obtained from the proposed model with the true solutions. However, it is to be noted the scope of the proposed *nested weighted Tchbycheff MO-BO* is applicable to any multi-objective black-box problem, such as a *diffusion bonded Compact Heat Exchanger* [82]. The road-map of this chapter is as follows: Section 5.2

provides an overview on single and multi-objective Bayesian optimization. Section 5.3 provides the weighted Tchebycheff black box multi-objective formulation for two case studies, a 2D multi-modal multi-objective benchmark problem and a cyclic reloaded thin tube design problem. Section 5.4 talks about different simple to complex regression models considered for the case study for the purpose of estimation of utopia points. Section 5.5 provides the proposed algorithm of the iterative model selection process implemented in the existing weighted Tchebycheff MO-BO framework. Section 5.6 compares the results of the *nested weighted Tchbycheff MO-BO* among other design architectures in terms of different performance parameters. Section 5.7 concludes chapter 5 with final thoughts.

## 5.2. Overview on Bayesian Optimization

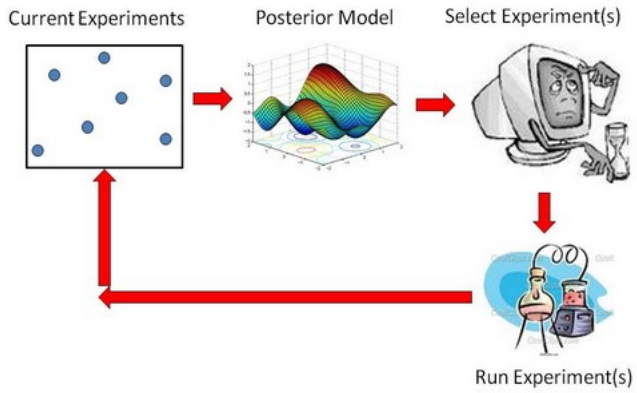


Figure 5.2. Bayesian Optimization Framework [106]

Bayesian optimization [7] is an emerging field of study in the sequential design methods. It is considered as a low-cost global optimization tool for design problems having expensive black-box objective functions. The general idea of the Bayesian optimization is to emulate an expensive unknown design space and find the local and global optimal locations while reducing the cost of function evaluation from expensive high-fidelity models. This approach has been widely used in many machine learning problems [92]–[96]. However, attempts have been made when the response is discrete like in consumer choice modelling problems where the responses are in terms of user

preference [7], [97]. The idea is to approximate the user preference discrete response function into continuous latent functions using Binomial-Probit model for two choices [98], [99] and polychotomous regression model for more than two choices where the user can state no preference [100].

### *5.2.1. Gaussian process model (GPM)*

BO adopts a Bayesian perspective and assumes that there is a prior on the function; typically, we use a Gaussian process (GP) prior. The overall Bayesian optimization approach has two major components: A predictor or Gaussian process model, and the acquisition function. As shown in figure 5.2, starting with a Gaussian prior, we build a posterior Gaussian process model, given the current available data from the expensive function evaluations. The surrogate GPM then predicts the outputs of any unsampled designs within the region of feasible design space. The uncertainty of these outputs for any unsampled designs near the observational data is small and increases as the unsampled designs are farther away from the observational data, thus related to kriging models where the errors are not independent. In order to incorporate and quantify uncertainty of the experimental or training data, one approach is to use a nugget term in the predictor GPM, which is largely discussed in the literature. It has been found that the nugget provides better a solution and computational stability framework [107], [108] as it mitigates the ill-conditioning of the correlation matrix. The technique is similar to Tikhonov regularisation where a small positive number $\vartheta$ is added on the main diagonal of the correlation matrix, which is called the nugget. Furthermore, GPM has also been implemented in high dimensional design space exploration [109] and big data problems [110], as an attempt to increase computational efficiency. As an alternative to GPs, random forest regression has been proposed as an expressive and flexible surrogate model in the context of sequential model-based algorithm configuration [104]. Although random forests are good interpolators in the sense that they output good predictions in the neighbourhood of training data, they are very poor extrapolators where the training data are far away [105]. This can lead to selecting redundant exploration (more experiments) in the non-interesting region as suggested by the acquisition function in the early iterations of the optimization, due to having

additional prediction error of the region far away from the training data. This motivates us to consider the GP model in Bayesian framework. However, in multi-objective settings, the GP model still fits each objective or response variables independently, thus assuming the objectives are uncorrelated. A survey of different GP packages available for different coding languages such as MATLAB, R, Python can be found in [111].

### *5.2.2. Acquisition function (AF)*

The second major component in Bayesian optimization is the acquisition function whose goal is to strategically select the best design locations for future experimentation, defined from the posterior simulations which are obtained from the GP model. The acquisition function predicts the improvement in learning of sampling new designs, thereby, guiding the search for the optimum and bringing sequential design into the BO. The improvement value depends on exploration (unexplored design spaces) and exploitation (region near high responses). Thus, the acquisition function gives a high value of improvement to the samples whose mean prediction is high, variance is high, or both. Thus, by maximizing the acquisition function, we strategically select design points which have the potential to have the optimal (maximum value of the unknown function) and gradually reduce the error to align with the true unknown function with iterations. Throughout the years, various formulations have been applied to define the acquisition functions. One such method is the *Probability of Improvement* (PI) [112] which is improvement based acquisition function. Jones in [113] notes that the performance of PI(·) "is truly impressive;… however, the difficulty is that the PI(·) method is extremely sensitive to the choice of the target. If the desired improvement is too small, the search will be highly local and will only move on to search globally after searching nearly exhaustively around the current best point. On the other hand, if the small-valued tolerance parameter $\varepsilon$ in PI(.) equation, as in [113], is set too high, the search will be excessively global, and the algorithm will be slow to fine-tune any promising solutions." Thus, *Expected Improvement* (EI) acquisition function [7] is widely used over PI which is a trade-off between exploration and exploitation. Another acquisition function is the *Confidence bound criteria* (CB) introduced by Cox and John [114], where the selection of points is based on the upper or lower confidence bound

of the predicted design surface for a maximization or minimization problem respectively. In multi-objective BO problems, the *Expected Improvement Hyper-volume* (EIHV) acquisition functions have been modelled to provide better performance [10], [11]. However, to increase the computational efficiency, [123] modified the EIHV acquisition function into the *Expected Hyper volume gradient-based* (EIHVG) acquisition function and proposed an efficient algorithm to calculate it. To reduce the computational cost, other acquisition functions like the *Max-value Entropy Search* (MESMO) [124] and *Predictive Entropy Search* (PESMO) [125] have been formulated. [126] proposed a multi-objective BO framework with preference over objectives on the basis of stability and attempting to focus on the Pareto front where preferred objectives are more stable. However, due to the computational complexity of all these MO-BO approaches with increasing number of objectives, the weighted Tchebycheff method has been augmented in MO-BO in [12] with a ridge regularization term to smoothen the converted single multi-objective function. Likewise, in previous chapter 4, we have implemented a weighted Tchebycheff method in MO-BO by introducing regression-based model calibration to estimate the parameter (utopia) of the multi-objective function. As stated earlier, the scope of this chapter is to modify the architecture in order to enhance the model performance.

## 5.3. Motivational Problems

In this section, we describe one benchmark problem and one design problem:

- *2-D Six-hump camel back* function and *Inversed-Ackley's Path* function
- *Thin tube design problem*

We introduce these problems, which will be explored in the case study, to aid in understanding the formulation of the regression model selection approach.

### *5.3.1. Benchmark Problem*

For the benchmark problem, we considered two popular global optimization test functions as our objectives: the *2-D Six-hump camel back* function and *Inversed-Ackley's Path* function [151]. These functions are drawn from the literature on evolutionary algorithms and global optimization, and were chosen in this chapter due

to their non-linearity and multi-modal nature and thereby having a reasonable complexity in the guided search towards the optimal solutions. We will treat these functions as black-box in our MO-BO architecture. Below is the formulation of the 2D benchmark problem:

*Maximize Objective1: 2-D Six-hump camel back* function:

$$\max_{x_1,\,x_2} Y_1 = \max_{x_1,x_2}\left(4 - 2.1x_1^2 + x_1^{\frac{4}{3}}\right)x_1^2 + x_1x_2 + (-4 + 4x_2^2)x_2^2 \tag{5.1}$$

*Maximize Objective2: 2-D Inversed-Ackley's Path* function:

$$\max_{x_1,\,x_2} Y_2 = \max_{x_1,\,x_2} a \times \exp\left(-b\sqrt{\frac{x_1^2+x_2^2}{2}}\right) + \exp\left(\frac{cos(cx_1)+\cos(cx_2)}{2}\right) - a - \exp(1) \tag{5.2}$$

where $a = 20; b = 0.2; c = 2\pi;\ -3 \le x_1 < 3;\ -2 \le x_2 < 2; x_1, x_2\ \neq 0.$

The values of *a*, *b* and *c* are considered as in [151].

### *5.3.2. Cyclic pressure-temperature loaded thin tube design problem*

For the design problem, we use the design of a thin tube under pressure-temperature cycling. As the tube is assumed to undergo constant loading of temperature and pressure, there will be risk of creep-fatigue failure which will vary with the design geometry. Fatigue damage is defined as cycling a test specimen at some fixed stress amplitude for enough cycles that it will develop micro-structural damage and eventually fail. Creep damage is defined as holding a test specimen at a fixed load for a long enough time that eventually it will develop micro-structural damage and fail. Creep-fatigue damage is therefore to do both of these simultaneously (e.g. a stress controlled cycle with a hold) such that the specimen will generally fail sooner than conducting the cycling or holding individually. The stated risk is defined based upon the location of the structural design in strain-defined regions such as elastic, shakedown, plastic or ratcheting. A similar example has been provided for thin tubes where the location of the designs can be numerically represented from a Bree Diagram [81] (fig. Appendix A.5.1) in terms of pressure and thermal stresses. Under cyclic loading, the elastic and shakedown region in the Bree diagram are considered as the safe region where no strain accumulation occurs or the growth of residual strain is practically diminishing when sufficient loading cycles are applied. However, plastic

and ratcheting in the Bree diagram are unsafe designs where the plastic strain accumulates until failure. Along with the risk, we have also considered the material cost of the tube. For a better tube design, we should minimize both the risk and cost functions. When the complexity of the design increases like in a diffusion bonded *Compact Heat Exchanger* [82], we cannot provide a numerical representation of such functions which define the location of designs. Also, considering different costs in the entire design process like material, component, manufacturing, assembly and quality checking makes the cost function hard to formulate. This makes both the objectives such as risk and cost functions to be black-box functions, representing the problem as a black-box multi-objective design problem for which we proposed the Bayesian framework in the chapter. Here, we assume the risk and cost functions for our case study problem are expensive black-box functions. We choose the design variables as radius ($R$), length ($L$), and thickness ($t$) of the tube. Next we state the experimental procedure for the formulation of the multi-objective functions and the constraints for the thin tube problem.

*5.3.2.1. Experimental procedure*

To formulate the objective of risk of creep-fatigue failure, we need to find the location of any design in terms of elastic, plastic, shakedown and ratcheting, and the respective strain accumulation. We represent these outputs as the responses from the expensive experiments. In this chapter, we consider the Bree diagram for a non-work-hardened material whose yield stress remains unchanged by changes in mean temperature as provided in Appendix A.5.1. For the sake of simplicity, we have ignored the further division of shakedown (S1, S2) and ratcheting (R1, R2) as shown in the figure, and assumed a single region of shakedown (S) and ratcheting (R), because the design risks are equivalent in the S1 and S2, and R1 and R2 regions, respectively. The three major steps we follow in the procedure are 1) Calculate Pressure and Temperature Stress of the design point, 2) Determine the region of the design in terms of elastic, plastic, shakedown and ratcheting and 3) Calculate the strain accumulation based on the location of the design. The detailed computation of the whole process for the thin tube can be found in [Section 3.3.1, chapter 3].

*5.3.2.2. Problem formulation of thin tube design*

The objective functions and the constraints of the thin tube problem is as follows:

$$\min_{R,L,t} Y_1 = \min_{R,L,t} f(\psi, \xi, k) \tag{5.3}$$

$$\min_{R,L,t} Y_2 = \min_{R,L,t} P\rho\pi tL(2R - t) \tag{5.4}$$

Subject to (Constraints):

$$P\big((\hat{\mu}(Y_1(R,L,t)|\boldsymbol{\Lambda})) \leq 0.5\big) \geq R \tag{5.5}$$

$$\frac{L_D}{2\pi Rt} - \sigma_y \leq 0 \tag{5.6}$$

$$L_D - \frac{\pi^3 E R^3 t}{4L^2} \leq 0 \tag{5.7}$$

$$\frac{R}{L} \leq \delta \tag{5.8}$$

Equation (5.3) is a distance function which measures the risk of creep-fatigue failure where $\psi \in \Psi$ is the region (elastic, shakedown, plastic and ratchetting) within the design space $\Psi$; $\xi$ is the total strain accumulation; $k$ is the $k^{th}$ iteration of the BO model. It is to be noted that in each iteration, with more experimental or training data (increase prior knowledge), the distance value for all the training data is re-evaluated. Equation (5.4) is the cost function where $P$ is the material cost per kg; $\rho$ is the density of the material. Equation (5.5) is the probabilistic constraint of creep-fatigue failure with Reliability factor, $R = 0.99$ where $\hat{\mu}(Y_1(R,L,t)|\boldsymbol{\Lambda})$ is the estimated mean of output objective, distance value, for the input design variables, given the converged posterior surrogate Gaussian Process model $\boldsymbol{\Lambda}$ of the MO-BO framework in the pre-stage [Section 3.4, chapter 3]. The value 0.5 is the threshold since we set this distance value at the transition boundary line between safe and unsafe region. For details, readers can look into the formulation of distance metrics, which builds eqns. 5.3 and 5.5, in chapter 3. Equations 5.6-5.8 are the deterministic constraint equations for normal stress, buckling load and aspect ratio respectively where $L_D = 1KN$ is the load exerted

on the wall of the thin tube, $\sigma_y = 205MPa$ is the yield stress, $E = 207GPa$ is the Young's modulus, $\delta = 0.025$ in this case study.

### *5.3.3. Weighted Tchebycheff multi-objective black-box function*

Finally, the weighted Tchebycheff multi-objective black-box function in our Bayesian optimization setting for either maximization (benchmark problem) or minimization (thin tube problem) of the multiple objectives is as follows:

$$\min_{\boldsymbol{X}} Y_{multi} = \min_{\boldsymbol{X}} \max_{i=1,2,..,N} \{w_i|\hat{\mu}(Y_i|\boldsymbol{\Delta_k}) - \widehat{\mu_k}(u_i)|\} \tag{5.9}$$

where $w_i$ is the weighting factor of $i^{th}$ objective; $N = 2$ is the total number of objectives; $\hat{\mu}(Y_i|\boldsymbol{\Delta_k})$ is the estimated mean value of the $i^{th}$ objective function, given the posterior surrogate Gaussian process model $\boldsymbol{\Delta_k}$, at iteration $k$ of the MO-BO; $\widehat{\mu_k}(u_i)$ is the estimated mean utopia value of the $i^{th}$ objective function, which has been calibrated from the selected regression model. Minimizing the maximum weighted distance from the utopia among the objective functions will provide the non-dominated solutions or Pareto-optimal solutions. Finally, eqn. 5.9 is transformed into maximizing the acquisition function of $Y_{multi}$, as $\max_{\boldsymbol{X}} U(-Y_{multi})$, thereby selecting samples for expensive function evaluations with higher likelihood of being a Pareto-optimal solution.

## 5.4. Regression Models for the thin tube design

In this section, we focus on the different simple-to-complex regression models, considered in this case study. Since the true nature of the design space or unknown objectives is assumed unknown (black-box), we have considered different flavours of regression models to understand their selection as the iteration of the MO-BO progress. In total, we have considered 7 models, used in regression analysis for estimation and prediction of outputs for given independent variables, including: 1. Mean model (MM), 2. Multiple linear regression model (MLR), 3. Log-transform of multiple linear regression model (log-MLR), 4. Bayesian multiple linear regression model (BMLR), 5. Second order polynomial model (SOP) (or quadratic model), 6. Support Vector Machine regression model (SVMR) and 7. GPM. It is to be noted that the design

architecture is not constrained to implement only these models, and any regression models can be opted out or introduced into the nested MO-BO framework at the start of the optimization (with any prior educative guess from existing similar problems and when the knowledge is very limited) or at the mid or later stage of the optimization (when we have better knowledge). However, for the sake of simplicity in model comparison, we have considered these models throughout the optimization process, assuming we have limited knowledge on the nature of the objectives to start with. Next, we have presented the formulation of fitting these models, using the sampled data in our case study. As our goal is to predict the utopia which is the optimal solution of an objective function independent of other objectives, we have considered $n = 2$ regression models for learning $n = 2$ objectives. The formulation of the models has been stated for the higher dimensional (3D) thin tube design; however, for the 2D benchmark problem (eqn. 5.1-5.2), the design variables $[R, L, t]$ can be replaced with $[x_1, x_2]$ in the following equations as required.

*Model 1: The* mean model (MM) is the simplest, only having intercepts in the regression model in equation (5.10-5.11):

$$\widehat{\mu_k}(Y_1|R, L, t) = \hat{\beta}_{0,1,k} \tag{5.10}$$

$$\widehat{\mu_k}(Y_2|R, L, t) = \hat{\beta}_{0,2,k} \tag{5.11}$$

where $\hat{\beta}_{0,1,k}$ ; $\hat{\beta}_{0,2,k}$ are the estimated regression coefficient (intercepts) for objective Eqn. (5.3) and (5.4), respectively, at iteration *k* of the MO-BO model; $\hat{\mu}(.|R, L, t)$ is the estimated mean of the objective function, given the sampled data from expensive function evaluations in the Bayesian optimization framework.

*Models 2 & 3*: Likewise, the equations for the estimated means of the objective functions fitted in MLR and log-MLR models are as follows:

$$\widehat{\mu_k}(Y_1|R, L, t) = \hat{\beta}_{0,1,k} + \hat{\beta}_{1,1,k}R + \hat{\beta}_{2,1,k}L + \hat{\beta}_{3,1,k}t \tag{5.12}$$

$$\widehat{\mu_k}(Y_2|R, L, t) = \hat{\beta}_{0,2,k} + \hat{\beta}_{1,2,k}R + \hat{\beta}_{2,2,k}L + \hat{\beta}_{3,2,k}t \tag{5.13}$$

$$\widehat{\mu_k}(Y_1|R, L, t) = e^{\widehat{\beta}_{0,1,k}} \times e^{\widehat{\beta}_{1,1,k}logR} \times e^{\widehat{\beta}_{2,1,k}logL} \times e^{\widehat{\beta}_{3,1,k}logt} \tag{5.14}$$

$$\widehat{\mu_k}(Y_2|R, L, t) = e^{\widehat{\beta}_{0,2,k}} \times e^{\widehat{\beta}_{1,2,k}logR} \times e^{\widehat{\beta}_{2,2,k}logL} \times e^{\widehat{\beta}_{3,2,k}logt} \tag{5.15}$$

where $\widehat{\boldsymbol{\beta}}_{.,\mathbf{1},\boldsymbol{k}} = \left(\hat{\beta}_{0,1,k},\ \hat{\beta}_{1,1,k},\ \hat{\beta}_{2,1,k},\ \hat{\beta}_{3,1,k}\right)^T$ ; $\widehat{\boldsymbol{\beta}}_{.,\mathbf{2},\boldsymbol{k}} = (\hat{\beta}_{0,2,k},\ \hat{\beta}_{1,2,k},\ \hat{\beta}_{2,2,k},\ \hat{\beta}_{3,2,k})^T$ are the vectors of estimated regression co-efficient (intercepts, slopes) for objective Eqn. (5.3) and (5.4) respectively at iteration $k$ of the MO-BO model. We considered full additive models per Eqn. (5.12-5.15), where both the objectives are a function of all predictor design variables (R, L and t). It is also to be noted that for the benchmark problem, the log-MLR models are avoided due to having negative values for the objective 2 (eqn. 5.2).

*Model 4*: In the Bayesian approach [142], [143], the estimation of regression coefficients for $i^{th}$ objectives and $k^{th}$ iteration of the MO-BO model, $\widehat{\boldsymbol{\beta}}_{.,\boldsymbol{i},\boldsymbol{k}} = \left(\hat{\beta}_{0,i,k},\ \hat{\beta}_{1,i,k},\ \hat{\beta}_{2,i,k},\ \hat{\beta}_{3,i,k}\right)^T$ are complex as we need to formulate the prior $p(\boldsymbol{\beta})$, likelihood function $\ell(Y|\boldsymbol{X},\boldsymbol{\beta})$, and posterior distribution $p(\boldsymbol{\beta}|\boldsymbol{X},Y)$. For BMLR, we set Gaussian (or normal) priors in eqns. 5.16, 5.17:

$$p\left(\boldsymbol{\beta}_{.,1,k}\right) \sim \boldsymbol{MVN}\left(\widehat{\boldsymbol{\mu}}_{\boldsymbol{\beta}_{.,\mathbf{1},\boldsymbol{k-1}}}, \widehat{\boldsymbol{cov}}^{\mathbf{2}}_{\boldsymbol{\beta}_{.,\mathbf{1},\boldsymbol{k-1}}} \boldsymbol{I_{p+1}}\right) \tag{5.16}$$

$$p\left(\boldsymbol{\beta}_{.,2,k}\right) \sim \boldsymbol{MVN}\left(\widehat{\boldsymbol{\mu}}_{\boldsymbol{\beta}_{.,\mathbf{2},\boldsymbol{k-1}}}, \widehat{\boldsymbol{cov}}^{\mathbf{2}}_{\boldsymbol{\beta}_{.,\mathbf{2},\boldsymbol{k-1}}} \boldsymbol{I_{p+1}}\right) \tag{5.17}$$

Therefore, the posterior distribution is defined as equations 5.18, 5.19:

$$p\left(\boldsymbol{\beta}_{.,1,k}\middle|Y_1,R,L,t\right) \propto l_k\left(Y_1\middle|R,L,t,\boldsymbol{\beta}_{.,1,k}\right)\ p\left(\boldsymbol{\beta}_{.,1,k}\right) \tag{5.18}$$

$$p\left(\boldsymbol{\beta}_{.,2,k}\middle|Y_2,R,L,t\right) \propto l_k\left(Y_2\middle|R,L,t,\boldsymbol{\beta}_{.,2,k}\right)\ p\left(\boldsymbol{\beta}_{.,2,k}\right) \tag{5.19}$$

where $\widehat{\boldsymbol{\mu}}_{\boldsymbol{\beta}_{.,\mathbf{1},\boldsymbol{k-1}}}, \widehat{\boldsymbol{\mu}}_{\boldsymbol{\beta}_{.,\mathbf{2},\boldsymbol{k-1}}}, \widehat{\boldsymbol{cov}}^{\mathbf{2}}_{\boldsymbol{\beta}_{.,\mathbf{1},\boldsymbol{k-1}}} \boldsymbol{I_{p+1}},\ \widehat{\boldsymbol{cov}}^{\mathbf{2}}_{\boldsymbol{\beta}_{.,\mathbf{2},\boldsymbol{k-1}}} \boldsymbol{I_{p+1}}$ are the estimated means and the variances, respectively, of the beta parameters for objectives 1 and 2 at iteration $k-1$ of the MO-BO model. $\boldsymbol{I_{p+1}}$ is the $(p+1)$ identity matrix where $p$ is the number of input design variables. Thus, the general idea is to compute the posterior distribution of the regression coefficients at the current iteration of MOBO model; the respective prior distribution is taken as the posterior distribution of the regression coefficients at the previous iteration. The BMLR has been implemented using a *Markov Chain Monte Carlo* (MCMC) approach (no. of Markov chain = 4, no. of warmup iter/chain = 1000, max. iter/chain = 10000) and using the *Gibb's sampling* (GB) algorithm to approximate the posterior distribution of regression coefficients.

*Model 5*: With increasing complexity by adding also square and the pairwise interaction terms of the predictor design variables, we define the quadratic or SOP model as follows:

$$\widehat{\mu_k}(Y_1|R,L,t) = \hat{\beta}_{0,1,k} + \hat{\beta}_{1,1,k}R + \hat{\beta}_{2,1,k}L + \hat{\beta}_{3,1,k}t + \hat{\beta}_{4,1,k}R^2 + \hat{\beta}_{5,1,k}L^2 + \hat{\beta}_{6,1,k}t^2 + \hat{\beta}_{7,1,k}RL + \hat{\beta}_{8,1,k}Lt + \hat{\beta}_{9,1,k}Rt \quad (5.20)$$

$$\widehat{\mu_k}(Y_2|R,L,t) = \hat{\beta}_{0,2,k} + \hat{\beta}_{1,2,k}R + \hat{\beta}_{2,2,k}L + \hat{\beta}_{3,2,k}t + \hat{\beta}_{4,2,k}R^2 + \hat{\beta}_{5,2,k}L^2 + \hat{\beta}_{6,2,k}t^2 + \hat{\beta}_{7,2,k}RL + \hat{\beta}_{8,2,k}Lt + \hat{\beta}_{9,2,k}Rt \quad (5.21)$$

*Models 6 & 7*: For the previous models, the errors are assumed independent. Thus, we considered the Support Vector Machine Regression model (SVMR) and the Gaussian process model (GPM) for the case studies where the errors are dependent. These models are altogether different from the earlier stated models, having different statistical approaches in formulation. SVMR and GPM are considered nonparametric techniques because they rely upon kernel functions. SVMR is a popular method in the domain of machine learning and widely used both in classification and regression problems for complex data [152], [153]. SVMR has the flexibility to define how much error is acceptable in the model and fit the data accordingly. Here, the objective is to minimize the sum of $l^2$ norm of the co-efficient vector, $\boldsymbol{\beta}$ and the mean $\varepsilon$-insensitive error, $|\,.\,|_\varepsilon$ of all the data. Thus, the optimization problem can be stated as:

$$\min \frac{1}{n}\sum_{j=1}^{n}\left(\left|y_j - f(\boldsymbol{S}_j)\right|_\varepsilon\right) + \left||\boldsymbol{\beta}|\right|^2 \quad (5.22)$$

$$\left|y_j - f(\boldsymbol{S}_j)\right|_\varepsilon = |z|_\varepsilon = \begin{cases} 0 & if\ |z| < \varepsilon \\ |z| - \varepsilon & otherwise \end{cases} \quad (5.23)$$

$$f(\boldsymbol{S}_j) = \boldsymbol{S}_j\boldsymbol{\beta} + b;\ \ \boldsymbol{S_j} = [R, L, t]_j\,; j = 1{:}n \quad (5.24)$$

where $\boldsymbol{S}_j$ is the $j^{th}$(row) sampled designs used for fitting the model; $y_j$ is the $j^{th}$(row) true output value; $b$ is the bias, $\varepsilon$ is the error margin and $n$ is the number of training sampled data (rows). The above eqns. 5.22-5.24 are the primal formulation where the primal variable is the co-efficient vector $\boldsymbol{\beta}$, for which the dual form is eqns. 5.25-5.26, which has been solved using the algorithm Sequential minimal optimization (SMO) [154]. The dual form of 5.22 can be written as, which is minimized w.r.t the Lagrange multipliers:

$$\min \varepsilon \sum_{j=1}^{n}(\alpha_j^+ + \alpha_j^-) + \sum_{j=1}^{n} y_j(\alpha_j^+ - \alpha_j^-) + \frac{1}{2}\sum_{i=1}^{n}\sum_{j=1}^{n}(\alpha_i^+ - \alpha_i^-)(\alpha_j^+ - \alpha_j^-)\, G(\boldsymbol{S_i}, \boldsymbol{S_j}) \quad (5.25)$$

$$\text{subject to } \sum_{j=1}^{n}(\alpha_j^+ - \alpha_j^-) = 0,\ 0 \leq \alpha_j^+, \alpha_j^- \leq C \quad (5.26)$$

where $\alpha_j^+, \alpha_j^-$ are the $j^{th}$(row) non-negative Lagrange multipliers (dual variables); $G(\boldsymbol{S_i}, \boldsymbol{S_j})$ is the kernel function between the sampled design, $\boldsymbol{S}$. $C$ is a user defined constant, which balance between model complexity and the approximation error. The primal variables, $\boldsymbol{\beta}(\alpha_j^+, \alpha_j^-)$ can be found as the linear combination of the training sampled designs as 5.27.

$$\boldsymbol{\beta}\left(\alpha_j^+, \alpha_j^-\right) = \sum_{j=1}^{n}(\alpha_j^+ + \alpha_j^-)\, \boldsymbol{S_j} \quad (5.27)$$

Finally, the estimated scores for the objectives $(Y_1, Y_2)$ for a new design $\boldsymbol{X}$ are of the form:

$$\widehat{\mu_k}(Y_1|\boldsymbol{X}) = \sum_{j=1}^{n} \hat{\alpha}_{1,j,k} \boldsymbol{G_k}\left(\boldsymbol{S_j}, \boldsymbol{X}\right) + \hat{b}_{1,k} \quad (5.28)$$

$$\widehat{\mu_k}(Y_2|\boldsymbol{X}) = \sum_{j=1}^{n} \hat{\alpha}_{2,j,k} \boldsymbol{G_k}\left(\boldsymbol{S_j}, \boldsymbol{X}\right) + \hat{b}_{2,k} \quad (5.29)$$

where $\hat{\alpha}_{i,j,k} = {\alpha_{i,j,k}}^+ - {\alpha_{i,j,k}}^-$ is the difference between the two non-negative $j^{th}$(row) Lagrange multipliers for the fitted SVMR model, estimating $i^{th}$ objective of the $k^{th}$iteration of MOBO model; $\boldsymbol{G_k}\left(\boldsymbol{S_j}, \boldsymbol{X}\right)$ is the Kernel function between each sampled design and the new design. In this paper, we considered the kernels as 'Gaussian' and 'linear' for the benchmark problem and the thin tube design, respectively; $\hat{b}$ is the bias estimate. It is to be noted that the SVMR can be efficient with different kernel functions or tuning of error margin $\varepsilon$. The proposed design architecture has the flexibility to modify SVMR models at any stage of the iteration $k$ of nested MO-BO, if required. However, for the sake of simplicity in the comparison, we have avoided that in this case study.

Like the SVMR, GPM is another tool extensively used in machine learning applications [155], [156]. GPM is attractive because of its flexible non-parametric nature and computational simplicity and is, therefore, generally applied within a Bayesian framework, which offers valid estimation and uncertainties in our prediction of function values in nonlinear black-box optimization problems. In our earlier work

as in chapter 3, we have used Gaussian process, fitted inside a Bayesian optimization framework, in the classification problem as well. The general form of the GP model, given the matrix of designs $\boldsymbol{S}$ for fitting, is as follows:

$$Y(\boldsymbol{S}) = \boldsymbol{S^T\beta} + z(\boldsymbol{S}) \tag{5.30}$$

where $\boldsymbol{S^T\beta}$ is the 2nd order polynomial regression model. $z(\boldsymbol{S})$ is a realization of a correlated Gaussian Process which is defined as follows:

$$z(\boldsymbol{S}) \sim GP\left(E[z(\boldsymbol{S})], cov\left(\boldsymbol{S}^i, \boldsymbol{S}^j\right)\right);\ \boldsymbol{S_j} = [R, L, t]_j;\ j = 1{:}n \tag{5.31}$$

$$E[z(\boldsymbol{S})] = 0, cov\left(\boldsymbol{S}^i, \boldsymbol{S}^j\right) = \sigma^2 R\left(\theta, \boldsymbol{S}^i, \boldsymbol{S}^j\right);\ i, j = 1{:}n \tag{5.32}$$

$$R\left(\theta, \boldsymbol{S}^i, \boldsymbol{S}^j\right) = \exp\left(-\sum_{m=1}^{p} \theta_m \left(s_m^i - s_m^j\right)^2\right); \tag{5.33}$$

$$\theta_m = \min_{\theta} |\mathrm{R}|^{1/n} \sigma^2 \tag{5.34}$$

Where $R\left(\boldsymbol{S}^i, \boldsymbol{S}^j\right)$ is the spatial correlation function; $|R|$ is the determinant of $R$; $\sigma^2$ is the overall scale parameter and $\theta_m$ is the correlation length parameter in dimension $m$ of $p$ dimension of $x$. The bound of $\theta_m$ is considered as $[1e^{-1}, 20]$ with starting value as 10, as suggested in [117]. These are termed as the hyper-parameters of GP model. The optimal $\theta_m$ is found as solving eqn. 5.34. In our model, we have used a Gaussian Spatial correlation function which is given as eqn. 5.33. The estimated score of the objectives $(Y_1, Y_2)$ for a new design $\boldsymbol{X}$ are of the form:

$$\widehat{\mu_k}(Y_1|\boldsymbol{X}) = \boldsymbol{X^T}\widehat{\boldsymbol{\beta}}_{.,1,k} + \boldsymbol{r(X)^T}\mathcal{R}^{-1}(\boldsymbol{Y_1(S)} - \boldsymbol{S^T}\widehat{\boldsymbol{\beta}}_{.,1,k}) \tag{5.35}$$

$$\widehat{\mu_k}(Y_2|\boldsymbol{X}) = \boldsymbol{X^T}\widehat{\boldsymbol{\beta}}_{.,2,k} + \boldsymbol{r(X)^T}\mathcal{R}^{-1}(\boldsymbol{Y_2(S)} - \boldsymbol{S^T}\widehat{\boldsymbol{\beta}}_{.,2,k}) \tag{5.36}$$

$$\boldsymbol{S} = [\boldsymbol{S_1}, \ldots., \boldsymbol{S_n}]^{\boldsymbol{T}};\ \boldsymbol{Y_q} = \left[y_{q,1}, \ldots., y_{q,n}\right]^{\boldsymbol{T}};\ \mathcal{R}^{-1} = R\left(\theta, \boldsymbol{S}^i, \boldsymbol{S}^j\right)^{-1};\ i, j = 1{:}n;$$

$$\boldsymbol{r(X)} = [R(\theta, \boldsymbol{S}^1, \boldsymbol{X}), \ldots., R(\theta, \boldsymbol{S}^n, \boldsymbol{X})]^T$$

where $\boldsymbol{r(X)}$ is the vector of correlation between each sampled design in $\boldsymbol{S}$ and new design $\boldsymbol{X}$; $\boldsymbol{Y_q(S)}$ is the vector of true responses ($q^{th}$ objectives) for the respective sampled designs in matrix $\boldsymbol{S}$; $\boldsymbol{S^T}\widehat{\boldsymbol{\beta}}_{.,q,k}$ is the estimated design $q^{th}$ output (objective) function matrix of all the sampled designs $\boldsymbol{S}$; $\mathcal{R}$ is the Gaussian spatial correlation matrix between the sampled designs, $\boldsymbol{S}$. It is to be noted the matrix $\mathcal{R}$ is symmetric and positive definite (from the bounds on $\theta_m$) and therefore, matrix $\mathcal{R}^{-1}$ exists and is also

symmetric. Thus, as the errors are dependent, the variability in the estimation of any new design which is nearer to the sampled design (used in fitting the model) is lesser than any new design which is farther from the sampled design.

## 5.5. Model Selection Criteria Procedure

The overall MO-BO design architecture with a brief version of the algorithm and the convergence criteria are provided in chapter 4. In the current chapter, we describe the model selection algorithm to estimate utopia values following a prediction root mean square error approach, which is nested in the weighted Tchebycheff MO-BO (highlighted in red, fig. 4.4). We call this the inner loop of the weighted Tchebycheff MO-BO. Figure 5.3 shows the detailed flow chart of the model selection procedure. The key point in the procedure is to compute two criteria, which together define the model selection criterion. In fig. 5.3, the steps (blocks) highlighted in blue, green and red are involved in criteria 1, criteria 2 and both criteria 1 and 2 respectively. The selection procedure is based upon the research objective to answer how good a certain model has estimated the certain parameters (utopia values); we do not consider the complexity of the model as part of the selection criteria. Our work aims to add flexibility to the model comparison among different families of models, which is formulated with different assumptions and statistical approaches, by focussing upon the measure of this goodness of fit in the estimation. This is the reason we have considered SVMR and GPM along with families of linear regression models, together with Bayesian and frequentist regression models. Also, the comparison ignores the trade-off between model accuracy and computational cost due to the increase of model parameters (e.g., number of regression co-efficient). This is because in the BO framework, this computational cost is negligible compared to the expensive function evaluations and we know with lower accuracy in estimation, there is higher chance to deviate from true optimal solutions. It is worthy to mention, in other problems where the research goal is different than stated here, further investigation is needed to ensure an appropriate model comparison and selection procedure.

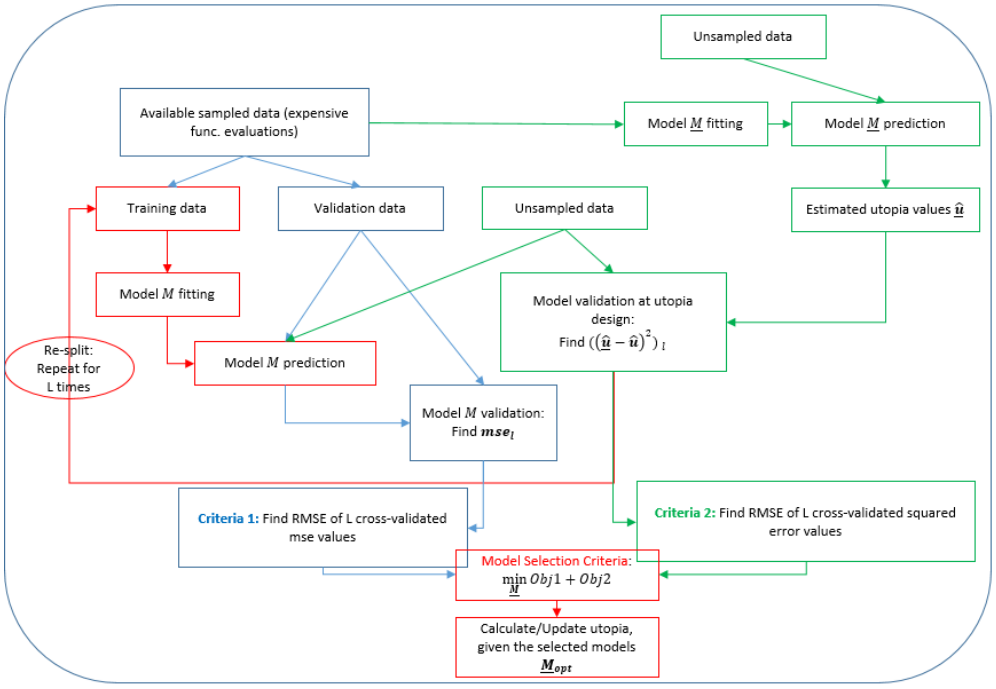


Figure 5.3. Model selection algorithm to estimate utopia (Inner loop of the MOBO)

### *5.5.1. Criterion 1: Global improvement*

The first criterion to consider in the model selection procedure is the overall *global improvement* by the model to estimate the designs across the feasible design space. Thus, criteria 1 is focused on selecting a model at iteration $k$ of the nested MO-BO model, which gives the best fit in general. With a best fit in general, the model has higher likelihood to provide better estimation of utopia values.

The steps to follow for computing criterion 1 are:

*Step 1: Training Data:* We define $\boldsymbol{X}$ as design input variables and $\boldsymbol{Y}$ as output functions. In our thin tube problem, we define $\boldsymbol{X} = [\boldsymbol{R}, \boldsymbol{L}, \boldsymbol{t}]$ as the matrix of design geometry containing radius, length and thickness of the thin tube and $\boldsymbol{Y} = [\boldsymbol{Y_1}, \boldsymbol{Y_2}]$ as the matrix of the distance (risk) and cost functions of the respective sampled designs. Create the feasible (validating constraints 5.5-5.8) sampled data matrix (guided from the acquisition function of eqn. 5.9), assuming at iteration $k$ of the MO-BO, $\boldsymbol{D_{f,k}} = [\boldsymbol{X_k}, \boldsymbol{Y}(\boldsymbol{X_k})]$ and $\boldsymbol{D_{f,k}} \in \boldsymbol{D_k}$.

*Step 2: Conduct Monte-Carlo cross-validation:*

Step 2a. Split $\boldsymbol{D_{f,k}}$ into two subsets of training $\boldsymbol{D_{f,k}^{T}}$ and validation $\boldsymbol{D_{f,k}^{V}}$ datasets without replacement at the proportion of $p^T$ and $p^V$ respectively where $p^T + p^V = 1$.

Step 2b. Given $\boldsymbol{D_{f,k}^{T}}$, fit all the pre-defined regression models to estimate objective $i$, $\mathbf{M}_{\boldsymbol{r,i,k}}$, where $r$ is the defined regression model number.

Step 2c. Estimate the objectives and create vectors of $\widehat{\boldsymbol{\mu_k}}(\boldsymbol{Y_i})$ for each input design in $\boldsymbol{D_{f,k}^{V}}$, given the regression model $\mathbf{M}_{\boldsymbol{r,i,k}}$.

Step 2d. Validate the estimated objectives in 2c with the true objective values in $\boldsymbol{D_{f,k}^{V}}$. Thus, calculate mean-squared-error $\epsilon_{1,i,l}$ to estimate objective $i$ and at iteration $l$ of the cross-validation for all the input designs $\boldsymbol{X_k^V}$ in $\boldsymbol{D_{f,k}^{V}}$.

$$\epsilon_{1,i,l} = \mu(\boldsymbol{Y_i}(\boldsymbol{X_k^V}) - \widehat{\boldsymbol{\mu_k}}(\boldsymbol{Y_i}(\boldsymbol{X_k^V})))^{\mathbf{2}} \tag{5.37}$$

Step 2e. Repeat Step 2a. - 2d. for $L$ times. In this case study, $L = 100$.

*Step 3: Define criterion 1:* Calculate root-mean-square of the vectors MC cross-validated mean-squared-errors of $i^{th}$ objective, $\boldsymbol{\epsilon_{1,i,.}}$. Thus criterion 1 at iteration $k$ of MO-BO for $i^{th}$ objective can be stated as,

$$\mathrm{E_{1,i,k}} = \sqrt{\mu(\boldsymbol{\epsilon_{1,i,.}})} \tag{5.38}$$

### *5.5.2. Criterion 2: Local improvement*

The second criterion is the local improvement by the model specific to our region of interest in the design space, which is the utopia region. It is to be noted that the purpose of the regression model is to have a good estimate at the utopia region, as a large error in any other region is not going to impact the MO-BO model performance. Although selecting a model with a good overall prediction accuracy as in criterion 1 has a likelihood of better estimation of the utopia region as well, it does not provide a guarantee of the best estimation among other models. In other words, comparing fitted model 1 and 2 as in fig. 5.4a using the training data (blue dots), although model 1 has higher error for the validation data (green dots), it has lower error in predicting utopia design (red dot). In this example, we see the overall better fit model 2 has high error at the utopia region, which is the region of interest. Thus, along with the global improvement, we have also focused on the second criteria on reducing the estimation

error specifically at the utopia region. However, doing so, the challenges lies that since the utopia design is unknown (red dot in figs. 5.4a, 5.4b), we will not know the true values of the objectives. This restricts the straightforward MC cross-validation as in section 5.5.1.

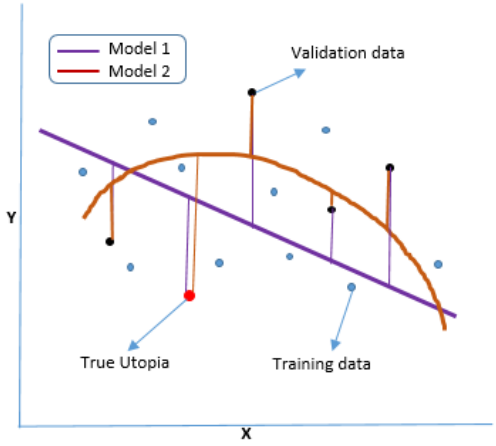


Figure 5.4a. Model Comparison: Model 1 has higher error on predicting validation data, but lower error on predicting utopia.

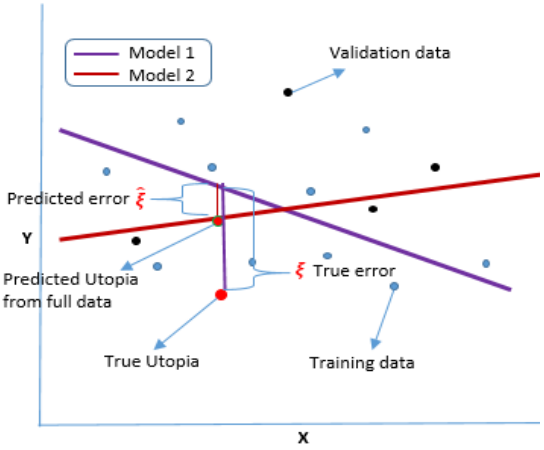


Figure 5.4b. Objective for Criteria 2: To minimize the error of predicted utopia between model 2 (full data) and model 1 (subsampled training data)

To mitigate this issue, we follow the assumption that fitting a model with more data will have higher likelihood for better estimation. Thus, the estimation error of the model, after fitting with the full feasible sampled dataset $\boldsymbol{D_{f,k}}$ is likely to be lower than that when fitted with feasible subsampled dataset $\boldsymbol{D_{f,k}^{T}}$. Following this, we assume that the reference utopia values for cross-validation are the estimated utopia values fit with the full feasible sampled dataset $\boldsymbol{D_{f,k}}$ (denoted by red dot on model 2 regression line in fig. 5.4b) and the criterion 2 is to select the model which minimize the predicted error $\hat{\xi}$ in fig. 5.4b. The steps to follow for computing criterion 2 are:

*Step 1: Training Data:* Same as stated in section 5.5.1. In addition, let $\boldsymbol{X_f} = [\boldsymbol{R_f}, \boldsymbol{L_f}, \boldsymbol{t_f}]$ be the feasible unsampled grid matrix for which the objective values are unknown.

*Step 2: Estimate utopia with full data:*

Step 2a. Given $\boldsymbol{D_{f,k}}$, fit all the pre-defined regression models to estimate objective $i$, $\underline{\mathbf{M}_{\boldsymbol{r,i,k}}}$, where $r$ is the defined regression model number.

Step 2b. Estimate the objectives and create vectors of $\underline{\widehat{\boldsymbol{\mu}_{\boldsymbol{k}}}}(\boldsymbol{Y_i})$ for each unsampled design $\boldsymbol{X_f}$, given the regression model $\underline{\mathbf{M}_{\boldsymbol{r,i,k}}}$.

Step 2c. Estimate the utopia of objective $i$, as the minimum of vectors $\underline{\widehat{\boldsymbol{\mu}_{\boldsymbol{k}}}}(\boldsymbol{Y_i})$:

$$\underline{\widehat{\mu_k}}(u_i) = \min_{R_f, L_f, t_f} (\underline{\widehat{\boldsymbol{\mu}_{\boldsymbol{k}}}}(\boldsymbol{Y_i})) \tag{5.39}$$

Store the estimated utopia $\underline{\widehat{\mu_k}}(u_i)$ and the respective design values, $\underline{\boldsymbol{x_{f,i,k}}} \in \boldsymbol{X_f}$.

*Step 3: Conduct Monte-Carlo cross-validation:*

Step 3a. Consider the same training $\boldsymbol{D_{f,k}^T}$ subsampled dataset and the fitted model $\mathbf{M}_{\boldsymbol{r,i,k}}$ as in step 2a and 2b, section 5.5.1.

Step 3b. Estimate the objective or utopia values $\widehat{\mu_k}(u_i)$ for respective input design $\underline{\boldsymbol{x_{f,i,k}}}$, given the regression model $\mathbf{M}_{\boldsymbol{r,i,k}}$.

Step 3c. Validate the estimated utopia values in 3b with the estimation done with full samples in 2c**.** Thus, calculate squared-error $\epsilon_{2,i,l}$ to estimate utopia of objective $i$ and at iteration $l$ of the cross-validation.

$$\epsilon_{2,i,l} = (\underline{\widehat{\mu_k}}(u_i) - \widehat{\mu_k}(u_i))^{\mathbf{2}} \tag{5.40}$$

Step 3d. Repeat Step 3a. – 3c. for $L$ times. In this case study, $L = 100$.

*Step 4: Define criterion 2:* Calculate root-mean-square of the MC cross-validated squared-errors of $i^{th}$ objective, $\boldsymbol{\epsilon_{2,i,.}}$. Thus the criterion 2 at iteration $k$ of MO-BO $i^{th}$ objective can be stated as,

$$\mathrm{E}_{2,\mathrm{i,k}} = \sqrt{\mu(\boldsymbol{\epsilon_{2,i,.}})} \tag{5.41}$$

Finally, the combined model selection criteria (among $r$ models) for $i^{th}$ objective to estimate utopia in the minimum of the addition of normalized values of eqns. 5.38 and 5.41 and can be stated as,

$$\min_{\underline{\mathbf{M}_{\boldsymbol{i,k}}}} |\mathrm{E}_{1,\mathrm{i,k}}| + |\mathrm{E}_{2,\mathrm{i,k}}| \tag{5.42}$$

where the optimal estimated solution is $\widehat{\mu_k}(u_i)_{opt} = \underline{\widehat{\mu_k}}\left(u_i|\underline{\mathbf{M}_{i,k,opt}}\right)$. This value is inputed into the weighted Tchebycheff black-box objective function (eqn. 5.9) for MO-BO model calibration.

## 5.6. Results

In this section, we present and discuss the results of comparing the proposed nested weighted Tchebycheff MO-BO model with other design architectures at convergence with respect to three major performance criteria. Those are as follows: 1) to maximize the overall prediction accuracy of utopia values, 2) to minimize the number of expensive function evaluations until convergence of MO-BO and 3) to maximize the overall accuracy of converged to true Pareto optimal solutions. We consider weighting factors on objectives distance and cost functions as $\boldsymbol{w_1} = [0, 0.1, .., 1]$ and $\boldsymbol{w_2} = 1 - \boldsymbol{w_1}$ respectively. We used the DACE package [117] in MATLAB for the regression and surrogate GP models. For fitting other regression models, we have used MATLAB built-in functions: *fitlm* (for fitting MM, MLR, log-MLR and SOP or Quadratic), *bayeslm* (for fitting BMLR) and *fitrsvm* (for fitting SVMR). The full nested weighted Tchebycheff MO-BO model with *Expected Improvement* type acquisition function has been coded in MATLAB 2018 and run in a machine with configuration of Windows 10, Intel Processor 3.4 GHz and 16 GB RAM.

### *5.6.1. Case study 1: Benchmark problem*

Firstly, we have presented the results for the multi-objective benchmark problem as referred in eqns. 5.1-5.2.

#### *5.6.1.1. Discussion on the proportion of models selected by nested MO-BO*

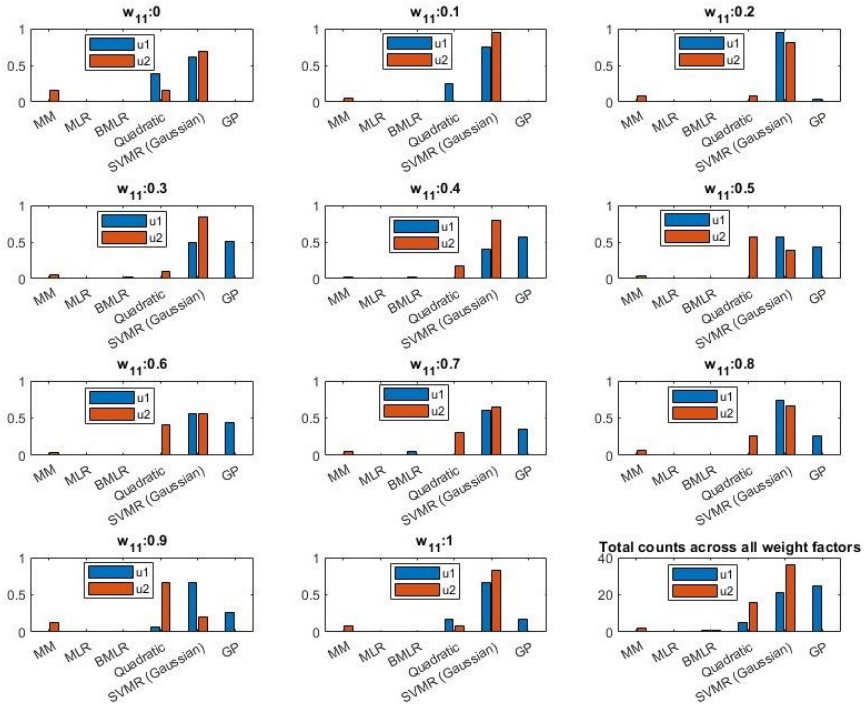


Figure 5.5. Proportion of regression models selected till nested MOBO convergence at various weighting factors for benchmark problem

Figure 5.5 shows the proportion of selecting each of the pre-defined six models for model calibration to estimate the model parameters (utopia) for the multi-objective optimization of the benchmark problem over *all iterations* at each weight combinations until convergence of the MO-BO. The bottom right figure is the total number of models selected across all *weight factors* of the objectives. To estimate utopia value for both objectives eqns. 5.1-5.2, we see the model selection varies among models with relatively higher complexities than the other pre-defined models, with high percentage for SVMR (Gaussian kernel) and GPM. As we know, both test functions are highly non-linear or multi-modal, the algorithm avoided the selection of simpler models; however, we do see a small proportion of simple linear models at the early stage of iteration. This could be because at the early stage, the data is limited and so the true nature of the objectives was not identified, and with sequential sampling of data, the MO-BO architecture has been guided to select better regression models as per fig. 5.5.

#### *5.6.1.2. Comparison of different MOBO architectures*

| Architecture* | | A | B | C |
|---|---|---|---|---|
| Euclidean norm (utopia) | Mean | 18 | 79.87 | 33.73 |
| | Std. | 16.16 | 70.69 | 55.4 |
| Func. eval. | Mean | 129 | 192 | 118 |
| Euclidean norm (Pareto optimal) | Mean | 20.08 | 95.91 | 16.26 |
| | Std. | 20.14 | 40.96 | 20.88 |

Table 5.1: MOBO design architectures performance comparison for benchmark problem

Table 5.1 shows the overall quantitative measurement of the performance of different MO-BO design architectures across the weighting factors, $\boldsymbol{w_1}$, in terms of the stated performance criteria for the benchmark problem. Figures 5.6-5.8 are the visualization of Table 5.1 at each weighting factors, $\boldsymbol{w_1}$. To achieve performance criteria 1 and 2, our objective is to minimize the Euclidean norms of utopia prediction and the Pareto-optimal solutions from the true values of utopia and the Pareto-optimal at different weight parameters, and eventually to minimize the mean Euclidean norms across all the weight parameters (Table 5.1). The true maximum values for both objectives of the benchmark problem are 162.9 and -0.2501 respectively. The true Pareto-optimal are obtained numerically from the exhaustive search using the weighted Tchebycheff method, where the true utopia values are known. With minimizing the mean Euclidean norms, we have focussed on minimizing the standard deviation of the Euclidean norms across different weight parameters. This will ensure that along with the overall minimal solution accuracy, the solution is also less variable across the weights or trade-offs between objectives. The architectures are summarized in Table 5.1 below:

- Architecture A: nested MO-BO with model selection criterion 1.
- Architecture B: nested MO-BO with model selection criterion 2.
- Architecture C: nested MO-BO with model selection criteria 1 and 2 (proposed).

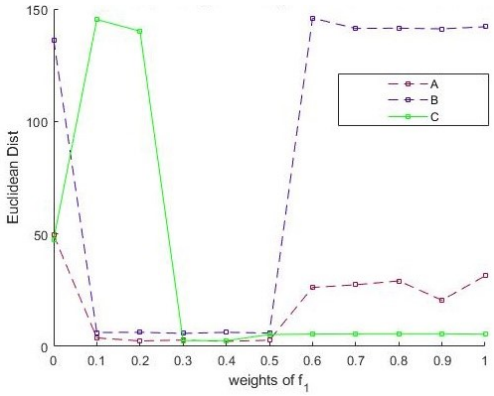


Figure 5.6. Euclidean norms between predicted and true utopia values for $w_1 = [0, 0.1, .., 1]$ (benchmark problem)

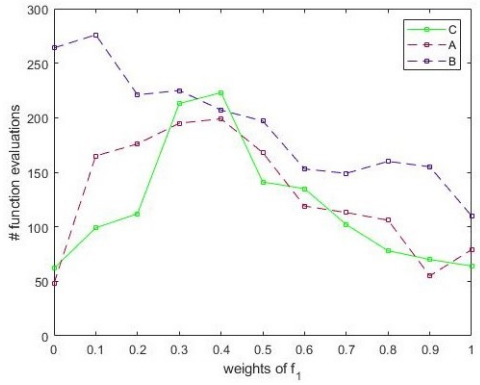


Figure 5.7. Total MOBO guided func. evaluation till convergence for $w_1 = [0, 0.1, .., 1]$ (benchmark problem)

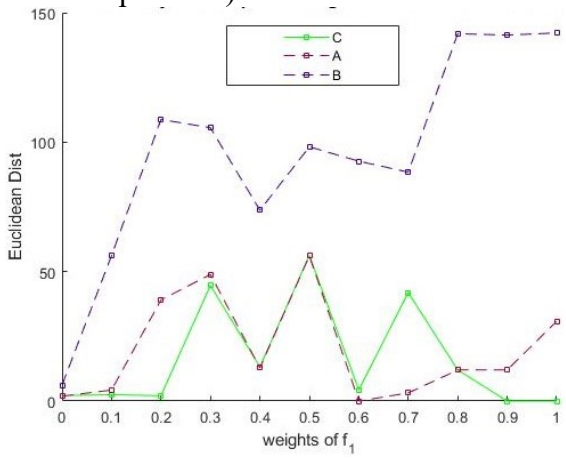


Figure 5.8. Euclidean norms between predicted and true Pareto-optimal values for $w_1 = [0, 0.1, .., 1]$ (benchmark problem)

### *5.6.2. Case study 2: Cyclic pressure-temperature loaded thin tube design problem*

Now, we have presented the results for the multi-objective thin tube design problem as referred in eqns. 5.3-5.8. Like the earlier problem, we have started with investigating the proportion of each regression model selection to capture the nature of the objectives for estimation of the utopia.

*5.6.2.1. Discussion on the proportion of models selected by nested MO-BO*

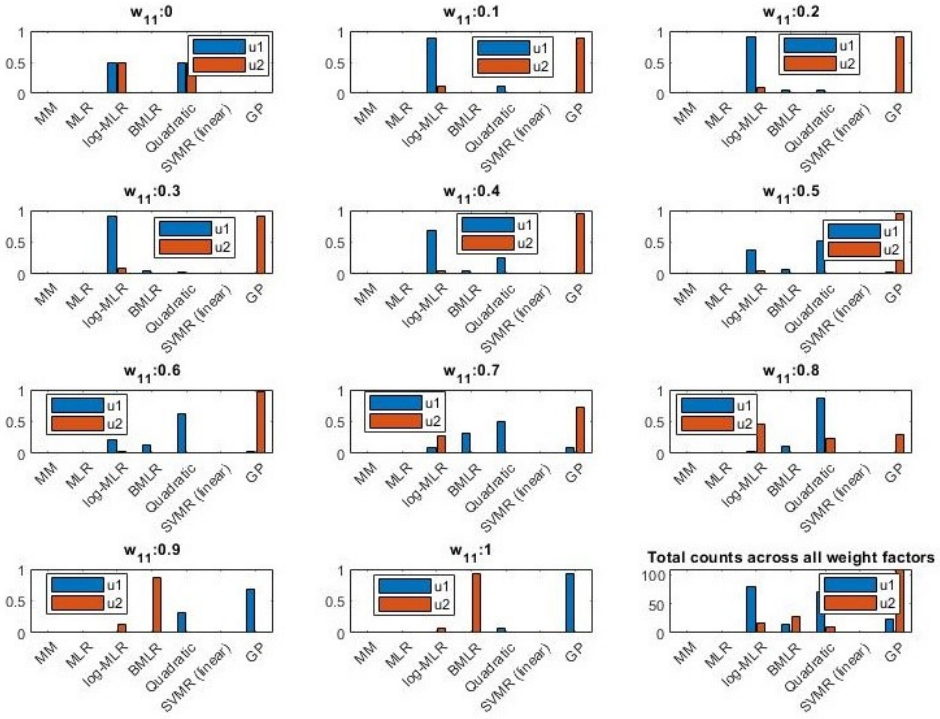


Figure 5.9. Proportion of regression models selected till nested MOBO convergence at various weighting factors for thin tube design problem

Figure 5.9 shows the proportion of selecting each of the pre-defined seven models for model calibration to estimate the model parameters (utopia) for the multi-objective optimization of the thin tube design over *all iterations* at each weight combinations until convergence of the MOBO. To estimate utopia values for objective eqn. 5.3, we see that model selection varies among log-MLR, BMLR, SOP and GP with higher percentage of log-MLR and SOP. As the weight of objective 1 increases, we see the model selection of utopia 1 shifts from log-MLR to SOP, thus trading off towards the linear model with higher complexities. Furthermore, we do not see any selection of MM, MLR and SVMR (linear kernel). Thus, changing the kernel function affects the selection of the SVMR model significantly as now the model is inefficient to capture any non-linearity of the objectives. This shows the nature of the objective is not fully linear and therefore, relatively simpler linear models considered in this case study are not appropriate here. However, we see a small proportion of Bayesian linear regression model due to its superiority over its frequentist version as it contains the prior

information of the regression coefficients. This result agrees with our linearity validation of the objectives when the MO-BO has been calibrated with only MLR models where the assumption was not perfectly met. One interesting observation is when we optimize with the full preference on objective 1 with $\boldsymbol{w_{11}} = 1$ (bottom middle figure), we see almost the whole proportion shifted to GP model. This is because of the special case that the multi-objective acquisition function of the MO-BO framework also guides the sampling at the objective 1 utopia region as we are giving importance entirely to minimizing objective 1. Thus, eventually with more sequential sampling in the utopia region, the architecture is flexible to use the benefit of error dependency of a Gaussian process as the prediction error of utopia will be much lower. This is the same reason why we see such a high percentage of GPM selection to estimate the utopia for objective eqn. 5.4. We started this MO-BO with the sampling done during the pre-optimization stage in chapter 3 where the objective is to locate the unknown creep-fatigue failure constraint (eqn. 5.5). This region is at the utopia of objective 2 since the minimization of the cost of tube will maximize risk, which eventually converges towards the creep-fatigue failure constraint. Thus, the architecture has the flexibility to choose regression models for estimation and calibration of the MO-BO based on the starting samples, weighting preferences of the multiple objectives and available sequential sampling guided by acquisition function.

*5.6.2.2. Comparison of different MOBO architectures*

| Architecture* | | A | B | C | D | E |
|---|---|---|---|---|---|---|
| Euclidean norm (utopia) | Mean | 0.1 | 0.145 | 0.083 | 0.103 | 0.057 |
| | Std. | 0.034 | 0.115 | 0.047 | 0.106 | 0.021 |
| Func. eval. | Mean | 492 | 487 | 508 | 596 | 690 |
| Euclidean norm (Pareto optimal) | Mean | 0.068 | 0.091 | 0.07 | 0.104 | 0.078 |
| | Std. | 0.03 | 0.033 | 0.03 | 0.038 | 0.039 |

Table 5.2: MOBO design architectures performance comparison for thin tube design

Table 5.2 shows the overall quantitative measurement of the performance of different MO-BO design architectures across the weighting factors, $\boldsymbol{w_1}$, in terms of the stated performance criteria for the thin tube problem. Figures 5.10-5.12 are the visualization

of the performance of different architectures at each weighting factors, $\boldsymbol{w_1}$. The true maximum values for both objectives of the thin tube problem are 0.1764 and 0.3545, respectively. Similarly, the true Pareto-optimal solutions are obtained from the exhaustive search with true utopia values. Table 5.2 is similar to Table 5.1, but also including two existing architectures D and E from chapter 4. Also, the line connecting black stars * in figs. 5.10 and 5.12 are the respective MO-BO model performance without any calibration or iterative estimation of utopia, considering a fixed value of (0, 0): this assumption leads to the worst estimation (as has been addressed in chapter 4). In this chapter, we are drawing comparisons among the architectures where estimation of utopia has been done, but with different procedures. The two existing architectures D and E, where utopia estimation is performed, in Table 5.2 are defined as below:

- Architecture A: nested MO-BO with model selection criterion 1.
- Architecture B: nested MO-BO with model selection criterion 2.
- Architecture C: nested MO-BO with model selection criteria 1 and 2 (proposed).
- Architecture D: MO-BO model integrated with only MLR.
- Architecture E: MO-BO model integrated with only BMLR.

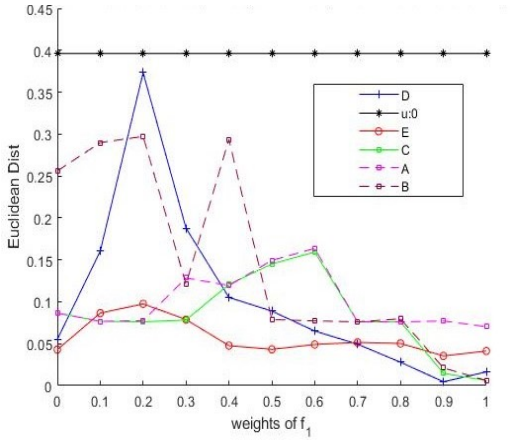


Figure 5.10. Euclidean norms between predicted and true utopia values for $w_1 = [0, 0.1, .., 1]$ (thin tube design)

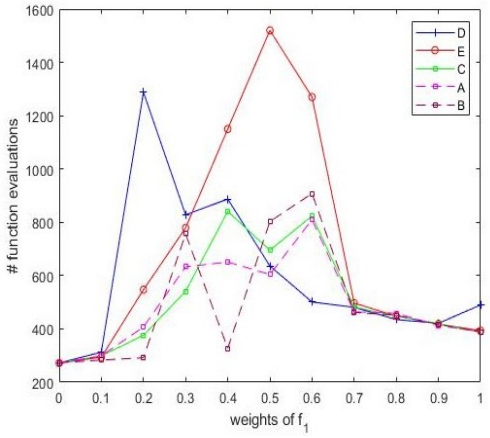


Figure 5.11. Total MOBO guided func. evaluation till convergence for $w_1 = [0, 0.1, .., 1]$ (thin tube design)

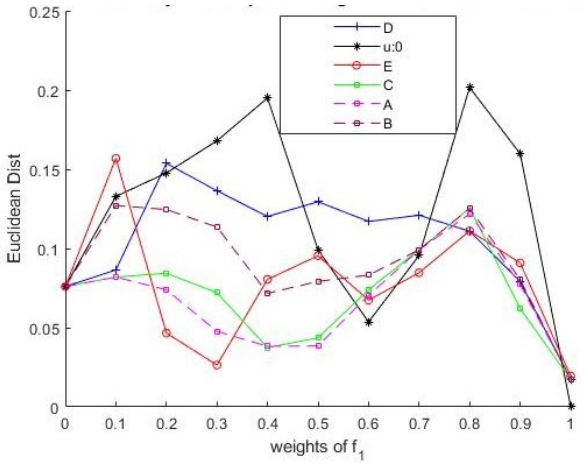


Figure 5.12. Euclidean norms between predicted and true pareto-optimal values for $w_1 = [0, 0.1, .., 1]$ (thin tube design)

*Sensitivity Analysis:* Finally, we also investigated with the sensitivity of the proportion of training and validation data $p^T$ and $p^V$, respectively, as mentioned in the algorithm 5.1 and 5.2, in the performance criteria. In doing the sensitivity analysis, we considered the proposed design architecture C with three test values of $p^T = 0.5, 0.7, 0.9$. Eventually, $p^V = 0.5, 0.3, 0.1$, respectively. It is to be noted, all the results shown for both case studies considered the setting of $p^T = 0.7$ and $p^V = 0.3$, thus can be considered as default setting in this chapter. We do not consider the case where the amount of training data is less than the validation data as this is not generally recommended in any model validation approach. Figures 5.13-5.15 and Table 5.3 show the performance of architecture C at three different proportional combinations of training and validation data in the regression model selection procedure, in terms of the three performance criteria. Similar performance results (mean and standard deviation values in Table 5.3) show that the proportion of the training and validation data did not provide any significant effect to the accuracy of the estimation of the utopia or the Pareto-optimal solution accuracy for the thin tube design. Although for most of the weight factors the total function evaluations are similar, we see a high increase in total function evaluation for the setting of $p^T = 0.5$ and $p^V = 0.5$ at $w_1 = 0.3$. This makes the mean function evaluation higher than the other two test cases for this particular case only.

| Architecture C | $p^T : p^V$ | 50:50 | 70:30 (default) | 90:10 |
|---|---|---|---|---|
| Euclidean norm (utopia) | Mean | 0.086 | 0.083 | 0.085 |
| | Std. | 0.047 | 0.047 | 0.048 |
| Func. eval. | Mean | 545 | 508 | 509 |
| Euclidean norm (Pareto optimal) | Mean | 0.07 | 0.07 | 0.07 |
| | Std. | 0.032 | 0.03 | 0.031 |

Table 5.3: Sensitivity analysis on proportion of training and validation data at regression model selection procedure for design architecture C (proposed) for thin tube design

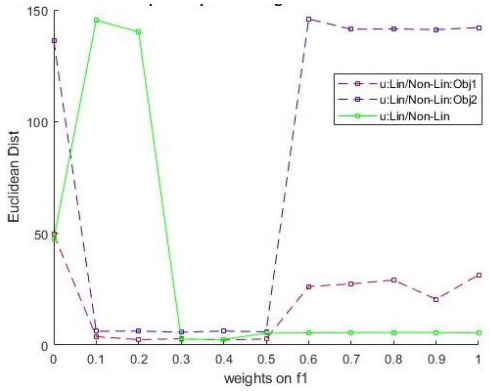


Figure 5.13. Euclidean norms between predicted and true utopia values for proposed architecture C at $w_1 = [0, 0.1, .., 1]$ (thin tube design)

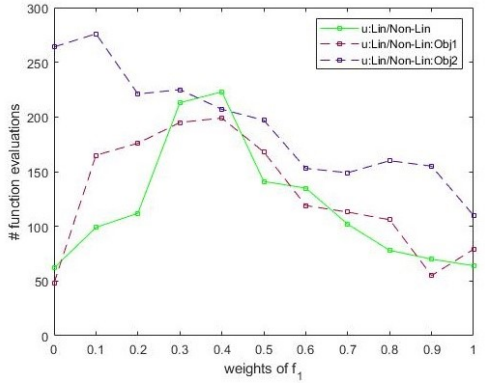


Figure 5.14. Total MOBO guided func. evaluation till convergence for proposed architecture C $w_1 = [0, 0.1, .., 1]$ (thin tube design)

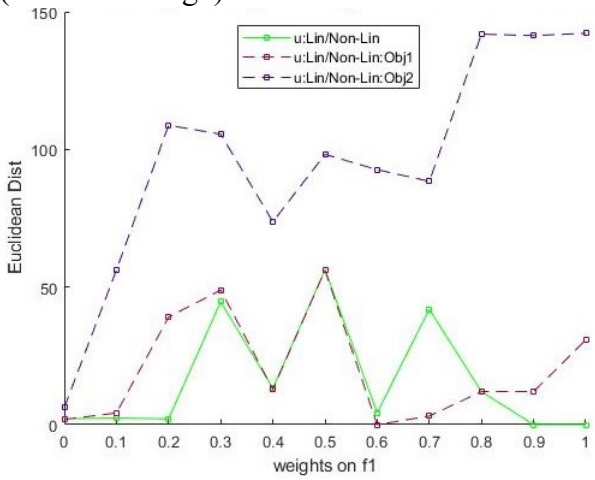


Figure 5.15. Euclidean norms between predicted and true pareto-optimal values for proposed architecture C $w_1 = [0, 0.1, .., 1]$ (thin tube design)

### *5.6.3. Discussion on the performance of different MOBO architectures for both case studies*

*Case Study 1: Benchmark problem:* In analysing the performance of different architectures, we can see architecture B performs the worst. This intuitively makes sense as the algorithm in 5.2 depends on the assumption of good overall fitting of the data by the reference model. As we did not consider the overall minimal error in fitting over the entire design space (algorithm in 5.1), the architecture D is prone to select the regression models only based on the utopia prediction error, where the error can be estimated from inappropriate reference models, thus resulting to an overall lower utopia Pareto-optimal solution accuracy. The total expensive function evaluations before convergence are also the highest for architecture B. However, the architectures A and C have an interesting comparison where we see the best (minimum) mean Euclidean norms between the estimated and true utopia across all weight combinations for architecture A, but best (minimum) mean function evaluations and mean Euclidean norms between the MO-BO converged and true Pareto-optimal solutions across all weight combinations for the proposed architecture C. With further investigation of C (fig. 5.8), we see high mean Euclidean norm of utopia and the respective standard deviation across all weight combinations are due to very high errors for only two weight combinations of $w_1 = 0.1, 0.2$. The accuracy of utopia estimation for other nine weight combinations are very minimal. However, with the high error in utopia estimation, the final optimal solutions accuracy of C is lower than A for these two weight combinations. Breaking down the utopia estimation accuracy (say for $w_1 = 0.2$), we find the absolute errors of utopia 1 from the true utopia for architectures A and C are 140.1 and 0.08, respectively. The same absolute errors of utopia 2 are 2.37 and 2.42, respectively. Thus for $w_1 = 0.2$, we have much higher preferences on objective eqn.5.2 than objective eqn. 5.1. Thus, although the Euclidean norm of utopias for C is higher than A, it has better estimation of utopia 2 for which the objective is highly preferred in the multi-objective optimization. This could be the reason why we see better optimal solutions even with overall higher Euclidean norm of utopias from true values, as the inaccuracy of utopia estimation is comparatively less penalized for the objectives with lower preferences (lower value of weights). We can check this intuitively by putting

$w_1 = 0$ in eqn. 5.9, which will have no effect on the optimal solution accuracy with the increase of the error in utopia 1 estimation, $\hat{\mu}(u_1)$.

*Case Study 2: Cyclic pressure-temperature loaded thin tube design:* To measure the performance from the comparison done based on the three criteria, Table 5.2 has been converted into scores as per Table 5.4. The score does not only tell the rank of the design architectures, but also provides the measure of how close or far way the performance of an architecture is from the best among them. It is to be noted we calculate the scores only for the mean Euclidean norms, but not for the standard deviation of the same. This is because we give first preference of minimizing the mean norms, as the design architecture having lower mean norms and higher standard deviations is better than higher mean norms and lower standard deviations. In case we have the same mean Euclidean norms for two architectures, the scores for standard deviation of the norms comes into play to break the tie.

| Architecture | A | B | C | D | E |
|---|---|---|---|---|---|
| **Criteria 1:** Utopia prediction accuracy (Mean Euclidean norm) | 51.1 | 0 | 70.5 | 47.7 | 100 |
| **Criteria 2:** Function evaluation | 97.5 | 100 | 89.7 | 46.3 | 0 |
| **Criteria 3:** Pareto-optimal solution accuracy (Mean Euclidean norm) | 100 | 36.1 | 94.4 | 0 | 72.2 |
| **Total Scores (out of 300)** | **248.6** | 136.1 | **254.6** | 94 | 172.2 |

Table 5.4: Design architecture performance metric for thin tube design (scores*)
Note*: Scores are between 0-100 with 100 being the best and is calculated from individual rows (1, 3 and 4) of Table 1, following the equation:

$$s_x = 100 - \left(\frac{x - x_{min}}{x_{max} - x_{min}} * 100\right)$$

From Table 5.4, we can see existing architecture D is among the lower scores in every criterion, with an overall worst performance (lowest total score) as the linearity assumption was found not to be met. Architecture E has the best scores in predicting utopia (criteria 1); the next best architecture is the proposed architecture C with a score

of 70.5. Architecture A is behind architecture E, with half the performance of the best architecture E. In reducing the expensive function evaluation cost (criteria 2), architectures A, B and C clearly outperform architectures D and E, which demonstrates the value of flexibility in selecting regression models with much faster convergence in reaching optimal solutions. Although architecture B has the best scores, the proposed architecture C is close in performance.

With respect to the accuracy of Pareto-optimal solutions (criteria 3), architectures B and D lag behind by significant margins. Both of these architectures also had the worst scores in predicting the utopia, which intuitively make sense as an incorrect prediction of utopia has more likelihood to give incorrect Pareto-optimal solutions. Also, architecture B, as in benchmark problem, turned out to be worst among A and C. Thus, for both the case studies, we see that although the region of interest is the utopia region, providing some priority on overall good fit in the selection criteria of the regression model is also necessary. Another interesting comparison between A and C is that although the architecture C performance score was much higher in predicting the utopia, it attains a slightly lower score in the accuracy of Pareto-optimal solution than A. As in the benchmark problem, we did a similar investigation and found the reason for this is due to the respective results at $w_1 = 0.3$ (refer fig. 5.9, 5.11). Thus, in this weight combination, higher penalization should be for the error in estimation utopia 2. However, we see both architectures have the same absolute error of 0.076. Thus, this could be due to another scenario where the utopia prediction is incorrect but along the direction of the weight combination as shown in Appendix A.5.2. However, an infinite number of such values are possible which is difficult to know, and while incorrect utopia predictions may lead to accurate Pareto solutions (by chance), the focus of this work is to estimate closer to the true utopia to generalize the design architecture for solving any similar problems, not only for this case study. The proposed architecture C is the second best in criteria 3 with only slightly behind the best architecture A. Finally, we see that the proposed architecture C has not out-performed in any of the performance criteria, but has the best all-around performance with the best score of

254.6. The next best is architecture A. Comparing the standard deviations, we see the same standard deviation for both A and C in the accuracy of Pareto-optimal solutions.

## 5.7. Conclusion

In this chapter, we presented a nested weighted Tchebycheff multi-objective Bayesian optimization framework, where the parameter (utopia values) of the acquisition function of the weighted Tchebycheff multi-objective function is estimated from regression analysis in order to calibrate the MO-BO for better performance. The utopia estimation is done from the chosen regression model among different pre-defined models with various complexities based on proposed selection criteria. The complete model selection procedure is nested with the MO-BO and is formulated to run iteratively as part of the model calibration. The results from the case study of cyclic pressure-temperature load thin tube design problem with two objectives of minimizing risk and cost, show that the introduction of the flexibility in model selection for calibration has given a much better all-round performance in better estimation of utopia, faster convergence to locate Pareto-optimal solutions and finally better accuracy in locating the Pareto-optimal solutions. The proposed nested MO-BO architecture is applicable to many black-box multi-objective optimization problems with minimal or no increase of model complexities with higher number of multiple objectives; and flexibility to define (at the start) or change (in-between iterations of MOBO) to any specific number or different families of regression models as necessary, in the comparison and selection procedure. Also, we can say that the proportion of training data and the validation data in the selection procedure in the proposed architecture is not sensitive in the thin tube design and therefore it is appropriate to use a fixed proportion, with larger training dataset, during the regression model selection procedure at every iteration of the MO-BO. The two selection criteria in choosing the regression model for estimation worked efficiently when coupled together in the nested MO-BO design architecture. Though considering only selection criteria 1 in the nested MO-BO competes well with the same considering both selection criteria, selection criteria 2 is still important to consider for this problem as the ultimate goal is focused only on efficient prediction of the utopia point.

### *5.7.1. Limitations and future work*

Based on the analysis from the results discussed in 6.3, the proposed design architecture can be improved by investigating the weighting combination between the model selection criteria 1 and 2, which will be addressed in the future. The default setting in this case study is equal preference, which is not optimal. As we understand from comparing architectures A and C in both the case studies, the weighting preference is likely to be higher on selection criteria 1. Also, another interesting factor which was found during the analysis of the case studies, other than estimation accuracy of utopia (considered in this chapter), which effects the Pareto-optimal solution accuracy is the dependency of the penalization of optimal solutions accuracy on the weight preferences on the multiple objectives. Although the focus of this chapter is on the weighted Tchebycheff method, the architecture is applicable to any other global criterion multi-objective optimization methods where prior knowledge of utopia is required. Finally, the full framework will be implemented in the complex high-dimensional design of a diffusion bonded heat exchanger.

**Acknowledgment**

This research was funded in part by DOE NEUP DE-NE0008533. The opinions, findings, conclusions, and recommendations expressed are those of the authors and do not necessarily reflect the views of the sponsor.

# APPENDIX A OF CHAPTER 5
FIGURES

A.1. Bree Diagram

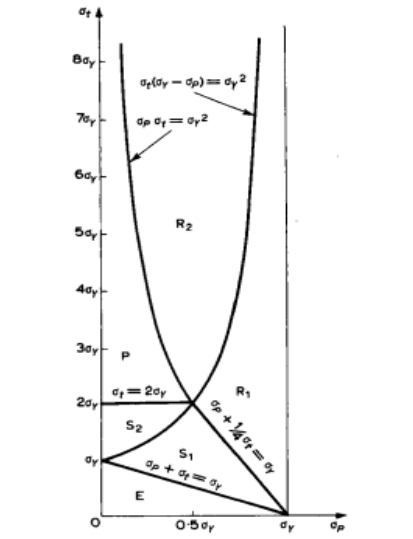


| Stress régime | Can behaviour |
|---|---|
| $R_1$ and $R_2$ | Ratchetting |
| $S_1$ and $S_2$ | Shakedown after first half-cycle |
| P | Plastic cycling |
| E | Elastic |

Figure A.5.1. Bree diagram of non-work-hardening material whose yield stress remain unchanged by the change in mean temperature [81]

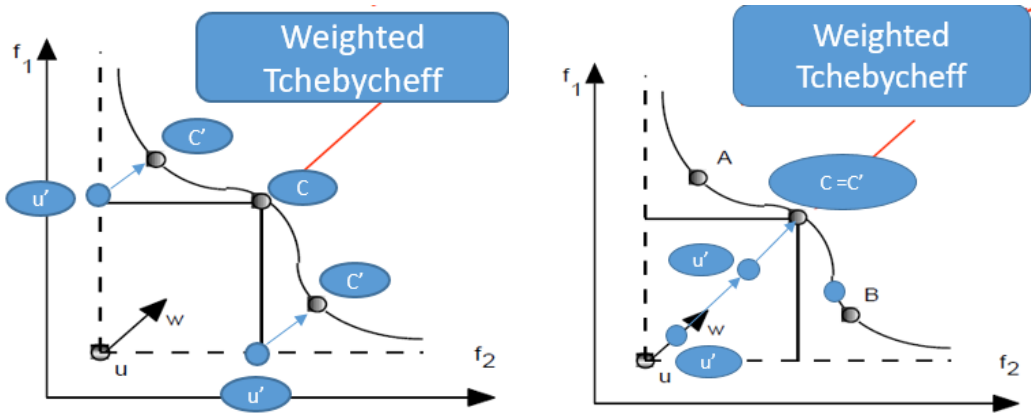


Figure A.5.2. (left) incorrect utopia at $u'$ lead to incorrect pareto-solutions at $C'$ with weight preferences between the objectives, $\boldsymbol{w}$. (right) incorrect utopia at $u'$ along the direction of weight preferences between the objectives, $\boldsymbol{w}$, still provide true pareto-solutions at $C$.

# CHAPTER 6

## General Conclusion

This dissertation is focused on complex design problems, representing towards realism in practical engineering design problems, for which many simple design optimization architectures are not adequate for finding optimal or efficient designs with high solution accuracy. In the early design phase, when the cost is comparatively low, finding true efficient designs from a complex architecture is necessary to minimize the likelihood of the designers falsely conducting costly experimental analysis or production of bad designs. On the other hand, an overly complex design architecture can contain excessive redundancy leading to high design cost and complexities. Thus, this work shows the development and investigation of different hybrid design optimization architectures, demonstrated on two case studies which focus on a global trade-off between model accuracy or efficiency vs complexities or cost.

The work in chapter 2 is of the domain of complex engineered systems, with early resilient system design and discontinuous design space (mixed integer problem) where the comparison has been made with simple single stage and sequential vs. a complex nested bi-level design architecture. The result in chapter 2 shows the bi-level architecture has potential to provide a better trade-off between multiple cost objectives in the integrated resilience system optimization, ultimately providing the best resilient designs. Although the bi-level design has higher model complexities, the results open a new direction in solving complex engineering system designs which are subject to high risk to failure consequences.

The work in chapter 3 is under the domain of complex black-box mechanical system design, with discontinuities (also representing here as an unknown constraint) due to discrete design domain. To solve this problem, this work starts with an artificially created continuous design space, then follows a domain partition approach, and a sequential Bayesian optimization (BO) architecture is built on this artificially created continuous design space. The architecture, once converged, provides a trained posterior surrogate model which is treated as a design classifier in order to partition the design space into two continuous design spaces along the discontinuity, also

represented here as the design feasibility classifier for the unknown safety measure constraint. This research also focused on building the classifier for the case with no pre-existing data, where data collection has high evaluation cost due to time, cost, etc. The BO architecture has the ability to guide the design sampling for expensive function evaluations towards maximum learning of the desired objectives at minimized evaluation cost, which other approaches do not exhibit, thereby reducing the overall design cost significantly.

The work in chapter 4 is extended to black-box optimization problems with multiple objectives. By developing a weighted Tchebycheff multi-objective Bayesian optimization (MOBO) architecture with a regression-based model calibration technique, the architecture does not introduce additional complexities in the formulation of acquisition function for a problem with large number of objectives; it also increases the solution quality from the iterative prediction of the unknown model parameters, such as the utopia values, through regression analysis.

Finally, the work in chapter 5 increased the flexibility of the design architecture in Chapter 4 by nesting a regression model selection procedure to estimate the utopia values, into the weighted Tchebycheff MOBO. The selection procedure handles uncertainty, coming from the unknown model parameters, into the MOBO design architecture. The results show that this flexibility in the choice of the regression model provides a much better estimate of utopia, increases the convergence rate of the MOBO model (lesser function evaluations) and ultimately leads to better optimal solutions.

Though the work in chapters 3-5 is applied on the complex mechanical system design in the domain of material science, it can be extended to any other fields of black-box design problems. However, for the work in Chapter 3 to other domain of problems, a new heuristic is required for transforming the original discontinuous design space to the artificially created continuous design space, before the BO is applied. Although the work in chapters 3-5 are interconnected, the work in chapter 3 can be considered independently. The results from these chapters has the potential to apply into large scale problems with the continuation of the research, thus bridging the gap between design optimization theory and its practical application.

Finally, we conclude this dissertation by listing the research accomplishments, current limitation and future directions.

### 6.1. Research Accomplishments

List of research accomplishments in this dissertations are as follow:

- Developed a nested Bi-level design architecture (in Python) for early integrated resilient system design.
- With an overall analysis and comparison with other simpler architectures, successfully showed the benefit of bi-level design in early resilient designs with handling different risk-level scenarios (research objective 1).
- Formulated an objective function to artificially create a continuous design space from the original discontinuous design space.
- Developed a sequential BO architecture (in MATLAB) with the acquisition function, formulated from the custom created objective function, guiding the sampling for expensive evaluation to learn the unknown discontinuity or safety measure constraints.
- With an overall analysis and comparison with other design classification ML approaches, successfully showed the benefit of the BO design in the black-box design classification or domain partitioning problem (research objective 2).
- Created a regression based calibration function (in MATLAB).
- Formulated the weighted Tchebycheff black-box multi-objective function and develop the weighted Tchebycheff MOBO design architecture in MATLAB by coupling with a calibration function.
- With an overall analysis and comparison with the non-calibrated MOBO architectures, successfully showed the benefit of the calibration function in MOBO in the black-box design optimization problem (research objective 3).
- Modified the regression based calibration function (fixed model) into a ‘flexible’ regression based calibration function with a model selection procedure.
- Nested the modified function into the existing weighted Tchebycheff MOBO.

- With an overall analysis and comparison with the non-flexible weighted Tchebycheff MOBO architectures, successfully showed the benefit of the model selection procedure in the nested weighted Tchebycheff MOBO architecture, with efficient handling of parameter uncertainty in the black-box design optimization problem (research objective 4).
- Finally, in answering research objectives 2, 3 and 4, developed a *two-stage BO-nested weighted Tchebycheff MO-BO design architecture.*

### 6.2. Limitations and Future Work

The limitations which can be addressed in future are as follows:

- As the drone resilience problem has relatively small finite solutions in the lower level to run an exhaustive search, we could guarantee a global optimal lower level solution, which guarantees the optimality of the bi-level problem. However, in extending to a large scale problem, this will not be the case due to having very large number of lower level solutions. Therefore, an investigation on the appropriate choice of optimization algorithm should be addressed in future, depending on the problem scale and complexities, in order to guarantee the true convergence of the bi-level design. Also, the polishing of the optimal solution of the continuous variables should be further investigated with other numerical algorithms.
- The BO model for the classification problem can be applied to any other field of black-box problem having a discontinuous design space, once a heuristic can be built to artificially create the continuous design space. As the heuristic changes with different domains of problem, we will need further investigation with different domain of problems while still following the common approach to tackle the discontinuous design space (domain partition technique) by optimizing the location of the discontinuity or constraint boundary (example -transition creep-fatigue line). Also, the extension of the approach to partition or classify into more than 2 domains or classes will be addressed in the future.
- The nested weighted Tchebycheff MOBO model for the optimization problem is applicable to any domain of black-box problems; however, the regression model

selection procedure can be improved with future investigation on the optimal preference for each selection criteria.

- Finally, the two stage BO-MOBO model can be considered for future implementation to a large scale problem, such as the design problem of 316 stainless steel diffusion bonded Hybrid Compact Heat Exchangers (H-CHX).

# BIBLIOGRAPHY


[1] J. Huo and L. Liu, "An Optimization Framework of Multiobjective Artificial Bee Colony Algorithm Based on the MOEA Framework," *Computational Intelligence and Neuroscience*, 2018. https://www.hindawi.com/journals/cin/2018/5865168/.

[2] J. Feng, W. Z. Shen, and Y. Li, "An Optimization Framework for Wind Farm Design in Complex Terrain," *Appl. Sci.*, vol. 8, no. 11, p. 2053, Nov. 2018, doi: 10.3390/app8112053.

[3] S. Rangarajan, C. T. Maravelias, and M. Mavrikakis, "Sequential-Optimization-Based Framework for Robust Modeling and Design of Heterogeneous Catalytic Systems," *J. Phys. Chem. C*, vol. 121, no. 46, pp. 25847–25863, Nov. 2017, doi: 10.1021/acs.jpcc.7b08089.

[4] A. Aubry, A. De Maio, A. Zappone, M. Razaviyayn, and Z.-Q. Luo, "A New Sequential Optimization Procedure and Its Applications to Resource Allocation for Wireless Systems," *IEEE Trans. Signal Process.*, vol. 66, no. 24, pp. 6518–6533, Dec. 2018, doi: 10.1109/TSP.2018.2868265.

[5] D. Nicolis, A. M. Zanchettin, and P. Rocco, "A Hierarchical Optimization Approach to Robot Teleoperation and Virtual Fixtures Rendering," *IFAC-Pap.*, vol. 50, no. 1, pp. 5672–5679, Jul. 2017, doi: 10.1016/j.ifacol.2017.08.1117.

[6] S. Ono and I. Yamada, "A hierarchical convex optimization approach for high fidelity solution selection in image recovery," in *Proceedings of The 2012 Asia Pacific Signal and Information Processing Association Annual Summit and Conference*, Dec. 2012, pp. 1–6.

[7] E. Brochu, V. M. Cora, and N. de Freitas, "A Tutorial on Bayesian Optimization of Expensive Cost Functions, with Application to Active User Modeling and Hierarchical Reinforcement Learning," *ArXiv10122599 Cs*, Dec. 2010, http://arxiv.org/abs/1012.2599.

[8] J. Cho, K. Lee, E. Shin, G. Choy, and S. Do, "How much data is needed to train a medical image deep learning system to achieve necessary high accuracy?," *ArXiv151106348 Cs*, Jan. 2016, http://arxiv.org/abs/1511.06348.

[9] X. Zhu, C. Vondrick, C. C. Fowlkes, and D. Ramanan, "Do We Need More Training Data?," *Int. J. Comput. Vis.*, vol. 119, no. 1, pp. 76–92, Aug. 2016, doi: 10.1007/s11263-015-0812-2.

[10] M. T. M. Emmerich, K. C. Giannakoglou, and B. Naujoks, "Single- and multiobjective evolutionary optimization assisted by Gaussian random field metamodels," *IEEE Trans. Evol. Comput.*, vol. 10, no. 4, pp. 421–439, Aug. 2006, doi: 10.1109/TEVC.2005.859463.

[11] M. Abdolshah, A. Shilton, S. Rana, S. Gupta, and S. Venkatesh, "Expected Hypervolume Improvement with Constraints," in *2018 24th International Conference on Pattern Recognition (ICPR)*, Aug. 2018, pp. 3238–3243, doi: 10.1109/ICPR.2018.8545387.

[12] A. Tran, M. Eldred, S. McCann, and Y. Wang, "srMO-BO-3GP: A sequential regularized multi-objective constrained Bayesian optimization for design

applications," *ArXiv200703502 Cs Stat*, Jul. 2020, http://arxiv.org/abs/2007.03502.

[13] I. Linkov *et al.*, "Changing the resilience paradigm," *Nat. Clim. Change*, vol. 4, no. 6, Art. no. 6, Jun. 2014, doi: 10.1038/nclimate2227.

[14] S. Hosseini, K. Barker, and J. E. Ramirez-Marquez, "A review of definitions and measures of system resilience," *Reliab. Eng. Syst. Saf.*, vol. 145, pp. 47–61, Jan. 2016, doi: 10.1016/j.ress.2015.08.006.

[15] B. Cottam, E. Specking, C. Small, E. Pohl, G. Parnell, and R. Buchanan, "Defining Resilience for Engineered Systems," *Eng. Manag. Res.*, vol. 8, no. 2, Art. no. 2, Aug. 2019, doi: 10.5539/emr.v8n2p11.

[16] W. Maul, G. Kopasakis, L. Santi, T. Sowers, and A. Chicattelli, "Sensor Selection and Optimization for Health Assessment of Aerospace Systems," in *AIAA Infotech@Aerospace 2007 Conference and Exhibit*, American Institute of Aeronautics and Astronautics.

[17] R. T. Rausch, K. F. Goebel, N. H. Eklund, and B. J. Brunell, "Integrated in-Flight Fault Detection and Accommodation: A Model-Based Study," *J. Eng. Gas Turbines Power*, vol. 129, no. 4, pp. 962–969, Oct. 2007, doi: 10.1115/1.2720517.

[18] S. Balachandran and E. Atkins, "Markov Decision Process Framework for Flight Safety Assessment and Management," *J. Guid. Control Dyn.*, vol. 40, no. 4, pp. 817–830, Aug. 2016, doi: 10.2514/1.G001743.

[19] S. Müller, A. Gerndt, and T. Noll, "Synthesizing Failure Detection, Isolation, and Recovery Strategies from Nondeterministic Dynamic Fault Trees," *J. Aerosp. Inf. Syst.*, vol. 16, no. 2, pp. 52–60, Nov. 2018, doi: 10.2514/1.I010669.

[20] A. Yildiz, M. U. Akcal, B. Hostas, and N. K. Ure, "Switching Control Architecture with Parametric Optimization for Aircraft Upset Recovery," *J. Guid. Control Dyn.*, vol. 42, no. 9, pp. 2055–2068, Apr. 2019, doi: 10.2514/1.G004180.

[21] D. R. Herber, "Advances in combined architecture, plant, and control desig," University of Illinois atUrbana-Champaign, 2017.

[22] T. Cui, J. T. Allison, and P. Wang, "A Comparative Study of Formulations and Algorithms for Reliability-Based Co-Design Problems," *J. Mech. Des.*, vol. 142, no. 3, Mar. 2020, doi: 10.1115/1.4045299.

[23] N. Yodo and P. Wang, "Resilience Allocation for Early Stage Design of Complex Engineered Systems," *J. Mech. Des.*, vol. 138, no. 9, Sep. 2016, doi: 10.1115/1.4033990.

[24] J. Wu and P. Wang, "Risk-Averse Optimization for Resilience Enhancement of Complex Engineering Systems under Uncertainties," *ArXiv200902351 Cs Eess*, Sep. 2020, http://arxiv.org/abs/2009.02351.

[25] J. R. Piacenza, K. J. Faller, M. A. Bozorgirad, E. Cotilla-Sanchez, C. Hoyle, and I. Y. Tumer, "Understanding the Impact of Decision Making on Robustness During Complex System Design: More Resilient Power Systems," *ASCE-ASME J Risk Uncert Engrg Sys Part B Mech Engrg*, vol. 6, no. 2, Jun. 2020, doi: 10.1115/1.4044471.

[26] D. Hulse, C. Hoyle, K. Goebel, and I. Y. Tumer, "Quantifying the Resilience-Informed Scenario Cost Sum: A Value-Driven Design Approach for Functional Hazard Assessment," *J. Mech. Des.*, vol. 141, no. 2, Feb. 2019, doi: 10.1115/1.4041571.

[27] "Multidisciplinary Design Optimization: A Survey of Architectures | AIAA Journal." https://arc.aiaa.org/doi/10.2514/1.J051895.

[28] J. T. Allison, "Complex system optimization: A review of analytical target cascading, collaborative optimization, and other formulations," The University of Michigan, 2004.

[29] P. He, C. A. Mader, J. R. R. A. Martins, and K. J. Maki, "DAFoam: An Open-Source Adjoint Framework for Multidisciplinary Design Optimization with OpenFOAM," *AIAA J.*, vol. 58, no. 3, pp. 1304–1319, 2020, doi: 10.2514/1.J058853.

[30] J. S. Gray, J. T. Hwang, J. R. R. A. Martins, K. T. Moore, and B. A. Naylor, "OpenMDAO: an open-source framework for multidisciplinary design, analysis, and optimization," *Struct. Multidiscip. Optim.*, vol. 59, no. 4, pp. 1075–1104, Apr. 2019, doi: 10.1007/s00158-019-02211-z.

[31] P. D. Ciampa and B. Nagel, "AGILE Paradigm: The next generation collaborative MDO for the development of aeronautical systems," *Prog. Aerosp. Sci.*, vol. 119, p. 100643, Nov. 2020, doi: 10.1016/j.paerosci.2020.100643.

[32] P. Piperni, A. DeBlois, and R. Henderson, "Development of a Multilevel Multidisciplinary-Optimization Capability for an Industrial Environment," *AIAA J.*, vol. 51, no. 10, pp. 2335–2352, Aug. 2013, doi: 10.2514/1.J052180.

[33] A. Papageorgiou, J. Ölvander, K. Amadori, and C. Jouannet, "Multidisciplinary and Multifidelity Framework for Evaluating System-of-Systems Capabilities of Unmanned Aircraft," *J. Aircr.*, vol. 57, no. 2, pp. 317–332, Dec. 2019, doi: 10.2514/1.C035640.

[34] H. von Stackelberg, *Market Structure and Equilibrium*. Berlin Heidelberg: Springer-Verlag, 2011.

[35] A. Biswas and C. Hoyle, "A Literature Review: Solving Constrained Non-Linear Bi-Level Optimization Problems With Classical Methods," presented at the ASME 2019 International Design Engineering Technical Conferences and Computers and Information in Engineering Conference, Nov. 2019, doi: 10.1115/DETC2019-97192.

[36] B. Colson, P. Marcotte, and G. Savard, "Bilevel programming: A survey," *4OR*, vol. 3, no. 2, pp. 87–107, Jun. 2005, doi: 10.1007/s10288-005-0071-0.

[37] S. C. Rismiller, J. Cagan, and C. McComb, "Stochastic Stackelberg Games for Agent-Driven Robust Design," presented at the ASME 2020 International Design Engineering Technical Conferences and Computers and Information in Engineering Conference, Nov. 2020, doi: 10.1115/DETC2020-22153.

[38] M. Labbé, P. Marcotte, and G. Savard, "A Bilevel Model of Taxation and Its Application to Optimal Highway Pricing," *Manag. Sci.*, vol. 44, no. 12-part-1, pp. 1608–1622, Dec. 1998, doi: 10.1287/mnsc.44.12.1608.

[39] A. Chen and K. Subprasom, "Analysis of regulation and policy of private toll roads in a build-operate-transfer scheme under demand uncertainty," *Transp.*

*Res. Part Policy Pract.*, vol. 41, no. 6, pp. 537–558, Jul. 2007, doi: 10.1016/j.tra.2006.11.009.

[40] "Defense Applications of Mathematical Programs with Optimization Problems in the Constraints on JSTOR." http://www.jstor.org/stable/169661.

[41] E. Roghanian, S. J. Sadjadi, and M. B. Aryanezhad, "A probabilistic bi-level linear multi-objective programming problem to supply chain planning," *Appl. Math. Comput.*, vol. 188, no. 1, pp. 786–800, May 2007, doi: 10.1016/j.amc.2006.10.032.

[42] A. Biswas, Y. Chen, N. Gibson, and C. Hoyle, "Bilevel Flexible-Robust Optimization for Energy Allocation Problems," *ASCE-ASME J Risk Uncert Engrg Sys Part B Mech Engrg*, vol. 6, no. 3, Sep. 2020, doi: 10.1115/1.4046269.

[43] P. Kall and S. Wallace, *Stochastic Programming.* 1994.

[44] G. B. Dantzig, "Linear Programming under Uncertainty," *Manag. Sci.*, vol. 1, no. 3/4, pp. 197–206, 1955.

[45] E. M. L. Beale, "On Minimizing a Convex Function Subject to Linear Inequalities," *J. R. Stat. Soc. Ser. B Methodol.*, vol. 17, no. 2, pp. 173–184, 1955, doi: https://doi.org/10.1111/j.2517-6161.1955.tb00191.x.

[46] P. Popela, J. Novotný, J. Roupec, D. Hrabec, and A. Olstad, "Two-stage Stochastic Programming for Engineering Problems.," *Eng. Mech.*, 2014.

[47] E. C. Finardi, B. U. Decker, and V. L. de Matos, "An Introductory Tutorial on Stochastic Programming Using a Long-term Hydrothermal Scheduling Problem," *J. Control Autom. Electr. Syst.*, vol. 24, no. 3, pp. 361–376, Jun. 2013, doi: 10.1007/s40313-013-0039-9.

[48] J. T. Allison and D. R. Herber, "Special Section on Multidisciplinary Design Optimization: Multidisciplinary Design Optimization of Dynamic Engineering Systems," *AIAA J.*, vol. 52, no. 4, pp. 691–710, Feb. 2014, doi: 10.2514/1.J052182.

[49] D. R. Herber and J. T. Allison, "Nested and Simultaneous Solution Strategies for General Combined Plant and Control Design Problems," *J. Mech. Des.*, vol. 141, no. 1, Jan. 2019, doi: 10.1115/1.4040705.

[50] K. W. Lee, W. Moase, A. Ooi, C. Manzie, and E. C. Kerrigan, "Optimization Framework for Codesign of Controlled Aerodynamic Systems," *AIAA J.*, vol. 54, no. 10, pp. 3149–3159, Jun. 2016, doi: 10.2514/1.J054711.

[51] N. Yodo and P. Wang, "Engineering Resilience Quantification and System Design Implications: A Literature Survey," *J. Mech. Des.*, vol. 138, no. 11, Nov. 2016, doi: 10.1115/1.4034223.

[52] J. Li and Z. Xi, "Engineering Recoverability: A New Indicator of Design for Engineering Resilience," presented at the ASME 2014 International Design Engineering Technical Conferences and Computers and Information in Engineering Conference, Jan. 2015, doi: 10.1115/DETC2014-35005.

[53] C. A. MacKenzie and C. Hu, "Decision making under uncertainty for design of resilient engineered systems," *Reliab. Eng. Syst. Saf.*, vol. 192, p. 106171, Dec. 2019, doi: 10.1016/j.ress.2018.05.020.

[54] B. D. Youn, C. Hu, and P. Wang, "Resilience-Driven System Design of Complex Engineered Systems," *J. Mech. Des.*, vol. 133, no. 10, Oct. 2011, doi: 10.1115/1.4004981.

[55] E. Specking *et al.*, "Assessing Engineering Resilience for Systems with Multiple Performance Measures," *Risk Anal.*, vol. 39, no. 9, pp. 1899–1912, 2019, doi: https://doi.org/10.1111/risa.13395.

[56] C. Small *et al.*, "Engineered Resilient Systems with Value Focused Thinking," *INCOSE Int. Symp.*, vol. 27, no. 1, pp. 1371–1385, 2017, doi: https://doi.org/10.1002/j.2334-5837.2017.00434.x.

[57] J. T. Margolis, K. M. Sullivan, S. J. Mason, and M. Magagnotti, "A multi-objective optimization model for designing resilient supply chain networks," *Int. J. Prod. Econ.*, vol. 204, pp. 174–185, Oct. 2018, doi: 10.1016/j.ijpe.2018.06.008.

[58] "A probabilistic detectability-based sensor network design method for system health monitoring and prognostics - Pingfeng Wang, Byeng D Youn, Chao Hu, Jong Moon Ha, Byungchul Jeon, 2015." https://journals.sagepub.com/doi/10.1177/1045389X14541496.

[59] C. Hoyle, I. Y. Tumer, A. F. Mehr, and W. Chen, "Health Management Allocation During Conceptual System Design," *J. Comput. Inf. Sci. Eng.*, vol. 9, no. 2, Jun. 2009, doi: 10.1115/1.3130775.

[60] B. Y. Yu, T. Honda, S. Zubair, M. H. Sharqawy, and M. C. Yang, "A Framework for System Design Optimization Based on Maintenance Scheduling With Prognostics and Health Management," presented at the ASME 2013 International Design Engineering Technical Conferences and Computers and Information in Engineering Conference, Feb. 2014, doi: 10.1115/DETC2013-12514.

[61] G. J. Kacprzynski, M. J. Roemer, and A. J. Hess, "Health management system design: Development, simulation and cost/benefit optimization," in *Proceedings, IEEE Aerospace Conference*, Mar. 2002, vol. 6, pp. 6–6, doi: 10.1109/AERO.2002.1036148.

[62] J. P. Malere, "Application of Linear Programming to Optimize the Cost-Benefit of an IVHM System," Sep. 2017, pp. 2017-01–2127, doi: 10.4271/2017-01-2127.

[63] A. F. Mehr and I. Y. Tumer, "A Multidisciplinary and Multiobjective System Analysis and Optimization Methodology for Embedding Integrated Systems Health Management (ISHM) Into NASA's Complex Systems," Jun. 2008, pp. 773–782, doi: 10.1115/DETC2006-99619.

[64] G. Niu and J. Jiang, "Prognostic control-enhanced maintenance optimization for multi-component systems," *Reliab. Eng. Syst. Saf.*, vol. 168, pp. 218–226, Dec. 2017, doi: 10.1016/j.ress.2017.04.011.

[65] R. Faturechi, E. Levenberg, and E. Miller-Hooks, "Evaluating and optimizing resilience of airport pavement networks," *Comput. Oper. Res.*, vol. 43, pp. 335–348, Mar. 2014, doi: 10.1016/j.cor.2013.10.009.

[66] E. Miller-Hooks, X. Zhang, and R. Faturechi, "Measuring and maximizing resilience of freight transportation networks," *Comput. Oper. Res.*, vol. 39, no. 7, pp. 1633–1643, Jul. 2012, doi: 10.1016/j.cor.2011.09.017.

[67] M. Mazidi, N. Rezaei, F. J. Ardakani, M. Mohiti, and J. M. Guerrero, "A hierarchical energy management system for islanded multi-microgrid clusters considering frequency security constraints," *Int. J. Electr. Power Energy Syst.*, vol. 121, p. 106134, Oct. 2020, doi: 10.1016/j.ijepes.2020.106134.

[68] X. Zhang, Z. Hu, and S. Mahadevan, "Bilevel Optimization Model for Resilient Configuration of Logistics Service Centers," *IEEE Trans. Reliab.*, pp. 1–15, 2020, doi: 10.1109/TR.2020.2996025.

[69] D. Hulse *et al.*, "fmdtools: A Fault Propagation Toolkit for Resilience Assessment in Early Design," engrXiv, Sep. 2020. doi: 10.31224/osf.io/d48k6.

[70] Daniel Hulse, Hongyang Zhang, arpanbiswas52, and walshh, *DesignEngrLab/fmdtools: v0.6.0-Multiple fault scenarios*. Zenodo, 2020.

[71] V. J. Bowman, "On the Relationship of the Tchebycheff Norm and the Efficient Frontier of Multiple-Criteria Objectives," in *Multiple Criteria Decision Making*, Berlin, Heidelberg, 1976, pp. 76–86, doi: 10.1007/978-3-642-87563-2_5.

[72] W. A. Mandal, "Weighted Tchebycheff Optimization Technique Under Uncertainty," *Ann. Data Sci.*, Mar. 2020, doi: 10.1007/s40745-020-00250-8.

[73] D. L. Olson, "Tchebycheff norms in multi-objective linear programming," *Math. Comput. Model.*, vol. 17, no. 1, pp. 113–124, Jan. 1993, doi: 10.1016/0895-7177(93)90095-G.

[74] A. M. Thike, S. Lupin, and Y. Vagapov, "Implementation of brute force algorithm for topology optimisation of wireless networks," in *2016 International Conference for Students on Applied Engineering (ICSAE)*, Oct. 2016, pp. 264–268, doi: 10.1109/ICSAE.2016.7810200.

[75] I. Fajfar, Á. Bűrmen, and J. Puhan, "The Nelder–Mead simplex algorithm with perturbed centroid for high-dimensional function optimization," *Optim. Lett.*, vol. 13, no. 5, pp. 1011–1025, Jul. 2019, doi: 10.1007/s11590-018-1306-2.

[76] "Implementing the Nelder-Mead simplex algorithm with adaptive parameters | SpringerLink." https://link.springer.com/article/10.1007/s10589-010-9329-3.

[77] "A unified optimization framework for microelectronics industry | Proceedings of the 8th annual conference on Genetic and evolutionary computation." https://dl.acm.org/doi/abs/10.1145/1143997.1144307.

[78] "Expensive Black-Box Model Optimization Via a Gold Rush Policy | Journal of Mechanical Design | ASME Digital Collection." https://asmedigitalcollection.asme.org/mechanicaldesign/article-abstract/141/3/031401/368491.

[79] B. Sharif, G. G. Wang, and T. Y. ElMekkawy, "Mode Pursuing Sampling Method for Discrete Variable Optimization on Expensive Black-Box Functions," *J. Mech. Des.*, vol. 130, no. 2, Feb. 2008, doi: 10.1115/1.2803251.

[80] A. Tran, T. Wildey, and S. McCann, "sBF-BO-2CoGP: A Sequential Bi-Fidelity Constrained Bayesian Optimization for Design Applications," presented at the ASME 2019 International Design Engineering Technical Conferences and

Computers and Information in Engineering Conference, Nov. 2019, doi: 10.1115/DETC2019-97986.

[81] J. Bree, “Elastic-plastic behaviour of thin tubes subjected to internal pressure and intermittent high-heat fluxes with application to fast-nuclear-reactor fuel elements,” *J. Strain Anal.*, vol. 2, no. 3, pp. 226–238, Jul. 1967, doi: 10.1243/03093247V023226.

[82] V. R. Saranam and B. K. Paul, “Feasibility of Using Diffusion Bonding for Producing Hybrid Printed Circuit Heat Exchangers for Nuclear Energy Applications,” *Procedia Manuf.*, vol. 26, pp. 560–569, Jan. 2018, doi: 10.1016/j.promfg.2018.07.066.

[83] F. Musumeci *et al.*, “An Overview on Application of Machine Learning Techniques in Optical Networks,” *IEEE Commun. Surv. Tutor.*, vol. 21, no. 2, pp. 1383–1408, Secondquarter 2019, doi: 10.1109/COMST.2018.2880039.

[84] M. Binkhonain and L. Zhao, “A review of machine learning algorithms for identification and classification of non-functional requirements,” *Expert Syst. Appl. X*, vol. 1, p. 100001, Apr. 2019, doi: 10.1016/j.eswax.2019.100001.

[85] B. Sekeroglu, S. S. Hasan, and S. M. Abdullah, “Comparison of Machine Learning Algorithms for Classification Problems,” in *Advances in Computer Vision*, Cham, 2020, pp. 491–499, doi: 10.1007/978-3-030-17798-0_39.

[86] G. Kurata, B. Xiang, and B. Zhou, “Improved Neural Network-based Multi-label Classification with Better Initialization Leveraging Label Co-occurrence,” in *Proceedings of the 2016 Conference of the North American Chapter of the Association for Computational Linguistics: Human Language Technologies*, San Diego, California, Jun. 2016, pp. 521–526, doi: 10.18653/v1/N16-1063.

[87] I. Kanellopoulos and G. G. Wilkinson, “Strategies and best practice for neural network image classification,” *Int. J. Remote Sens.*, vol. 18, no. 4, pp. 711–725, Mar. 1997, doi: 10.1080/014311697218719.

[88] O. T. Inan, L. Giovangrandi, and G. T. A. Kovacs, “Robust Neural-Network-Based Classification of Premature Ventricular Contractions Using Wavelet Transform and Timing Interval Features,” *IEEE Trans. Biomed. Eng.*, vol. 53, no. 12, pp. 2507–2515, Dec. 2006, doi: 10.1109/TBME.2006.880879.

[89] Y. Li, W. Xie, and H. Li, “Hyperspectral image reconstruction by deep convolutional neural network for classification,” *Pattern Recognit.*, vol. 63, pp. 371–383, Mar. 2017, doi: 10.1016/j.patcog.2016.10.019.

[90] G. Nasierding, G. Tsoumakas, and A. Z. Kouzani, “Clustering based multi-label classification for image annotation and retrieval,” in *2009 IEEE International Conference on Systems, Man and Cybernetics*, Oct. 2009, pp. 4514–4519, doi: 10.1109/ICSMC.2009.5346902.

[91] R. C. Barros, R. Cerri, A. A. Freitas, and A. C. P. L. F. de Carvalho, “Probabilistic Clustering for Hierarchical Multi-Label Classification of Protein Functions,” in *Machine Learning and Knowledge Discovery in Databases*, Berlin, Heidelberg, 2013, pp. 385–400, doi: 10.1007/978-3-642-40991-2_25.

[92] D. Lizotte, T. Wang, M. Bowling, and D. Schuurmans, “Automatic Gait Optimization with Gaussian Process Regression.,” Jan. 2007, pp. 944–949.

[93] D. Lizotte, “Practical Bayesian Optimization,” Jan. 2008.

[94] V. M. Cora, “Model-based active learning in hierarchical policies,” University of British Columbia, 2008.
[95] M. Frean and P. Boyle, “Using Gaussian Processes to Optimize Expensive Functions,” in *AI 2008: Advances in Artificial Intelligence*, Berlin, Heidelberg, 2008, pp. 258–267, doi: 10.1007/978-3-540-89378-3_25.
[96] R. Martinez-Cantin, N. de Freitas, E. Brochu, J. Castellanos, and A. Doucet, “A Bayesian exploration-exploitation approach for optimal online sensing and planning with a visually guided mobile robot,” *Auton. Robots*, vol. 27, no. 2, pp. 93–103, Aug. 2009, doi: 10.1007/s10514-009-9130-2.
[97] W. Chu and Z. Ghahramani, “Extensions of gaussian processes for ranking: semisupervised and active learning,” *Learn. Rank*, p. 29, 2005.
[98] L. L. Thurstone, “A law of comparative judgment,” *Psychol. Rev.*, vol. 34, no. 4, pp. 273–286, 1927, doi: 10.1037/h0070288.
[99] F. Mosteller, “Remarks on the Method of Paired Comparisons: I. The Least Squares Solution Assuming Equal Standard Deviations and Equal Correlations,” in *Selected Papers of Frederick Mosteller*, S. E. Fienberg and D. C. Hoaglin, Eds. New York, NY: Springer, 2006, pp. 157–162.
[100] C. C. Holmes and L. Held, “Bayesian auxiliary variable models for binary and multinomial regression,” *Bayesian Anal.*, vol. 1, no. 1, pp. 145–168, Mar. 2006, doi: 10.1214/06-BA105.
[101] L. Shu, P. Jiang, X. Shao, and Y. Wang, “A New Multi-Objective Bayesian Optimization Formulation With the Acquisition Function for Convergence and Diversity,” *J. Mech. Des.*, vol. 142, no. 9, Sep. 2020, doi: 10.1115/1.4046508.
[102] S. Sarkar *et al.*, “Multifidelity and Multiscale Bayesian Framework for High-Dimensional Engineering Design and Calibration,” *J. Mech. Des.*, vol. 141, no. 12, Dec. 2019, doi: 10.1115/1.4044598.
[103] T. Sexton and M. Y. Ren, “Learning an Optimization Algorithm Through Human Design Iterations,” *J. Mech. Des.*, vol. 139, no. 10, Oct. 2017, doi: 10.1115/1.4037344.
[104] F. Hutter, H. H. Hoos, and K. Leyton-Brown, “Sequential Model-Based Optimization for General Algorithm Configuration,” in *Learning and Intelligent Optimization*, Berlin, Heidelberg, 2011, pp. 507–523, doi: 10.1007/978-3-642-25566-3_40.
[105] B. Shahriari, K. Swersky, Z. Wang, R. P. Adams, and N. de Freitas, “Taking the Human Out of the Loop: A Review of Bayesian Optimization,” *Proc. IEEE*, vol. 104, no. 1, pp. 148–175, Jan. 2016, doi: 10.1109/JPROC.2015.2494218.
[106] “Javad Azimi Homepage.” http://javad-azimi.com/Research.html (accessed Jan. 04, 2020).
[107] I. Andrianakis and P. Challenor, “The effect of the nugget on Gaussian process emulators of computer models,” *Comput. Stat. Data Anal.*, vol. 56, pp. 4215–4228, Dec. 2012, doi: 10.1016/j.csda.2012.04.020.
[108] A. Pepelyshev, “The Role of the Nugget Term in the Gaussian Process Method,” in *mODa 9 – Advances in Model-Oriented Design and Analysis*, Heidelberg, 2010, pp. 149–156, doi: 10.1007/978-3-7908-2410-0_20.

[109] W. Xing, S. Y. Elhabian, V. Keshavarzzadeh, and R. M. Kirby, "Shared-Gaussian Process: Learning Interpretable Shared Hidden Structure Across Data Spaces for Design Space Analysis and Exploration," *J. Mech. Des.*, vol. 142, no. 8, Aug. 2020, doi: 10.1115/1.4046074.

[110] R. Bostanabad, Y.-C. Chan, L. Wang, P. Zhu, and W. Chen, "Globally Approximate Gaussian Processes for Big Data With Application to Data-Driven Metamaterials Design," *J. Mech. Des.*, vol. 141, no. 11, Nov. 2019, doi: 10.1115/1.4044257.

[111] C. B. Erickson, B. E. Ankenman, and S. M. Sanchez, "Comparison of Gaussian process modeling software," *Eur. J. Oper. Res.*, vol. 266, no. 1, pp. 179–192, Apr. 2018, doi: 10.1016/j.ejor.2017.10.002.

[112] H. J. Kushner, "A New Method of Locating the Maximum Point of an Arbitrary Multipeak Curve in the Presence of Noise," *J. Basic Eng.*, vol. 86, no. 1, pp. 97–106, Mar. 1964, doi: 10.1115/1.3653121.

[113] D. R. Jones, "A Taxonomy of Global Optimization Methods Based on Response Surfaces," *J. Glob. Optim.*, vol. 21, no. 4, pp. 345–383, Dec. 2001, doi: 10.1023/A:1012771025575.

[114] D. D. Cox and S. John, "A statistical method for global optimization," in *[Proceedings] 1992 IEEE International Conference on Systems, Man, and Cybernetics*, Oct. 1992, pp. 1241–1246 vol.2, doi: 10.1109/ICSMC.1992.271617.

[115] "Diagnostics for Gaussian Process Emulators: Technometrics: Vol 51, No 4." https://www.tandfonline.com/doi/abs/10.1198/TECH.2009.08019.

[116] H. Chen, J. L. Loeppky, J. Sacks, and W. J. Welch, "Analysis Methods for Computer Experiments: How to Assess and What Counts?," *Stat. Sci.*, vol. 31, no. 1, pp. 40–60, Feb. 2016, doi: 10.1214/15-STS531.

[117] H. B. Nielsen, S. N. Lophaven, and J. Søndergaard, "DACE - A Matlab Kriging Toolbox," 2002, https://orbit.dtu.dk/en/publications/dace-a-matlab-kriging-toolbox.

[118] D. Meyer *et al.*, *e1071: Misc Functions of the Department of Statistics, Probability Theory Group (Formerly: E1071), TU Wien*. 2019.

[119] F. original by L. B. and A. Cutler and R. port by A. L. and M. Wiener, *randomForest: Breiman and Cutler's Random Forests for Classification and Regression*. 2018.

[120] B. Greenwell, B. Boehmke, J. Cunningham, and G. B. M. Developers (https://github.com/gbm-developers), *gbm: Generalized Boosted Regression Models*. 2019.

[121] A. Al-Dujaili and S. Suresh, "Revisiting norm optimization for multi-objective black-box problems: a finite-time analysis," *J. Glob. Optim.*, vol. 73, no. 3, pp. 659–673, Mar. 2019, doi: 10.1007/s10898-018-0709-z.

[122] P. Važan, Z. Červeňanská, J. Kotianová, and J. Holík, "Problems of a Utopia Point Setting in Transformation of Individual Objective Functions in Multi-Objective Optimization," *Res. Pap. Fac. Mater. Sci. Technol. Slovak Univ. Technol.*, vol. 27, no. 45, pp. 64–71, Sep. 2019, doi: 10.2478/rput-2019-0027.

[123] K. Yang, M. Emmerich, A. Deutz, and T. Bäck, "Multi-Objective Bayesian Global Optimization using expected hypervolume improvement gradient," *Swarm Evol. Comput.*, vol. 44, pp. 945–956, Feb. 2019, doi: 10.1016/j.swevo.2018.10.007.

[124] Z. Wang and S. Jegelka, "Max-value Entropy Search for Efficient Bayesian Optimization," *ArXiv170301968 Cs Math Stat*, Jan. 2018, http://arxiv.org/abs/1703.01968.

[125] D. Hernández-Lobato, J. M. Hernández-Lobato, A. Shah, and R. P. Adams, "Predictive Entropy Search for Multi-objective Bayesian Optimization," *ArXiv151105467 Stat*, Feb. 2016, http://arxiv.org/abs/1511.05467.

[126] M. Abdolshah, A. Shilton, S. Rana, S. Gupta, and S. Venkatesh, "Multi-objective Bayesian optimisation with preferences over objectives," *ArXiv190204228 Cs Stat*, Nov. 2019, http://arxiv.org/abs/1902.04228.

[127] V. Bhaskar, Santosh K. Gupta, and Ajay K. Ray, "APPLICATIONS OF MULTIOBJECTIVE OPTIMIZATION IN CHEMICAL ENGINEERING," *Rev. Chem. Eng.*, vol. 16, no. 1, pp. 1–54, Mar. 2000, doi: 10.1515/REVCE.2000.16.1.1.

[128] L. Grandinetti, F. Guerriero, D. Laganà, and O. Pisacane, "An Approximate ε-Constraint Method for the Multi-objective Undirected Capacitated Arc Routing Problem," in *Experimental Algorithms*, Berlin, Heidelberg, 2010, pp. 214–225, doi: 10.1007/978-3-642-13193-6_19.

[129] M. J. Rentmeesters, W. K. Tsai, and Kwei-Jay Lin, "A theory of lexicographic multi-criteria optimization," in *Proceedings of ICECCS '96: 2nd IEEE International Conference on Engineering of Complex Computer Systems (held jointly with 6th CSESAW and 4th IEEE RTAW)*, Oct. 1996, pp. 76–79, doi: 10.1109/ICECCS.1996.558386.

[130] W. Zhang and S. Fujimura, "Improved Vector Evaluated Genetic Algorithm with Archive for Solving Multiobjective PPS Problem," in *2010 International Conference on E-Product E-Service and E-Entertainment*, Nov. 2010, pp. 1–4, doi: 10.1109/ICEEE.2010.5660926.

[131] "Improved rank-niche evolution strategy algorithm for constrained multiobjective optimization | Emerald Insight." https://www.emerald.com/insight/content/doi/10.1108/02644400810874949/full/html.

[132] C. A. Coello Coello and M. S. Lechuga, "MOPSO: a proposal for multiple objective particle swarm optimization," in *Proceedings of the 2002 Congress on Evolutionary Computation. CEC'02 (Cat. No.02TH8600)*, May 2002, vol. 2, pp. 1051–1056 vol.2, doi: 10.1109/CEC.2002.1004388.

[133] K. Deb, A. Pratap, S. Agarwal, and T. Meyarivan, "A fast and elitist multiobjective genetic algorithm: NSGA-II," *IEEE Trans. Evol. Comput.*, vol. 6, no. 2, pp. 182–197, Apr. 2002, doi: 10.1109/4235.996017.

[134] Y. Cui, Z. Geng, Q. Zhu, and Y. Han, "Review: Multi-objective optimization methods and application in energy saving," *Energy*, vol. 125, pp. 681–704, Apr. 2017, doi: 10.1016/j.energy.2017.02.174.

[135] R. T. Marler and J. S. Arora, “Survey of multi-objective optimization methods for engineering,” *Struct. Multidiscip. Optim.*, vol. 26, no. 6, pp. 369–395, Apr. 2004, doi: 10.1007/s00158-003-0368-6.
[136] S. Kuiper, “Introduction to Multiple Regression: How Much Is Your Car Worth?,” *J. Stat. Educ.*, vol. 16, no. 3, p. null, Nov. 2008, doi: 10.1080/10691898.2008.11889579.
[137] T. Plotts, “A Multiple Regression Analysis of Factors Concerning Superintendent Longevity and Continuity Relative to Student Achievement,” *Seton Hall Univ. Diss. Theses ETDs*, Jan. 2011, [Online]. Available: https://scholarship.shu.edu/dissertations/484.
[138] S. Rong and Z. Bao-wen, “The research of regression model in machine learning field,” *MATEC Web Conf.*, vol. 176, p. 01033, 2018, doi: 10.1051/matecconf/201817601033.
[139] J. D. Williams, “A Regression Approach to Experimental Design,” *J. Exp. Educ.*, vol. 39, no. 2, pp. 83–90, 1970.
[140] J. Real, C. Forné, A. Roso-Llorach, and J. Martínez-Sánchez, “Quality Reporting of Multivariable Regression Models in Observational Studies: Review of a Representative Sample of Articles Published in Biomedical Journals,” *Medicine (Baltimore)*, vol. 95, no. 20, May 2016, doi: 10.1097/MD.0000000000003653.
[141] L. C. R. P. Watagoda and D. J. Olive, “Inference For Multiple Linear Regression After Model or Variable Selection.”
[142] O. Seidou, J. J. Asselin, and T. B. M. J. Ouarda, “Bayesian multivariate linear regression with application to change point models in hydrometeorological variables,” *Water Resour. Res.*, vol. 43, no. 8, 2007, doi: 10.1029/2005WR004835.
[143] T. Chen and E. Martin, “Bayesian linear regression and variable selection for spectroscopic calibration,” *Anal. Chim. Acta*, vol. 631, no. 1, pp. 13–21, Jan. 2009, doi: 10.1016/j.aca.2008.10.014.
[144] D. C. Woods, A. M. Overstall, M. Adamou, and T. W. Waite, “Bayesian design of experiments for generalized linear models and dimensional analysis with industrial and scientific application,” *Qual. Eng.*, vol. 29, no. 1, pp. 91–103, Jan. 2017, doi: 10.1080/08982112.2016.1246045.
[145] M. Peruzzi and D. B. Dunson, “Bayesian Modular and Multiscale Regression,” 2018.
[146] C. Elster *et al.*, “A Guide to Bayesian Inference for Regression Problems,” 2015.
[147] A. Saltelli, Ed., *Sensitivity analysis*, Paperback ed. Chichester: Wiley, 2008.
[148] H. M. Wagner, “Global Sensitivity Analysis,” *Oper. Res.*, vol. 43, no. 6, pp. 948–969, Dec. 1995, doi: 10.1287/opre.43.6.948.
[149] Y. Xiong, W. Chen, K.-L. Tsui, and D. W. Apley, “A better understanding of model updating strategies in validating engineering models,” *Comput. Methods Appl. Mech. Eng.*, vol. 198, no. 15, pp. 1327–1337, Mar. 2009, doi: 10.1016/j.cma.2008.11.023.
[150] E. Keshavarzi, K. Goebel, I. Y. Tumer, and C. Hoyle, “Model Validation in Early Phase of Designing Complex Engineered Systems,” presented at the ASME 2018 International Design Engineering Technical Conferences and

Computers and Information in Engineering Conference, Nov. 2018, doi: 10.1115/DETC2018-85137.
[151] H. Pohlheim, “Examples of Objective Functions (GEATbx.com).” 2006.
[152] H. Yang, L. Chan, and I. King, “Support Vector Machine Regression for Volatile Stock Market Prediction,” in *Intelligent Data Engineering and Automated Learning — IDEAL 2002*, Berlin, Heidelberg, 2002, pp. 391–396, doi: 10.1007/3-540-45675-9_58.
[153] M. A. Patil *et al.*, “A novel multistage Support Vector Machine based approach for Li ion battery remaining useful life estimation,” *Appl. Energy*, vol. 159, pp. 285–297, Dec. 2015, doi: 10.1016/j.apenergy.2015.08.119.
[154] G. W. Flake and S. Lawrence, “Efficient SVM Regression Training with SMO,” *Mach. Learn.*, vol. 46, no. 1, pp. 271–290, Jan. 2002, doi: 10.1023/A:1012474916001.
[155] E. Snelson, “Flexible and efficient Gaussian process models for machine learning,” 2007. https://discovery.ucl.ac.uk/id/eprint/1445855/.
[156] M. Seeger, “GAUSSIAN PROCESSES FOR MACHINE LEARNING | International Journal of Neural Systems,” 2004. https://www.worldscientific.com/doi/abs/10.1142/S0129065704001899.